6-9-2016

The Smoluchowski equation in population dynamics and the spread of infection

Satomi Sugaya

Satomi Sugaya

Candidate

Physics and Astronomy

Department

This dissertation is approved, and it is acceptable in quality and form for publication:

Approved by the Dissertation Committee:

V. M. Kenkre , Chairperson

D. Dunlap

K. Lidke

M. Moses

THE SMOLUCHOWSKI EQUATION IN POPULATION DYNAMICS AND THE SPREAD OF INFECTION

by

SATOMI SUGAYA
B.A., Lewis & Clark College, Portland, OR, May 2006
M.S., New Mecixo Institude of Mining and Technology,
Socorro, NM, May 2010
M.S., The Univerisyt of New Mexico, Albuquerque, NM, May 2016

DISSERTATION

Submitted in Partial Fulfillment of the
Requirements for the Degree of

Doctor of Philosophy

Physics

The University of New Mexico
Albuquerque, New Mexico

May 2016

Dedication

To my mother Reiko, my father Tatsuo, my sister Miyako, my brother Ippei, the dog Lucky, and myself. We survived. The chain is broken and we are free. Good work!

Acknowledgments

The completion of this degree came in a relatively short stretch of a long road. First and foremost, this would not have been possible without my thesis adviser Professor Nitant Kenkre. I have been very fortunate to have been able to work with him not only as my thesis adviser but also as a person.

The Consortium of the Americas for Interdisciplinary Science has been my home at UNM since I started here in 2010. Much gratitude goes to the director, Nitant Kenkre, and the unique members (as unique as the director) of the consortium. I appreciate the wide range of topics we shared and discussed in lengths, and especially for the amount of laughter our group generated, which was (and is) truly special. Special thanks for Professor Dunlap.

I would like to thank the Program in Interdisciplinary Biological & Biomedical Sciences (PiBBs) for the opportunity for me to participate in a unique and diverse scientific community, and for granting me a fellowship between 2013-2015. My Ph.D. project would not have been possible without PiBBs.

My last semester at UNM had been supported by the Megumi Yamamoto Memorial Fund. I would like to thank Professor Rudolf and Professor Deutsch for helping me through an unexpected medical condition that emerged during my last semester by this mean.

The last stride of my degree was intense in every aspect. It is not an overstatement to say that I was able to keep going because of my friends, especially my office mates Anastasia, Matt, Tzu-Cheng, and Wesley. Besides their intelligent inputs and insightful conversations I had with them, their supportive presence and great characters made my life better. I would like to thank Adrian for helping me with numerical methods. Also, I would like to thank all of my friends here at the physics department. Lastly, I would like to thank Andy for the support and encouragement he gave me all the way.

The Smoluchowski Equation in Population Dynamics and the Spread of Infection

by

Satomi Sugaya

B.A., Lewis & Clark College, Portland, OR, May 2006

M.S., New Mexico Institute of Technology and Mining,

Socorro, NM, May 2010

M.S., The University of New Mexico, Albuquerque, NM, May 2014

Physics, University of New Mexico, 2016

Abstract

This dissertation is a report on an interdisciplinary investigation consisting of an application of random walk techniques to problems in ecology, particularly to the spread of Hantavirus epidemic among rodents that live on an open terrain. The population of mice that we consider is made up of infectious disease-carrying mice and susceptible mice that are disease-free, and each mouse has its own home range around which it executes a random walk. We describe an event of infection transmission in such a population via reaction-diffusion theory. Our simple model consists of two mice, one infected and the other susceptible, the disease being passed upon encounter as the two mice move on the terrain. The existence of home ranges of the mice is included in the model by representing each mouse to be a Smoluchowski random walker. Such a simple model is appropriate for a dilute population where

only one infected-susceptible mice pair is considered to meet at a time. However the calculation helps the understanding of underlying microscopic processes of an epidemic outbreak in an arbitrary population density.

The two-mice model is formulated in an arbitrary number of dimensions and explicit calculation in 1-dimension is performed first. We uncover an interesting effect of the home ranges on the characteristics of infection-transmission event. We find that there is an optimal configuration of the home ranges for which infection-transmission occurs most efficiently. Furthermore, the practical application of our model to higher dimensions requires an extension of the theory to circumvent a seemingly well-known problem in reaction-diffusion theory that the 'reaction' site cannot be a 0-dimensional object for problems considered in higher dimension than 1. We develop a detailed resolution and present a practical extension with an explicit calculation demonstrated in 2-dimensions.

Our work is, thus, useful in two ways. One is the further development of reaction-diffusion theory to tethered random walkers and dimensions higher than 1. The other is to gain insights into the practical problem of the spread of the Hantavirus epidemic.

Contents

Chapter 1

Introduction

1.1 Motivation

In this thesis, we report an interdisciplinary investigation consisting of an application of random walk techniques to problems in ecology, particularly to the spread of epidemics such as the Hantavirus. The main topic of this work consists of a further development of some tools of non-equilibrium statistical mechanics: the Smoluchowski equation [1], reaction-diffusion theory, non-Gaussian random walks, and the defect technique [2–12] ; and their application specifically to the spread of Hantavirus among rodents moving on open terrain. We will give a detailed description of the non-equilibrium tools in the next chapter. In the following, we present the relevant background on epidemics in general and Hantavirus in particular. In Section 1.2 we will also give the outline of this thesis.

1.1.1 Background

In an epidemic outbreak, an infectious disease spreads among a population of susceptible individuals. The symptom of the infection varies widely as well as its duration depending on the nature of the disease [13]. The field of mathematical epidemiology studies population dynamics using mathematical models. In their seminal work [13], Anderson and May started a major branch of research by studying the subject by the use of coupled ordinary differential equations. Their objects of research are universally known as, for instance, the SI (susceptible-infected) and SIR (susceptible-infected-recovered) models. Such models are used widely and the application can be found, for example, in a review given in ref. [14]. Despite their success, these models are appropriate only for a well-mixed host population of an infectious disease, and fail to capture the spatial elements in the system, the movement of the populations, and the space-dependent interactions of the population. Inclusion of space in population dynamics equations was introduced independently by many authors, and such models have been used widely [15–24].

A series of investigations of the Hantavirus epidemic among a rodent species, *peromyscus maniculatus*, was conducted [25–33] following the epidemic outbreak of a strain of Hantavirus, called the Sin Nombre Virus, among the rodents that in turn caused the Hantavirus Polmonary Syndrome (HPS) among humans in 1993, in the Southwest region of the United States. The symptoms of HPS start out similar to a flu, followed by a pneumonia-like condition with lungs filling with fluids, causing upto 70% mortality rate [33]. Unlike its effects on humans a Hantavirus infection does not affect the rodents; an infected rodent carries a chronic infection without ill effects; it is also found that an infection does not get passed to offspring [25].

Our investigation stems from theoretical work done by Kenkre and collaborators in the last decade at UNM, starting with ref. [18]. Abramson and Kenkre in ref. [18] captured major features of the observed spatio-temporal patterns of the Hantavirus spread in New Mexico. The model treated the logistic growth [34] of the infected and susceptible populations combined with their movement on the terrain and the space-dependent interaction between them, with a parameter that characterized the environmental resources. The movement of mice was treated as random walks. The logistic element models resource-limited population growth. It curbs the growth by the competition for the limited resource.

The temporal pattern of the virus outbreak predicted by the Abramson-Kenkre model described well the observation of 1993 Hantavirus outbreak following the El Niño in the previous year that boosted the habitability of the environment through increased precipitation followed by a warm winter [32]. The other observed character of the Hantavirus infection is its spatial pattern, where the existence of patches of infected mice were identified. Such patches are referred to as *refugia* [18], and they contract and expand depending on the environmental factor, becoming a source of an infection spread when the environment is favorable [31]. The Abramson-Kenkre model also predicted satisfactorily such refugia of infection where the resources are abundant.

Furthermore, Abramson et. al., in [19,23,35], described *how* the infection spreads from refugia when the condition is favorable. They found that the infection spreads as a wave front. First, the front of susceptible population spreads out to the areas that are unoccupied by the mice, and then following the spread of the susceptible mice, the front of the infection develops. A large variety of observations based on the Abramson-Kenkre model were explained and predictions were made at UNM in

the ensuing decade [18,19,21,23,35–42] including even an extinction of refugia of the virus, modulated by the environmental condition [22,43].

During the explicit quantitative application of the theory to the accumulated data of the motion of the mice, it was found that the mice moved like random walkers attracted to central locations. These were understood as home range centers [38,40,41]. This finding called for a profound modification in the theory [21] with an introduction of the Smoluchowski equation [41] and a detailed study of home ranges and epidemic spread was conducted [38, 39, 41]. The theory was used to estimate the diffusion constant and the size of the home ranges of the mice. The first mention of the Smoluchowski equation in the context of animal home ranges seems to have been made by Okubo [15]. The actual task of incorporating home ranges was undertaken first in the Ph.D. thesis of MacInnis [44].

The double role of the present thesis is to develop tools for reaction-diffusion theory in the context of tethered random walkers with the help of the Smoluchowski equation; and to apply the tools to the study of the spread of epidemics via model investigations comprising of small (two-mouse) systems. The ultimate aim is to use the result from such two-mouse calculations to develop a kinetic theory of spread of epidemics incorporating the existence of home ranges.

1.2 Outline

In Chapter 2, we present the important tools of this thesis, objects of non-equilibrium statistical mechanics, viz., the Smoluchowski equation and the reaction-diffusion theory via the defect technique. The former describes the probability density of a ran-

dom walker that is also attracted to a central location. In the latter, the term "diffusion" indicates that there is a moving entity, and "reaction" means something happens to the entity as it moves when it reaches a particular configuration. Specifically, we give an overview of a mathematical technique called the defect technique that makes it practical for a reaction-diffusion approach to our problem.

In the remaining chapters, we present the applications of the Smoluchowski equation and the defect technique. In Chapter 4, we analyze our model of an infectious disease transmission between two mice, one carrying an infection and the other without it but susceptible to it. In this problem, each mouse is thought to be a Smoluchowski random walker where the attractive center represents the center of the home range. We are interested in the effect of the home ranges of the mice on the probability of the susceptible mouse obtaining the infection, the infection probability.

We know from the exciton annihilation analysis performed earlier by Kenkre [5] that a two-walker reaction-diffusion problem in an arbitrary number of dimensions can always be mapped to a single-walker reaction-diffusion problem in twice the number of dimensions. This point is elaborated in 4.2. Thus, in Chapter 3, a trapping scenario of a Smoluchowki random walker is discussed, where the walker is captured by a stationary trap. The expression for the probability to survive the trap, the survival probability, is given. We find a counter-intuitive effect of the existence of the attractive center on the survival probability.

In Chapter 5, we present an extension to the infection model presented in Chapter 4 for its application to a higher dimension, circumventing the seemingly well-known reaction-diffusion problem: the Laplace transform of a key quantity in finding the infection probability cannot be found when the "reaction" takes place at a

mathematical point in higher dimensions. An explicit calculation in 2-dimensions is given to demonstrate the use of the extension and to verify that the effect found in the previous chapter is generalized to higher dimensions.

In Chapter 6, we give a summary of this thesis and make brief remarks on building a kinetic model for an epidemic spread with home range consideration.

Chapter 2

The Underlying Smoluchowski Equation and the Defect Technique

2.1 Motivation

In this chapter, we introduce the tools for building our understanding of a transmission of an infectious disease between two animals that have respective home ranges. First, in Section 2.2, we introduce the Smoluchowski equation that is used to model the probability density to find such an animal at a certain location at a given time. We give the solution and discuss its important characteristics pertinent to our study. In Section 2.3, we present the general framework of the defect technique [2] that enables us to study the infection-transmission between such animals in a reaction-diffusion scenario.

2.2 The Smoluchowski Equation

This equation was developed by M. Smoluchowski to study coagulation phenomena [1], where he considered particles that are attracted to the center of an attractive potential to aggregate when they reach a certain radius of the potential center. This well-known equation describes the probability density of an entity that moves randomly but is also attracted to a central location. We here present the equation and discuss the feature of the solution in detail.

We first give a brief overview of a pure random walker. Consider an n-dimensional random walker whose position is given by the vector $\boldsymbol{r} = (r_1, r_2, \ldots, r_n)$. If no attractive center is involved, the equation of motion for the probability density, $P(\boldsymbol{r}, t)$ to find the walker at position $\boldsymbol{r}$ at time t is given by

$$\frac{\partial P(\boldsymbol{r}, t)}{\partial t} = D\nabla^2 P(\boldsymbol{r}, t), \tag{2.1}$$

where D is called the diffusion constant, and the equation is called the diffusion equation. This equation can be straightforwardly solved by the use of Fourier transform. The well-known solution is given by

$$P(\boldsymbol{r}, t) = \int_{-\infty}^{\infty} d^n r' \, \Pi_D(\boldsymbol{r}, \boldsymbol{r}', t) P(\boldsymbol{r}', 0), \tag{2.2}$$

where $P(\boldsymbol{r}', 0)$ is the initial condition of the walker, and $\Pi_D(\boldsymbol{r}, \boldsymbol{r}', t)$ is the propagator (the subscript D is for diffusion),

$$\Pi_D(\boldsymbol{r}, \boldsymbol{r}', t) = \left(\frac{1}{\sqrt{4\pi D t}}\right)^n \prod_{\beta=1}^{n} e^{-\frac{(r_\beta - r'_\beta)^2}{4Dt}}, \tag{2.3}$$

where β labels each dimension. For a delta-function initial condition, $P(\boldsymbol{r}', 0) = \delta^n(\boldsymbol{r}' - \boldsymbol{r}^0)$, where the initial location has the β-th component r^0_β, the solution of equation (2.1) is

$$P(\boldsymbol{r}, t) = \left(\frac{1}{\sqrt{4\pi D t}}\right)^n \prod_{\beta=1}^{n} e^{-\frac{(r_\beta - r^0_\beta)^2}{4Dt}}. \tag{2.4}$$

Thus, the probability density of the walker is characterized by the Gaussian centered at $\boldsymbol{r}^0$ with the width $\sigma_D = \sqrt{2Dt}$. The mean position of the walker, which is the center of the Gaussian, obviously given by the first moment of $\boldsymbol{r}$ as

$$\langle \boldsymbol{r} \rangle = \int_{-\infty}^{\infty} d^n r \; \boldsymbol{r} P(\boldsymbol{r}, t) = \boldsymbol{r}^0, \tag{2.5}$$

is the initial location of the walker. The mean squared displacement (MSD), *i.e.*, the average of square distance traveled by the walker, is given by the difference between the second moment, $\langle \boldsymbol{r}^2 \rangle$, and the square of the mean:

$$\text{MSD} = \langle \boldsymbol{r}^2 \rangle - \langle \boldsymbol{r} \rangle^2 = n \cdot 2Dt = n \cdot \sigma_D^2. \tag{2.6}$$

Hence, the MSD grows linearly in time, indicating that the walker will eventually disappear to infinity. We note that, as seen in the last equality of the above equation, the MSD is proportional to the square of the width (the variance) of the Gaussian.

We now introduce the primary equation used in this thesis to describe the behavior of the probability density, $P(\boldsymbol{r}, t)$, of a random walker who is also attracted to a central location. Letting such central location be the origin without loss of generality, the equation of motion for $P(\boldsymbol{r}, t)$ is given by the Smoluchowski equation,

$$\frac{\partial P(\boldsymbol{r}, t)}{\partial t} = \gamma \nabla \cdot (\boldsymbol{r} P(\boldsymbol{r}, t)) + D \nabla^2 P(\boldsymbol{r}, t), \tag{2.7}$$

where the second term on the right hand side is the diffusion term as described above, and the first term arises due to the motion of the walker being attracted toward the origin, with strength γ. The word "tethered" will be used in the following to describe this home-bound motion of the walker throughout this thesis. When the term multiplying $P(\boldsymbol{r}, t)$ in this term ($\boldsymbol{r}$) is expressed as a gradient of a potential $U(\boldsymbol{r})$, the potential takes the form $U(\boldsymbol{r}) = (\gamma/2)(r_1^2 + r_2^2 + \cdots + r_n^2)$, which is the form of an attractive harmonic potential. The solution of equation (2.7) is presented and discussed below.

2.2.1 Solution of the Homogeneous Smoluchowski Equation and its Physical Significance

For the purpose of generality of use we will now relax the assumption that the location of attraction lies at the origin. It is now placed at an arbitrary location, $\boldsymbol{r}_h = (h_1, h_2, \ldots, h_n)$. The equation for $P(\boldsymbol{r}, t)$ then becomes

$$\frac{\partial P(\boldsymbol{r}, t)}{\partial t} = \nabla \cdot \left[\gamma \left(\boldsymbol{r} - \boldsymbol{r}_h\right) P(\boldsymbol{r}, t)\right] + D\nabla^2 P(\boldsymbol{r}, t). \tag{2.8}$$

This equation is solved by the method of characteristic in Fourier space, which is a standard procedure that can be found in a text book [45]. Nevertheless, the step by step method is provided in Appendix A for completeness. The solution to equation (2.8) is given by

$$P(\boldsymbol{r}, t) = \int_{-\infty}^{\infty} d^n \boldsymbol{r} \Pi(\boldsymbol{r}, \boldsymbol{r}', t) P(\boldsymbol{r}', 0), \tag{2.9}$$

where $P(\boldsymbol{r}', 0)$ is the initial condition of the walker, and $\Pi(\boldsymbol{r}, \boldsymbol{r}', t)$ is the propagator given by

$$\Pi(\boldsymbol{r}, \boldsymbol{r}', t) = \left(\frac{1}{\sqrt{4\pi D\mathcal{T}(t)}}\right)^n \prod_{\beta=1}^{n} e^{-\frac{\left(r_\beta - h_\beta - (r'_\beta - h_\beta)e^{-\gamma t}\right)^2}{4D\mathcal{T}(t)}}. \tag{2.10}$$

The function $\mathcal{T}(t)$ is given by

$$\mathcal{T}(t) = \frac{(1 - e^{-2\gamma t})}{2\gamma}. \tag{2.11}$$

Hence, for a delta-function initial condition, $P(\boldsymbol{r}', 0) = \delta^n(\boldsymbol{r}' - \boldsymbol{r}^0)$, the solution is

$$P(\boldsymbol{r}, t) = \left(\frac{1}{\sqrt{4\pi D\mathcal{T}(t)}}\right)^n \prod_{\beta=1}^{n} e^{-\frac{\left(r_\beta - h_\beta - (r^0_\beta - h_\beta)e^{-\gamma t}\right)^2}{4D\mathcal{T}(t)}}. \tag{2.12}$$

This is also a Gaussian that we refer to as the Smoluchowski Gaussian. It exhibits richer features compared to equation (2.3) for an unconstrained random walker.

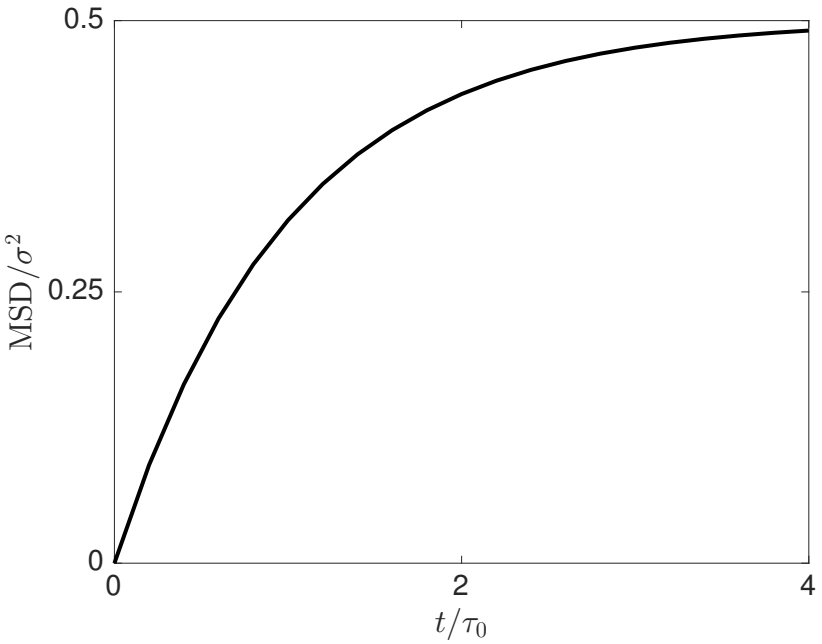

Figure 2.1: The mean square displacement (MSD) for a Smoluchowski random walker, given in equation (2.15), is plotted for 1-dimension against time, where the MSD is scaled to the square of the Smoluchowski width, $\sigma^2 = 2D/\gamma$. The time is expressed as a ratio to the diffusive time for the walker to travel to the attractive center from its initial location, $\tau_0 = x_0^2/2D$. The MSD starts at 0 at $t = 0$ and saturates to the steady-state value.

One unique feature is of the width, $\sigma(t)$, we here define as

$$\sigma(t) = \sqrt{4D\mathcal{T}(t)} = \sqrt{\frac{4D(1 - e^{-2\gamma t})}{2\gamma}}. \tag{2.13}$$

As seen in its time-dependence, it *saturates* in its value as a function of time, due to the behavior of $\mathcal{T}(t)$. We denote the saturation value, *i.e.*, the steady-state value, of $\sigma(t)$ by σ:

$$\sigma = \sqrt{\frac{2D}{\gamma}}. \tag{2.14}$$

Such behavior of $\sigma(t)$, in turn, gives the same saturating character to the MSD, which is given by

$$\text{MSD} = n \cdot 2D\mathcal{T}(t) = n \cdot \frac{1}{2}\sigma^2(t). \tag{2.15}$$

Notice the stark difference compared to the MSD found for a pure random walker which grows linearly in time. This saturating MSD indicates that in the steady-state, there is a *finite* probability density to find the tethered random walker somewhere in space particularly around the center of attraction. Figure 2.1 depicts the MSD given in equation (2.15) (scaled to σ^2) plotted against time (scaled to τ_0, the characteristic time for the walker to travel to the potential center from its initial location by a purely random motion, the diffusive time). It starts at 0 at $t = 0$ and saturates to the steady-state value. We chose $n = 1$ but the behavior is identical for higher dimensions.

The other peculiar feature of the solution of the Smoluchowski equation is that of the mean position of the walker, which is given by

$$\langle \boldsymbol{r} \rangle(t) = \boldsymbol{r}_h + \left(\boldsymbol{r}^0 - \boldsymbol{r}_h\right) e^{-\gamma t}. \tag{2.16}$$

This is a *time-dependent* quantity unlike that of a 'pure' (an unconstrained) random walker, where it starts from being at the initial position, $\boldsymbol{r}^0$, at $t = 0$, and shifts to the potential-center location, $\boldsymbol{r}_h$, in a long time. This behavior of the mean position and the MSD eventually gives $P(\boldsymbol{r}, t)$ as

$$P(\boldsymbol{r})_{ss} = \left(\frac{1}{\sqrt{\pi}\sigma}\right)^n \prod_{\beta=1}^{n} e^{-\frac{\left(r_\beta - h_\beta\right)^2}{\sigma^2}}, \tag{2.17}$$

which is another Gaussian centered at the potential-center location with the constant width σ. The subscript ss stands for steady-state.

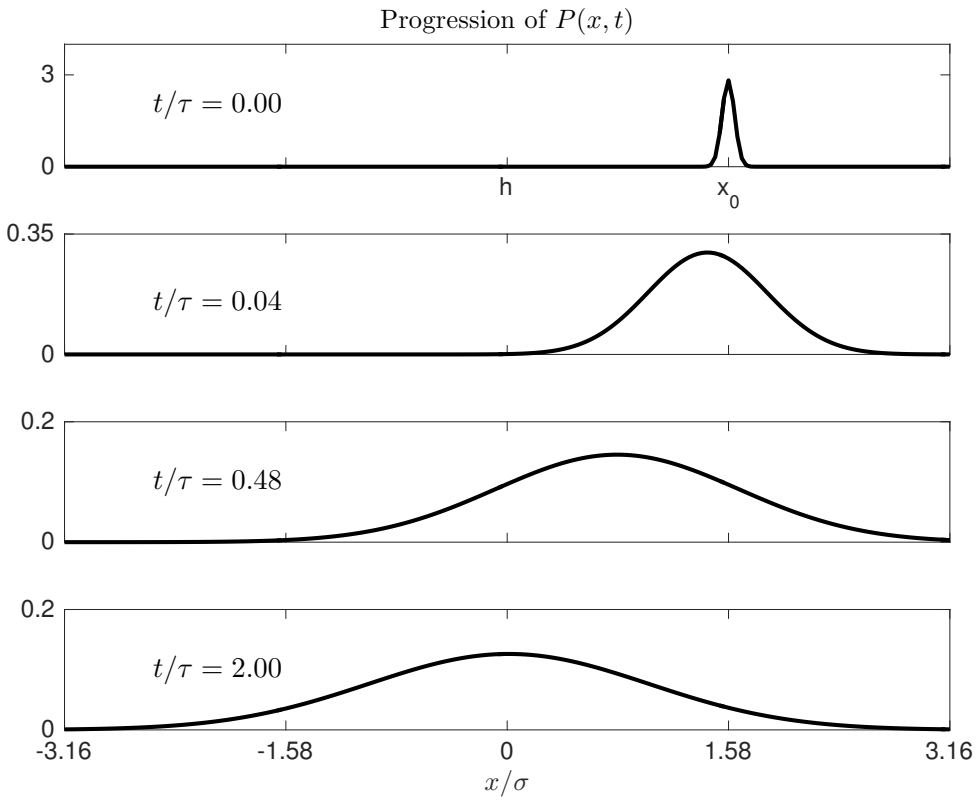

Figure 2.2: The Smoluchowski density in one dimension, $P(x,t)$ plotted against x (scaled to $\sigma = \sqrt{D/\gamma}$) at four different times, which is scaled to the diffusive time $\tau = (x_0 - h)^2/2D$ to travel the distance between the initial location and the potential center. These are t/τ =0, 0.04, 0.48, and 2.0. The walker was initially placed at $x_0 = 1.58$ and the center of the potential was set to be the origin. From top to bottom, the mean position of $P(x,t)$ moves from x_0 to h as the width settles to its steady-state value, σ, here taken to be 3.20.

In order to illustrate the behavior of the Smoluchowski Gaussian, we show in Figure 2.2, the spatial profile of $P(x,t)$ at different times for a 1-dimensional walker.

Specifically, $P(x,t)$ is given by

$$P(x,t) = \frac{1}{\sqrt{4\pi D\mathcal{T}(t)}} e^{-\frac{\left(x-h-(x^0-h)e^{-\gamma t}\right)^2}{4D\mathcal{T}(t)}}, \tag{2.18}$$

where $r_1 \equiv x$, $r_1^0 \equiv x^0$, and $h_1 \equiv h$. From the top to bottom panel, the temporal progression of $P(x,t)$ is shown at four different times, which is scaled to $\tau = (x_0 - h)^2/2D$, the diffusive time to travel the distance between the initial location and the potential center, and whose values are $t/\tau = 0$, 0.04, 0.48, and 2.0, respectively. The horizontal axis of the spatial variable x is scaled to the steady-state width σ. The probability density of the walker starts out being centered at the initial location of the walker (top panel), and shifts towards the potential-center location h as seen in the progression of $P(x,t)$ in each panel. As the mean of $P(x,t)$ migrates to h, the width of the Gaussian also approaches the Smoluchowski width. Now that the property of Smoluchowski equation and its solution were discussed in detail, we next present a mathematical method central to solving the reaction-diffusion equations that are studied in this thesis.

2.3 The Defect Technique and the ν-function Method

We here present the general framework of the defect technique [2–12] through the simplest possible example: trapping of a random walker via a reaction-diffusion scenario. While the example may be found in the work of numerous authors (as in the references listed above), our notation here follows that of a recent review [12].

Consider a particle in a discrete space with an arbitrary number of dimensions, whose probability to be found on m-th site at time t is denoted by $P_m(t)$. We consider a trapping problem of this particle by stationary traps located arbitrarily throughout

the space that capture the particle at a rate $\mathcal{C}$, when they are visited by the particle. The characteristics of the motion of the particle is to be specified for each problem at hand, and here we present a general prescription. The equation of motion for $P_m(t)$ is given by the reaction-diffusion equation

$$\frac{dP_m(t)}{dt} = \text{motion term} - \mathcal{C}\sum_r{}' \delta_{m,r} P_m(t), \tag{2.19}$$

where the "motion term" describes the portion of the equation of $P_m(t)$ arising from the motion of the particle, e.g., with or without translational invariance, and is assumed to be linear in $P_m(t)$. The second term, $-\mathcal{C}\sum_r{}' \delta_{m,r} P_m(t)$, describes the trapping event where the particle gets captured at a rate $\mathcal{C}$, when it visits a trap site r, which is described by the Kronecker delta function, $\delta_{m,r}$. The prime denotes the summation over such trap (reaction) sites.

Let the propagator and the solution to the homogeneous problem be denoted by $\Psi_{m,n}(t)$ and $\eta_m(t)$, respectively. Then, given the initial condition, $P_n(0)$, of the particle, $\eta_m(t)$ is given by

$$\eta_m(t) = \sum_n \Psi_{m,n}(t) P_n(0). \tag{2.20}$$

By the Green function method, the solution to the inhomogeneous equation (equation (2.19)) is given, in terms of $\eta_m(t)$ and $\Psi_{m,n}(t)$ by

$$P_m(t) = \eta_m(t) - C\sum_r{}' \int_0^t dt'\, \Psi_{m,r}(t-t') P_r(t'). \tag{2.21}$$

The Laplace transform of this equation is given by

$$\widetilde{P}_m(\epsilon) = \tilde{\eta}_m(\epsilon) - \mathcal{C}\sum_r{}' \widetilde{\Psi}_{m,r}(\epsilon)\widetilde{P}_r(\epsilon), \tag{2.22}$$

where the tildes denote Laplace transforms and ϵ is the Laplace variable.

The common quantity of interest in a trapping problem is the total survival probability, that is the probability that the particle have survived the capture by the traps at time t. We denote this quantity by $\mathcal{Q}(t)$, and it is defined as

$$\mathcal{Q}(t) = \sum_m P_m(t). \tag{2.23}$$

In the Laplace domain, this quantity becomes

$$\widetilde{\mathcal{Q}}(\epsilon) = \frac{1}{\epsilon}\left[1 - \sum_r{}' \widetilde{P}_r(\epsilon)\right], \tag{2.24}$$

via equation (2.22), where the summation over all the site of $\tilde{\eta}_m(\epsilon)$ and $\Psi_{m,r}(\epsilon)$ yields $1/\epsilon$. It is also straightforward to obtain the rate of disappearance of the particle by summing over equation (2.19), which yields

$$\frac{d\mathcal{Q}(t)}{dt} = 1 - \mathcal{C}\sum_r{}' P_r(t). \tag{2.25}$$

Thus, the calculation of $\mathcal{Q}(t)$ boils down to finding the quantity $\sum_r' P_r(t)$, which is the total probability to find the particle at one of the trap sites, given the initial condition, in the *presence* of the traps.

We proceed by summing over the trap sites of equation (2.22). Doing so gives

$$\sum_s{}' \widetilde{P}_s(\epsilon) = \sum_s{}' \tilde{\eta}_s(\epsilon) - \mathcal{C}\sum_s{}'\sum_r{}' \widetilde{\Psi}_{s,r}(\epsilon)\widetilde{P}_r(\epsilon). \tag{2.26}$$

It is practically impossible to solve equation (2.26) exactly unless the locations of the r and s in the summations are simply related as in a periodic situation [6]. The idea of defining the average, which we refer to as the ν-function method, was first suggested to surmount this problem to generalize the analysis for one trap to an arbitrary concentration of traps by Kenkre in [6]. Its applications are found in a study of sensitized luminescence [7, 8], and have been recently reviewed [12]. We

define the quantity $\nu_r(t)$ by

$$\nu_r(t) = \sum_s{}' \Psi_{s,r}(t), \tag{2.27}$$

which is the probability to find the particle at a specific trap site r given that it was at any one of the trap sites before. While $\nu_r(t)$ depends on r generally, it becomes independent of r in highly symmetrical situations or in an average sense. We now consider the ensemble average of $\nu_r(t)$ and remove the r-dependence [6, 7]. The average quantity, $\nu(t)$, is defined by summing $\nu_r(t)$ over the trap sites and dividing by the total number of traps:

$$\nu(t) = \frac{\sum_r' \sum_s' \Psi_{s,r}(t)}{\sum_r'}. \tag{2.28}$$

Additionally, we define the quantity $\mu(t)$ to be

$$\mu(t) = \sum_s{}' \eta_s(t), \tag{2.29}$$

which is the probability to find the particle at a trap site at time t given the initial condition. With this quantity and the averaging approximation of $\nu(t)$, equation (2.26) is now solved for $\sum_r' \widetilde{P}_r(\epsilon)$ as

$$\sum_r{}' \widetilde{P}_r(\epsilon) = \frac{\tilde{\mu}(\epsilon)}{1 + \mathcal{C}\tilde{\nu}(\epsilon)}. \tag{2.30}$$

Thus we arrive at the expression of the survival probability in the Laplace domain as

$$\widetilde{\mathcal{Q}}(\epsilon) = \frac{1}{\epsilon}\left[1 - \frac{\tilde{\mu}(\epsilon)}{1/\mathcal{C} + \tilde{\nu}(\epsilon)}\right]. \tag{2.31}$$

The key quantities in finding $\mathcal{Q}(\epsilon)$ are then the functions $\mu(t)$ and $\nu(t)$, which are found solely in terms of the *homogeneous* propagator $\Psi_{m,n}(t)$. These are the probability to find the particle at one of the trap sites at time t, given the initial condition ($\mu(t)$), and given that it was at a trap site before ($\nu(t)$).

Chapter 3

Emergence of a Counterintuitive Consequence of Trapping of Tethered Random Walkers

3.1 Introduction

In this chapter, we take a first step towards developing a theory for an infection transmission between a pair of mice by studying the simplest reaction-diffusion scenario: trapping of a single Smoluchowski random walker by a stationary trap. This study of a trapping of a single 'tethered' random walker addresses the effect of the attractive potential on the trapping phenomena, and in turn, provides us with a fundamental understanding of the effect of the home ranges on the infection problem.

In our analysis of the survival probability, we specifically study how it responds to the varied strength of the attractive potential. For a trap placed at the center of the potential, we can predict the effect easily. Because the potential attracts the

walker to its center, placing the trap at the center will be beneficial to its capture, and a stronger potential should make the capture even easier. On the other hand, the effect of the potential is not clear when the trap is placed arbitrarily, and such condition is the main focus of this chapter.

In section 3.2, we present the framework for this trapping problem of a single Smoluchowski walker. The survival probability for this specific problem is defined and the expression of its Laplace transform is given. In section 3.3, the survival probability is analyzed for varying values of the potential strength, for three distinct configurations of the trap and walker's initial location placements. Finally, in section 3.4 the accuracy of the numerical procedures used in this study is discussed in detail, and the summary is given in section 3.5.

3.2 The Equation of Motion and the Survival Probability

Consider a Smoluchowski random walker in 1-dimension. Its position is given by x and the potential center is located at $x = h$, which we set to be the origin without loss of generality, *i.e.*, $h = 0$. Such a walker is tethered to the origin as it performs a random walk. A trap is placed arbitrarily at x_r, and when the walker visits x_r, it captures the walker at a certain rate $\mathcal{C}_1$, where the subscript 1 denotes the 1-dimensional rate. The equation of motion for the probability density $P(x,t)$ of the walker to be found at location x at time t is given by the inhomogenesou Smoluchowski equation

$$\frac{\partial P(x,t)}{\partial t} = \frac{\partial}{\partial x}\gamma x P + D\frac{\partial^2 P}{\partial x^2} - \mathcal{C}_1\delta(x-x')P(x,t), \tag{3.1}$$

where, as in equation (2.7), γ is the strength of attraction to the potential center and D is the diffusion constant. The first two terms on the right hand side represent the

tethering and the random motions, respectively. The last term $-\mathcal{C}_1\delta(x-x')P(x,t)$ describes the capture event by the trap: when the walker visits the trap, $\delta(x-x')P(x,t)$, it gets captured (the negative sign) at a rate $\mathcal{C}_1$. The general homogeneous propagator in n-dimensions is given in equation (2.10), and for this case in 1-dimension with $h=0$, it reduces to

$$\Pi(x,x',t)=\frac{1}{\sqrt{4\pi D\mathcal{T}(t)}}e^{-\frac{\left(x-x'e^{-\gamma t}\right)^2}{4D\mathcal{T}(t)}}, \tag{3.2}$$

where $\mathcal{T}(t)$ is given in equation (2.11). The walker's survival probability, $\mathcal{Q}(t)$ defined in equation (2.23) for a discrete space in the last chapter becomes

$$\mathcal{Q}(t)=\int_{-\infty}^{\infty}dx\ P(x,t) \tag{3.3}$$

for this problem, in a continuous space. Its Laplace transform for this specific problem is given by

$$\widetilde{\mathcal{Q}}(\epsilon)=\frac{1}{\epsilon}\left[1-\frac{\tilde{\mu}(\epsilon)}{1/\mathcal{C}_1+\tilde{\nu}(\epsilon)}\right]. \tag{3.4}$$

The functions $\mu(t)$ and $\nu(t)$ are given by

$$\mu(t)=\int_{-\infty}^{\infty}dx'\Pi(x_r,x',t)P(x',0), \tag{3.5}$$

$$\nu(t)=\Pi(x_r,x_r,t), \tag{3.6}$$

where $P(x',0)$ is the initial condition of the walker. As seen in their definitions, $\mu(t)$ is the probability (density) to find the walker at the trap location given the initial condition at time t, while $\nu(t)$ is the probability density to find the walker at the trap site at time t given that it was there before (the self-propagator at the trap location). We note that, $\nu(t)$ in this problem is an exact quantity because we only have a single trap. Using this result, we next investigate the effect of the attractive potential on the walker's survival probability.

3.3 Counterintuitive Consequence of Trapping of Tethered Random Walkers

The effect of the attractive potential on the survival probability of the walker may not be immediately clear upon mere reflection as follows. Suppose that the walker is initially farther away from the center of the potential compared to the location of the trap. At first, the walker moves towards the trap as it is attracted towards the potential center. This motion is favorable for the capture of the walker because in the process of moving towards the potential center, it also moves toward the trap. However, the tethering motion becomes unfavorable for the capture once the walker moves beyond the location of the trap. In this case, the walker is attracted toward the potential center and away from the trap.

In order to systematically investigate how the tethering motion of the walker affects its survival probability, $\mathcal{Q}(t)$, we consider three distinct placements of the trap and the initial condition of the walker and study the resulting $\mathcal{Q}(t)$ for each case. The trap location denoted by x_r and the initial location of the walker denoted by x_0 are chosen to be separated by an arbitrary distance, L, apart. This distance L is kept fixed. The first of three distinct configurations of x_r and x_0 is their symmetric placement with respect to the potential center location h. We again take $h = 0$ without loss of generality, and the trap and the initial conditions are set to be at $x_r = -L/2$ and $x_0 = L/2$. For this case, the walker moves towards the trap due to the potential until it reaches the origin, and is kept away form the trap once it is there. The other configurations are asymmetric. One of these configurations places the trap at $x_r = 0$ and the initial location at $x_0 = L$. With this configuration, the potential acts to move the walker always towards the trap. This is not true for the converse situation *i.e.*, if the trap at $x_r = L$ and the initial condition at $x_0 = 0$.

All of the three cases require numerical procedures to evaluate the survival probability $\mathcal{Q}(t)$ due to the complex form of the Smoluchowski propagator. In order to obtain the Laplace transform of the survival probability given in equation (3.4), numerical integration of the functions $\mu(t)$ and $\nu(t)$ in equations (3.5) and (3.6) are necessary to calculate the Laplace transforms. Specifically, $\tilde{\mu}(\epsilon)$ is defined by

$$\tilde{\mu}(\epsilon) = \int_0^\infty dt\, \mu(t) e^{-\epsilon t}, \tag{3.7}$$

and similarly done for $\tilde{\nu}(\epsilon)$. These functions are then used to evaluate the Laplace transform of the survival probability, $\widetilde{\mathcal{Q}}(\epsilon)$, via equation (3.4), which is then numerically inverted [46, 47] to arrive at the time domain result, $\mathcal{Q}(t)$.

The localized initial condition of the walker at x_0 yields $\mu(t)$ to be given by

$$\mu(t) = \Pi(x_r, x_0, t), \tag{3.8}$$

while $\nu(t)$ is as given in equation (3.6). The Laplace transform of the survival probability given in equation (3.4) then becomes

$$\widetilde{Q}(\epsilon) = \frac{1}{\epsilon}\left[1 - \frac{\tilde{\Pi}(x_r, x_0, \epsilon)}{1/\mathcal{C}_1 + \tilde{\Pi}(x_r, x_r, \epsilon)}\right]. \tag{3.9}$$

With the numerical procedures described above, we calculate $\mathcal{Q}(t)$ for varying values of γ, for each configuration of x_r and x_0. The result for the symmetric placement of x_r and x_0 is given first.

3.3.1 Symmetric Placement of the Trap and the Initial Walker Location

For clarity, the experimental scheme is shown in Figure 3.1. The initial location denoted by the circle is placed at $x_0 = L/2$ and the trap denoted by the asterisk

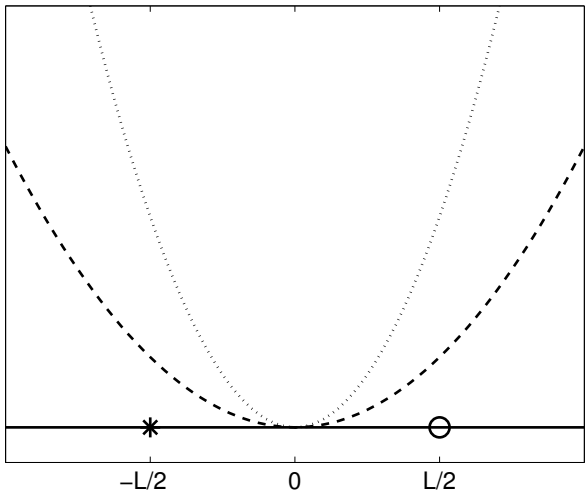

Figure 3.1: Conceptual picture of the attractive potential and the configuration of the trap (asterisk) and the initial location (circle) placements, which are placed symmetrically with respect to the center of the potential that is taken to be the origin. Let the trap and the initial location be separated by the distance L. For this configuration, $\mathcal{Q}(t)$ is computed for the diffusion limit, $L/\sigma = 0$, (solid horizontal line), and finite values of L/σ.

is placed at $x_r = -L/2$, symmetrically with respect to the center of the attractive potential at the origin, distance L apart. The straight solid line on which the trap and the initial location are drawn depicts the diffusion limit where there is no potential ($\gamma \to 0$) and when the walker's motion is described by a pure random walk. The strength of the attraction to the potential center is given by the dimensionless parameter L/σ. The parabolic lines illustrate the attractive potentials that account for the tethering motion of the walker, with the dotted line showing the stronger effect than the dashed one. The survival probability of the walker $\mathcal{Q}(t)$ is calculated for different potential strengths. For this specific placement of x_r and x_0, the Laplace transform of the survival probability via equation (3.9) becomes

$$\widetilde{Q}(\epsilon) = \frac{1}{\epsilon}\left[1 - \frac{\widetilde{\Pi}(-L/2, L/2, \epsilon)}{1/\mathcal{C}_1 + \widetilde{\Pi}(-L/2, -L/2, \epsilon)}\right]. \tag{3.10}$$

The Laplace transforms of $\Pi(-L/2, L/2, t)$ and $\Pi(-L/2, -L/2, t)$ need to be computed numerically by calculating integrals, for instance,

$$\widetilde{\Pi}(-L/2, L/2, \epsilon) = \int_0^\infty dt\, \Pi(-L/2, L/2, t) e^{-\epsilon t}. \tag{3.11}$$

From the expression given in equation (3.10), $\mathcal{Q}(t)$ is calculated numerically as mentioned above.

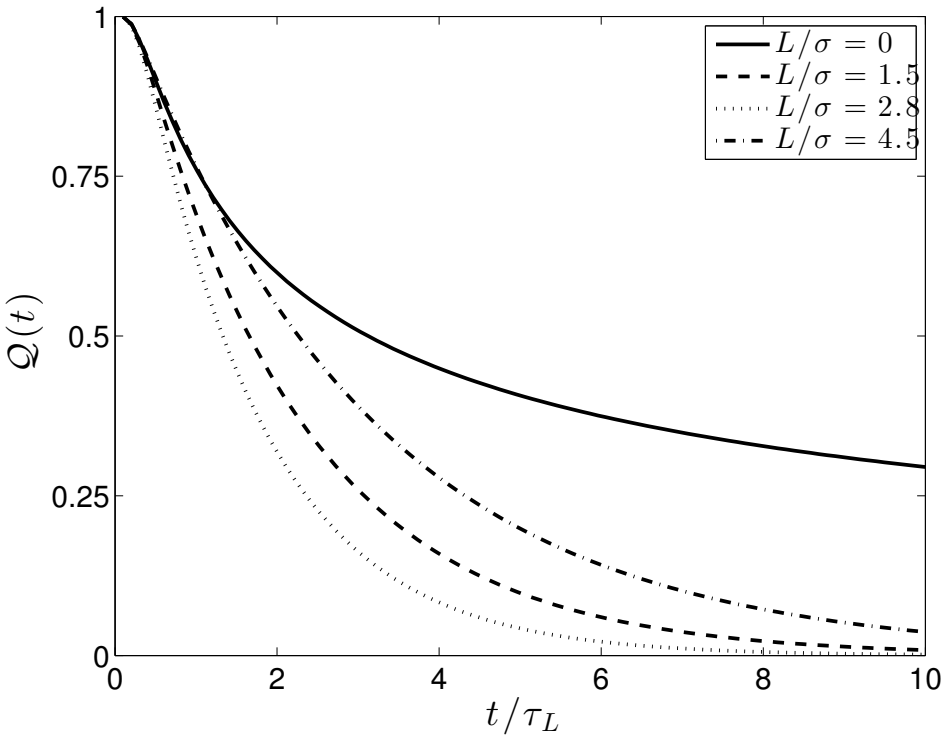

Figure 3.2: Numerically obtained survival probability, $\mathcal{Q}(t)$, plotted against time (scaled to τ_L, the diffusive time for the walker to travel the distance L by a pure random motion), for values of $L/\sigma = 0$, 1.5, 2.8, 4.5. We find that $\mathcal{Q}(t)$ behaves nonnomotonically as the value of L/σ is varied, as seen in panel (b) of Figure 3 of ref. [48].

The result is surprising, as shown in Figure 3.2, where $\mathcal{Q}(t)$ is plotted against the dimensionless time t/τ_L, where $\tau_L = L^2/2D$ is the diffusive time, that is the

time it takes for the walker to traverse the distance L by a pure random walk. Each $\mathcal{Q}(t)$-curve corresponds to a value of the potential strength γ, where the value of γ is cast in terms of the dimensionless parameter $L/\sigma = L/\sqrt{2D/\gamma}$; the smaller value of γ gives the smaller value of L/σ and vice versa. The surprising result in this experiment is the non-monotonic progression of $\mathcal{Q}(t)$-curve as a function of L/σ.

To see this, follow each $\mathcal{Q}(t)$ curve in Figure 3.1 for each increased value of L/σ. The lowest value of L/σ is zero and the corresponding curve is depicted by the solid line (the topmost curve). When the potential is turned on, say for $L/\sigma = 1.5$, the corresponding survival probability decays faster as seen in the dashed line, indicating that the introduction of the potential is beneficial to the capture. The same behavior of $\mathcal{Q}(t)$ is seen for the further strengthened γ as seen in the dotted curve for $L/\sigma = 2.8$ appearing below the dashed curve. However, when γ is made stronger, $L/\sigma = 4.5$, this trend reverses, as depicted in the dash-dotted curve which rises above the previous two (dashed and dotted) curves. This reveals that varying the strength of the attractive potential in a monotonic manner produces a non-monotonic response in the survival probability of the walker. In other words, we have found the existence of an optimal value of the potential strength that yields the maximal efficiency in the capture of the walker for a given placement of the trap and the initial condition.

3.3.2 Origin of the Non-monotonic Effect

The physical origin of the observed non-monotonic behavior of the walker's survival probability $\mathcal{Q}(t)$ as a function of the potential strength γ is understood by analyzing $\mathcal{Q}(t)$ in the capture limited situation where making a steady-state approximation in $\mu(t)$ is sound. We specify what is meant by the capture limit below. Although this

explanation involves approximations, it is instructive and insightful.

The capture limit is the situation in which the capture rate, $\mathcal{C}_1$, is small, such that $1/\mathcal{C}_1$ overwhelms $\tilde{\nu}(\epsilon)$ in its effects in equation (3.4), and where the expression for $\widetilde{\mathcal{Q}}(t)$ can be written as

$$\widetilde{\mathcal{Q}}(\epsilon) \sim \frac{1}{\epsilon}\left[1 - \mathcal{C}_1\tilde{\mu}(\epsilon)\right]. \tag{3.12}$$

The second term in the parentheses has been significantly simplified, where instead of it begin the product of $\tilde{\mu}(\epsilon)$ and $1/\left(1/\mathcal{C}_1 + \tilde{\nu}(t)\right)$, it is now given by $\mathcal{C}_1\tilde{\mu}(\epsilon)$. This simplification affords a straightforward expression in the time domain:

$$\frac{d\mathcal{Q}(t)}{dt} \sim -\mathcal{C}_1\mu(t) = -\mathcal{C}_1\int_{-\infty}^{\infty} dx'\,\Pi(x_r, x', t)P(x', 0). \tag{3.13}$$

The middle expression says that, in the capture limit, the time rate of change of the probability for the walker to survive the trap is essentially the product of $\mu(t)$ and the capture rate $\mathcal{C}_1$. In the right most term, the definition of $\mu(t)$ in terms of the homogeneous propagator $\Pi(x_r, x', t)$ and the initial condition $P(x', 0)$, as given in equation (3.5), is written explicitly. We remind ourselves that $\mu(t)$ is the probability density to find the walker at the trap location x_r at time t in the *absence* of the trapping phenomena. In this experiment, $P(x', 0) = \delta(x' - x_0)$, and therefore $\mu(t)$ is given by

$$\mu(t) = \Pi(x_r, x_0, t) \equiv P(x_r, x_0, 0), \tag{3.14}$$

where the equivalence for the right most term is given to emphasize that $\mu(t)$ in this case is the probability density of finding the walker at the trap site x_r at time t given the localized initial placement at x_0, and *not* the propagator. Substituting this $\mu(t)$ in equation (3.13) gives

$$\frac{d\mathcal{Q}(t)}{dt} \sim -\mathcal{C}_1 P(x_r, x_0, t). \tag{3.15}$$

Therefore, in the limit of small capture rate $\mathcal{C}_1$, the time rate of change of the survival probability simply depends on the product of the capture rate $\mathcal{C}_1$ and the probability density to find the walker at the trap location x_r at time t, given it was initially at x_0.

In the capture limit, it is fair to say that the walker visits the trap site many times before it gets captured in such a manner that that characteristic time it takes for the capture event becomes long compared to the time it takes for the homogeneous solution, *i.e.*, $\mu(t)$, to come to its steady-state. On this premise, we replace $\mu(t) = P(x_r, x_0, t)$ in equation (3.15) with its steady-state expression, which we denote by $P_{ss}(x)$, where the subscript ss stands for the steady-state. For the purpose of the following, we replace x_r by x here. The expression of $P(x, x_0, t)$ is (via equation (3.14)) given by

$$P(x, x_0, t) = \frac{1}{\sqrt{4\pi D\mathcal{T}(t)}} e^{-\frac{\left(x - x_0 e^{-\gamma t}\right)^2}{4D\mathcal{T}(t)}}. \tag{3.16}$$

In the steady-state, the time dependent elements of this solution behave as $\mathcal{T}(t) \to 1/2\gamma$ and $e^{-\gamma t} \to 0$, yielding the steady-state expression,

$$P_{ss}(x) = \frac{1}{\sqrt{\pi}\sigma} e^{-\frac{x^2}{\sigma^2}}. \tag{3.17}$$

Replacing $P(x_r, x_0, t)$ in the right hand side of the equation (3.15) by this $P_{ss}(x)$, $d\mathcal{Q}(t)/dt$ becomes

$$\frac{d\mathcal{Q}(t)}{dt} \sim -\mathcal{C}_1 P_{ss}(x) = -\mathcal{C}_1 \frac{1}{\sqrt{\pi}\sigma} e^{-\frac{x^2}{\sigma^2}}. \tag{3.18}$$

Then, in the capture limit, the walker's survival probability is given by

$$\mathcal{Q}(t) \sim 1 - \mathcal{C}_1 P_{ss}(x) \cdot\ t = 1 - \mathcal{C}_1 \frac{1}{\sqrt{\pi}\sigma} e^{-\frac{x}{\sigma^2}} \cdot\ t, \tag{3.19}$$

where the constant of integration is appropriately chosen to be unity. We demonstrate that the non-monotonic behavior of the survival probability as a function of

the potential strength is explained by the behavior of $P_{ss}(x)$ with respect to the Smoluchowski width σ below.

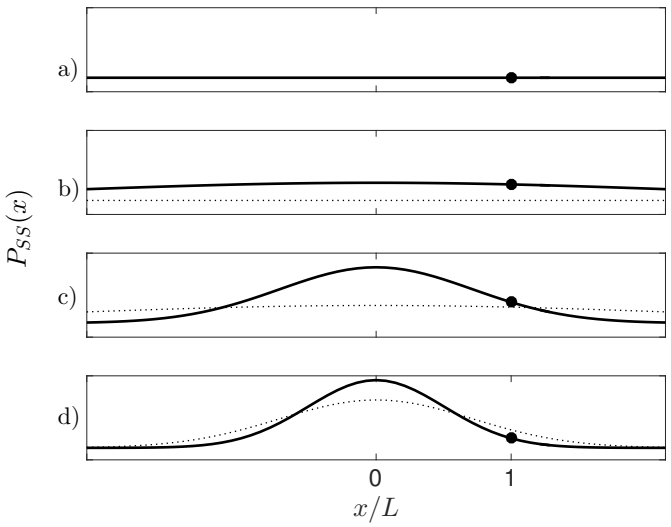

Figure 3.3: Steady-state Smoluchowski distribution plotted against x scaled to L for different values of L/σ, varying from 0, 0.4, 1.4, and 2.0, in panels a)-d), respectively. For b)-d), the dotted line shows the curve in the previous panel drawn to scale for an easy comparison. The spacial dimension x is in an arbitrary unit. The black dot provides an arbitrary reference location.

In Figure 3.3, the spatial profile of $P_{ss}(x)$ is plotted for different values of σ. We observe the value of $P_{ss}(x)$ at a fixed location where a trap would be placed arbitrarily. The profile of $P_{ss}(x)$ is given by the solid line and the arbitrarily chosen location is denoted with a filled circle. Each panel corresponds to a value of σ. From a) to d) the panels are ordered in the increasing value of the nondimensionalized width, L/σ. The actual values taken are, from a) to d), L/σ= 0, 0.4, 1.4, and 2.0, respectively. In b) through d) the dotted lines show $P_{ss}(x)$ shown in the previous panel, each drawn to scale. The diffusion limit case ($\gamma \to 0$) is given in panel a). In this case, σ diverges and hence $P_{ss}(x)$ is zero everywhere, so is the value of $Pss(x)$ at the filled

circle. As the potential is strengthened, $P_{ss}(x)$ becomes finite everywhere in space. Consequently, the value of $P_{ss}(x)$ at the circle increases as shown in panel b). In the next panel, c), γ is increased further yielding a narrower σ and for this particular observation point, the value of $P_{ss}(x)$ increases. However, as shown in the last panel, d), the value at the circle decreases compared to the previous instance because σ has become smaller such that the trap location is well outside of the peak of the Gaussian.

Thus, the value of $P_{ss}(x)$ at a fixed point exhibits non-monotonic behavior as a function of potential strength, and this is responsible for the observed behavior of the survival probability of the walker. We note that the potential center location is excluded from this phenomenon because at the center of the potential, the value of $P_{ss}(0)$ increases monotonically as σ is narrowed.

We now analytically examine equation (3.19). We are interested in the behavior of $\mathcal{Q}(t)$ as a function of σ. From a routine method we learn in calculus, we know that taking the derivative of $\mathcal{Q}(t)$ with respect to σ and setting it to zero tells us about the existence and the condition for its extremum value. Calculating $\partial\mathcal{Q}(t)/\partial\sigma$ and setting it to zero yields the condition

$$x = \sigma. \tag{3.20}$$

Thus $\mathcal{Q}(t)$ takes an extremum value when the condition $x = \sigma$ is met. Additionally, evaluating the second derivative with respect to σ and evaluating it at $x = \sigma$ gives

$$\left.\frac{\partial^2\mathcal{Q}(t)}{\partial\sigma^2}\right|_{x=\sigma} = -\mathcal{C}_1\left.\frac{\partial^2 P_{ss}(x)}{\partial\sigma^2}\right|_{x=\sigma} > 0. \tag{3.21}$$

This result says that the extremum of $\mathcal{Q}(t)$ when $x = \sigma$ is a *minimum*. This is true for all x except for $x = 0$: the potential center location. Hence we show that the survival probability of the walker has a maximum value at $x = \sigma$, yielding the

non-monotonic effect.

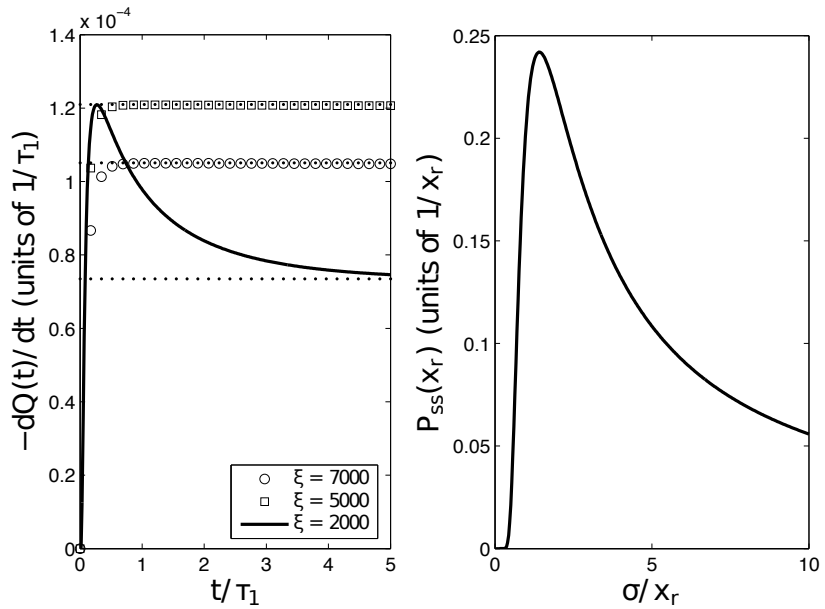

Figure 3.4: Extent of accurary of the small capture rate approximation of the survival probability given by Eq. (3.18), as in Figure 6 of ref. [48]. The left panel shows the numerical (exact) solution for $dQ(t)/dt$ (the decay rate) for three values of $\xi = 2\sqrt{\pi}\gamma\sigma/\mathcal{C}_1$. The approximation is represented by the three asymptotic (constant) values and shows that it is adequate at long times. Thus, the non-monotonic effect emerges in this regime. The right panel shows $P_{ss}(x_r)$ as a function of σ in units of $L/2$. Since, in the approximation, $P_{ss}(x_r)$ is proportional to the decay rate, its peaking behavior is a clear manifestation of the non-monotonic effect.

We have given an explanation for the non-monotonic variation of the walker's survival probability as a function of varied strength of the tethering motion of the walker in the capture limit. To provide validity to this approximation, we have plotted the exact numerical solution of $d\mathcal{Q}(t)/dt$ and its approximate form given in equation (3.18) against t in the right panel of Figure 3.4 for three different values of $\mathcal{C}_1$. The time is scaled to τ_1 and $d\mathcal{Q}(t)/dt$ to $1/\tau_1$. The lines depicted by the circle, square, and the solid line are the exact values found by a numerical procedure,

and three dotted lines are the corresponding values given by the approximation in equation (3.18). The different values of $\mathcal{C}_1$ are reflected in the values of the corresponding dimensionless variable $\xi = 2\sqrt{\pi}\gamma\sigma/\mathcal{C}_1$, where circle, square, and the solid lines correspond to $\xi = 7000$, 5000, and 2000, respectively. A larger value of ξ corresponds to a smaller value of $\mathcal{C}_1$. For each value of ξ, the exact solutions converges to the approximation. As seen in the circle and the square lines, the exact solution reaches its approximate values for smaller $\mathcal{C}_1$ quickly and the agreement is excellent. This provides the validity (and its extent) of the capture limit expression, and the replacement of $\mu(t)$ by $P_{ss}(x)$. On the right panel of the same figure, the steady-state distribution $P_{ss}(x_r)$ at the trap site x_r is plotted against σ, where $P_{ss}(x_r)$ is scaled to $1/x_r$ and σ to x_r, and it shows a non-monotonic variation as a function of σ/x_r as expected.

3.3.3 The Result for the Other Configurations of x_r and x_0

In the analysis of the survival probability $\mathcal{Q}(t)$ obtained for the symmetrical placement of x_r and x_0, we have shown that the non-monotonic behavior of $\mathcal{Q}(t)$ is caused by the behavior of $P_{ss}(x)$ at the trap location with respect to σ. Additionally, it was found that such behavior of $\mathcal{Q}(t)$ will not be present when the trap is placed at the center of the attractive potential. Given this understanding, we can formulate expectations of behavior of $\mathcal{Q}(t)$ under varied potential strength for the other configurations of x_r and x_0.

For $x_r = 0$ and $x_0 = L$, we expect a monotonic variation of $\mathcal{Q}(t)$ as a function of γ. In other words, it is straightforward to understand that when the trap is placed centrally, the frequency for the walker to visit the trap site is positively correlated

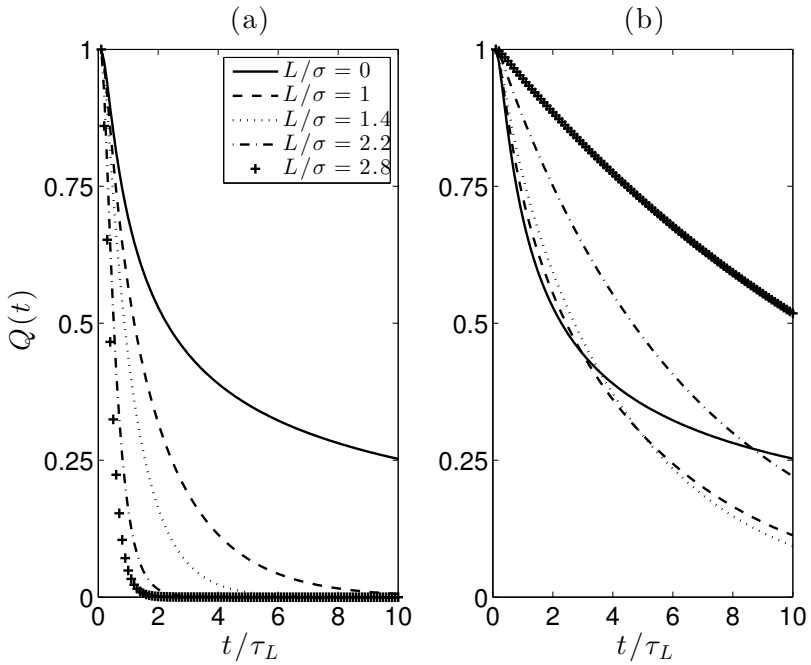

Figure 3.5: The behavior of $\mathcal{Q}(t)$ for different values of γ for asymmetric configurations of x_r and x_0 are plotted against time (scaled to τ_L), as in Figure 4 of ref. [48]. The dimensionless quantity that reflects the value of γ is L/σ, whose values taken here are 0, 1, 1.4, 2.2, 2.8. The left panel presents $\mathcal{Q}(t)$ for the case of central trap placement, $x_r = 0$ and $x_0 = L$, where $\mathcal{Q}(t)$ curves monotonically faster decay for increased values of γ. The right panel shows the result for the configuration $x_r = L$ and $x_0 = 0$, where the non-monotonic behavior of $\mathcal{Q}(t)$ is seen.

with its increased tethering tendency to the potential center. The survival probability for this case is plotted against time, which is scaled to τ_L in the left panel of Figure 3.5, where the progression of $\mathcal{Q}(t)$ as a function of L/σ confirms this point. On the other hand, for the other configuration of the trap location and the initial walker locations, $x_r = L$ and $x_0 = 0$, we should recover the non-monotonic behavior of the survival probability as a function of the potential strength. This point is confirmed in the plot of $\mathcal{Q}(t)$ against time (scaled to τ_L) given in the right panel of the same figure.

We note that, for the centrally placed *perfect* trap, *i.e.*, the trap with an infinite

capture rate, analytic expressions can be obtained. Spendier has shown [48, 49] that $\widetilde{\mathcal{Q}}(\epsilon)$ can be expressed in terms of the Whittaker-W function when the trap is placed centrally. Furthermore, when the trap is perfect, the Laplace transform can be inverted exactly and the survival probability is given by

$$Q(t) = 1 - \left(\frac{\mathrm{e}^{2\gamma t} - 1}{\pi^2 \gamma \tau_1}\right)^{\frac{1}{4}} e^{\frac{-\gamma\tau_1}{e^{2\gamma t}-1}} \; W_{-\frac{1}{4},\frac{1}{4}}\left(\frac{\gamma\tau_1}{e^{2\gamma t}-1}\right). \tag{3.22}$$

The W is the Whittaker W-function, which is defined in Ref. [50] as

$$W_{\kappa,\mu}(z) = e^{-\frac{z}{2}} z^{\frac{1}{2}+\mu} U\left(\frac{1}{2} + \mu - \kappa, 1 + 2\mu, z\right), |\arg\, z| < \pi \tag{3.23}$$

where U is the confluent hypergeometric function,

$$U\,(a, b, c) = \frac{1}{\Gamma(a)} \int_0^\infty e^{-ct} t^{a-1} \,(1+t)^{b-a-1}\, dt. \tag{3.24}$$

This result can be simplified to

$$Q(t) = \mathrm{erf}\left(\frac{x_0/\sigma}{\sqrt{e^{2\gamma t} - 1}}\right), \tag{3.25}$$

and is found in [48].

The evaluation of $\mathcal{Q}(t)$ required numerical methods. We discuss the accuracy and the extent of validity of these methods next.

3.4 Accuracy of the Numerical Methods

In this investigation, two numerical means were used to study the system. As mentioned earlier, one is the numerical integration of $\mu(t)$ and $\nu(t)$ to obtain their Laplace transforms, $\tilde{\mu}(\epsilon)$ and $\tilde{\nu}(\epsilon)$. The other is the numerical inverse transformation of $\widetilde{\mathcal{Q}}(\epsilon)$, equation (3.4), through the algorithm given in [46, 47] to obtain $\mathcal{Q}(t)$. We have also

found the numerical solution of the starting differential equation (equation (3.1)), to find $P(x,t)$, and computation of $\mathcal{Q}(t)$ through equation (3.3). The agreement yielded between the resulting $\mathcal{Q}(t)$ obtained from both methods gave us confidence in the accuracy of the numerical methods. We have investigated also the accuracy and the limitation of the numerical solution of the differential equation. This was done by testing the numerical solution of the homogeneous Smoluchowski equation against the analytic one. The details are presented next.

Numerically solving a differential equation, using such programs as Matlab, (usually) requires discretization of the equation. Therefore, we begin by discretizing the Smoluchowski equation in one dimension (equation (3.1) without the capture term), which yields

$$\frac{dP_m(t)}{dt} = F\left[P_{m+1} + P_{m-1} - 2P_m\right] + f\left[(m+1)P_{m+1} - (m-1)P_{m-1}\right]. \quad (3.26)$$

Here $P_m(t)$ is the probability for the walker to occupy a site m at time t, the nearest-neighbor hopping rate is F, and the rate caused by the attractive potential is f. The center of the potential is at $m = 0$. Let a be the inter-site distance (the lattice constant). Then relations that gives the equation of motion in the the continuum limit are

$$a \to 0, \quad F \to \infty, \quad Fa^2 \to D, \quad f = \gamma/2,$$
$$ma \to x, \quad P_m(t)/a \to P(x,t).$$

Therefore, using these correspondences and by writing $m_0 = x_0/a$, the discrete counterpart of the analytic propagator expression given in equation (3.2) becomes

$$a\Pi(x, x_0, t) = \sqrt{\frac{f/F}{\pi(1 - e^{-4ft})}} e^{-\frac{(m - m_0 e^{-2ft})^2}{(1 - e^{-4ft})}} = \Pi_{m,m_0}(t). \quad (3.27)$$

To investigate the extent of the accuracy of the method, the numerical solution of $\Pi_{m,m_0}(t)$ is compared against this equation above.

We used periodic boundary conditions with a total of 2001 lattice sites, with $f/F = 0.1$ and the initial condition $m_0 = 10$. The result of the comparison is shown in Figures 3.6 and 3.7. The time is scaled to $1/Ft$. Figure 3.6 shows the time-evolution of the probability density at three different locations, and Figure 3.7 shows the spatial distribution of the probability density at three different times. The numerical solution is depicted by circles, while the analytic solution is given by solid lines. We find the agreement to be excellent and thus demonstrate that the numerical procedure is generally satisfactory.

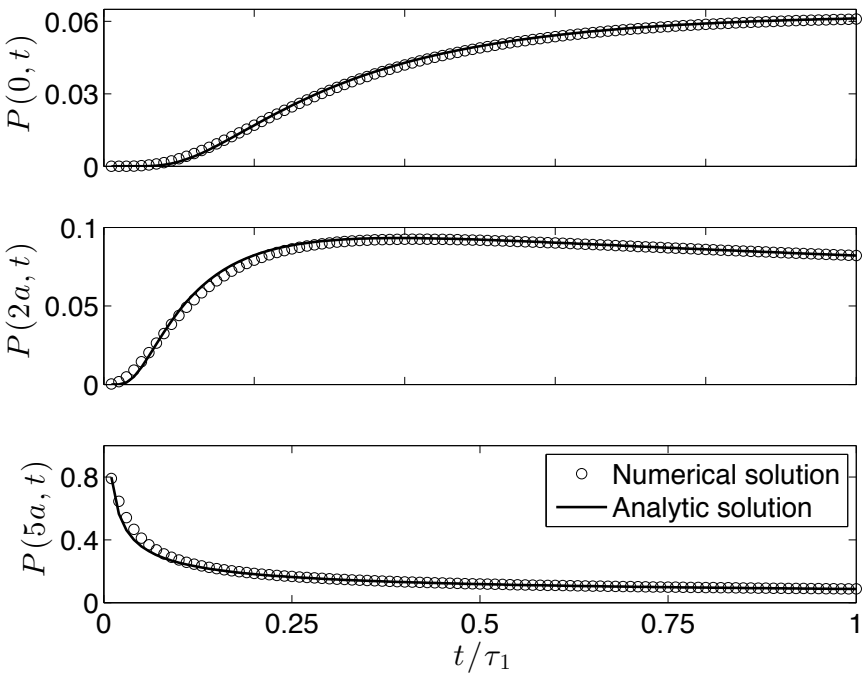

Figure 3.6: The analytic and numerical solutions of the probability density, in their time-evolution, at three arbitrary locations are plotted for comparison, as in Figure 7 of ref. [48]. The three locations are $x = 0$, 2, and 5 in units of the lattice constant a. The initial condition is taken to be $P(x, 0) = \delta(x - 5a)$, the ratio of the potential-to-random hopping rate to be $f/F = 0.01$, and the total number of lattice points to be 2001. Time is scaled to $1/\tau_1$.

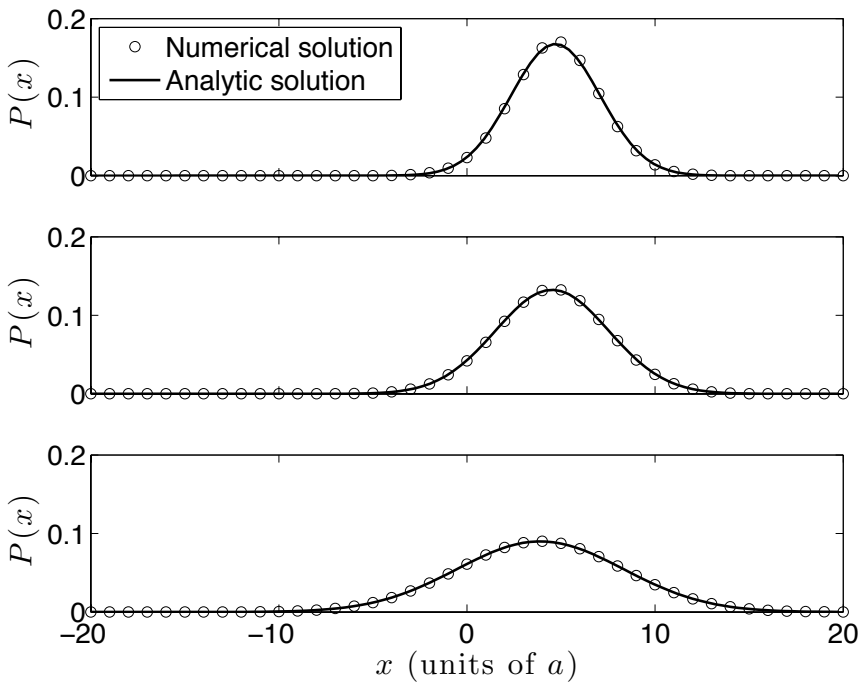

Figure 3.7: The analytic and numerical solutions of the probability density, in their spatial profile, at three different times are plotted for comparison, as in Figure 8 of ref. [48]. An excellent agreement is seen. The specific parameters (the number of lattice points, f/F, and the initial condition) are the same as in Fig. 3.6. The three panels correspond to the value of $t/\tau_1 = 0.24$, 0.40, 1 from top down, respectively.

The accuracy of our numerical procedure depends on the ratio f/F, where the smaller value yields a more accurate result. The square of this quantity is inversely proportional to the equilibrium Smoluchowski width. Therefore, the corresponding length to the Smoluchowski width in the discrete space should not be smaller than

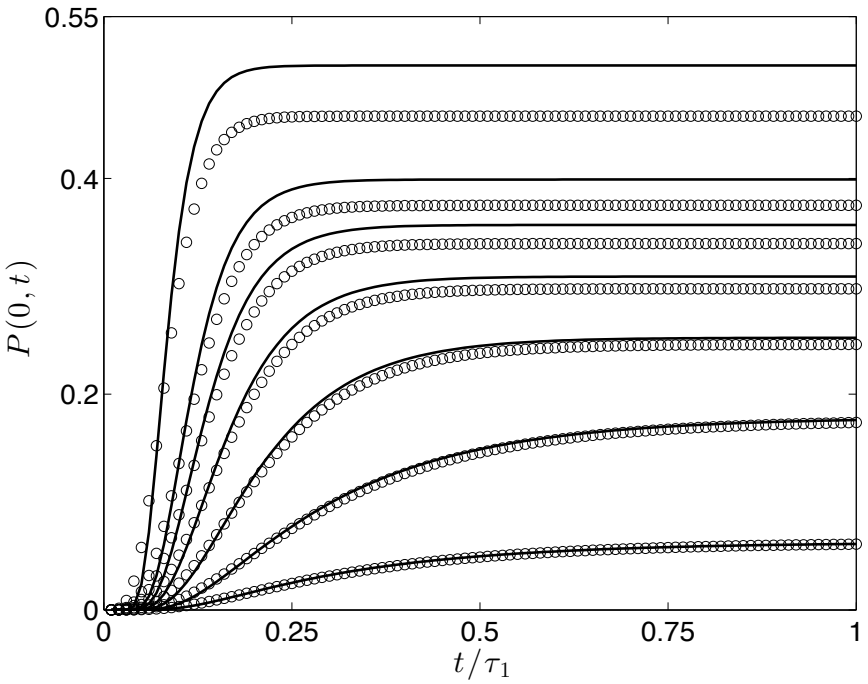

Figure 3.8: The analytic and numerical solutions of the probability density as a function of time, at the origin, is plotted for various values of f/F, as in Figure 9 of ref. [48]. The discretization procedure develops inaccuracy as f/F becomes larger from $0.01, 0.1, 0.2, 0.3, 0.4, 0.5$ to 0.8, from the lowest to the top-most curve, respectively. The progression of f/F corresponds to narrowing Smoluchowski width. As in Figs. 3.6 and 3.7, the numerical and analytic solutions are respectively given by the circles and the solid lines. Other parameters are as in Figs. 3.6 and 3.7. In the top four curses, noticeable departures are observed.

the lattice constant, a, of the discretization, where the numerical method (based on the discretization of the differential equation) begins to yield inaccurate results with the growing value of $a/\sigma = \sqrt{f/F}$. Figure 3.8 demonstrates this limit of accuracy, by presenting the evolution of the probability density at site $m = 0$ for different values of f/F. Our numerical solution starts to show deviation from the analytic solution when f/F exceeds 0.15.

In conclusion, for sufficiently small f/F the discretization of the differential equation is a reasonably accurate procedure (because it reproduces the analytic results well), and that for large f/F, it is best to use the Laplace inversion numerical procedure as the discretization method fails.

3.5 Summary

An analysis for an idealized situation of a *centrally* placed *perfect* trap was available earlier [48, 49]. However it had limited applicability because of the restrictions of perfect capture and central placement. We conducted here a more general case of an arbitrary trap placement with a finite capture rate. For this case, numerical procedures were employed to compute the survival probability of the walker. We found that there is an optimal potential strength for the most efficient capture of the walker per given trap location. This is a non-intuitive result, and is reflected in the non-monotonic behavior of the survival probability as a function of the increased potential strength.

An approximate, but instructive explanation was provided in the motion limit of our problem where the survival probability can be appropriately expressed as a product of the capture rate and the steady-state probability density of the walker in the absence of the trap. This argument finds that the value of the steady-state density at the arbitrarily chosen trap location has a maximum when the value of the steady-state width equals the distance of the trap location from the potential center. This behavior of the steady-state distribution with respect to the steady-state width is reflected on the non-monotonic behavior of the survival probability. The accuracy of the numerical methods used were confirmed and a detailed discussion was given.

Our study of the literature has found no considerable advances in the theory of trapping of a Smoluchowski walker except in two studies [51,52]. In the former of the references, no position dependence is considered in the capture phenomena, and the main emphasis is placed on anomalous diffusion, which is a type of diffusion whose mean square displacement depends non-linearly on time. The latter reference only considers a perfect trap placed at the potential center. Our present investigation addresses the trapping phenomenon more generally. While trapping of a Smoluchowski walker might be of interest in a variety of fields of research [53–56], our focus of the study in this thesis is to use the results for a theory we develop for the spread of epidemics. This, we do in the next chapters in this thesis.

The work presented here has been done in collaboration with Spendier and Kenkre and is published in ref. [48].

Chapter 4

Transmission of Infection in the Spread of Epidemics

4.1 Introduction

In this chapter, we apply the results from the trapping problem to our simple model of infection transmission among a mice population in an epidemic outbreak of a Hantavirus. This model is appropriate in a dilute limit of a population density of mice where only two mice are considered to meet at a time. Such pair-wise model also describes an underlying microscopic processes of an epidemic spread in a larger population. We model the mice as Smoluchowski random walkers where the attractive potential acts to confine the mice to their respective home ranges, and the infection-passing interaction occurs as the two mice meet. Further description of the model is provided in the next section.

Here, we are interested in the infection probability of the susceptible mouse, especially how this quantity is affected by the strength of confinement of the mice to their

home ranges. In addition to the infection probability, we develop a single quantity called the effective infection rate that also characterizes an infection event.

Our model for an infection transmission between two mice in an arbitrary dimension is presented in Section 4.2, where we make clear the equivalence between the infection and the trapping problems. The infection probability is defined and its expression in the Laplace space is given. In Section 4.3, we give an explicit result in 1-dimension and present the non-monotonic effect of the confinement on the infection probability of the susceptible mouse. Additionally, it is shown that an analytic expression is possible for the infection probability in the limit of no confinement. The effective rate of infection is developed in Section 4.4 along with its non-monotonic dependency on the confinement parameter.

4.2 Model for the Two-Walker Infection Problem

Our simple model considers infection transmission between only two mice, one carrying an infectious disease and the other initially being *not* infected but susceptible to infection. The transmission of infection is marked by the event of the susceptible mouse catching the disease from the infected one upon meeting. We consider that the disease is passed on at a certain rate rather than being transmitted one hundred percent of the time whenever the two meet. The analysis of a model consisting of only two mice is appropriate to a dilute population where both of the susceptible and the infected populations are sparse enough that practically only two mice meet at a time. The theory applies to any number of dimensions, say s-dimensions.

Let the location of the infected mouse be denoted by $\boldsymbol{r}_1 = (x_1^1, x_1^2, \ldots, x_1^s)$ and

that of the susceptible mouse by $\boldsymbol{r}_2 = (x_2^1, x_2^2, \ldots, x_2^s)$, where the subscripts 1 and 2 are for the infected and the susceptible mice, respectively. The home-center locations for these mice are denoted respectively by $\boldsymbol{R}_1 = (h_1^1, h_1^2, \ldots, h_1^s)$ and $\boldsymbol{R}_2 = (h_2^1, h_2^2, \ldots, h_2^s)$. We consider that these mice are of the same species such that they share the diffusion constant, D, and the strength of the attraction to their homes, γ, in common. When the mice meet, *i.e.*, $\boldsymbol{R}_1 = \boldsymbol{R}_2$, the infection is passed at a rate $\mathcal{C}$. The transmission of infection can be characterized by the equation of motion for the joint probability density, $P(\boldsymbol{r}_1, \boldsymbol{r}_2, t)$, to find the infected mouse at $\boldsymbol{r}_1$ and the susceptible one at $\boldsymbol{r}_2$ at a given time. The configuration that the first mouse is infected *and* the second is susceptible (not infected) vanishes when the susceptible mouse gets the disease. The equation of motion for $P(\boldsymbol{r}_1, \boldsymbol{r}_2, t)$ is then given by

$$\begin{aligned}\frac{\partial P(\boldsymbol{r}_1, \boldsymbol{r}_2, t)}{\partial t} &= \nabla_1 \cdot \left[\gamma \left(\boldsymbol{r}_1 - \boldsymbol{R}_1\right) P(\boldsymbol{r}_1, \boldsymbol{r}_2, t)\right] + \nabla_2 \cdot \left[\gamma \left(\boldsymbol{r}_2 - \boldsymbol{R}_2\right) P(\boldsymbol{r}_1, \boldsymbol{r}_2, t)\right] \\ &\quad + D\left(\nabla_1^2 + \nabla_2^2\right) P(\boldsymbol{r}_1, \boldsymbol{r}_2, t) - \mathcal{C}\delta(\boldsymbol{r}_1 - \boldsymbol{r}_2) P(\boldsymbol{r}_1, \boldsymbol{r}_2, t). \qquad (4.1)\end{aligned}$$

Here the Smoluchowski motions of the mice are described by the first three terms on the right hand side. The first two terms represent the motion due to the attraction of the mice to their respective homes, with the locations of the potential-centers being the center of their home ranges. The third term stands for their pure random motions. Infection transmission is given by the last term, $-\mathcal{C}\delta(\boldsymbol{r}_1 - \boldsymbol{r}_2)P(\boldsymbol{r}_1, \boldsymbol{r}_2, t)$, where $\delta(\boldsymbol{r}_1 - \boldsymbol{r}_2)P(\boldsymbol{r}_1, \boldsymbol{r}_2, t)$ describes the meeting of the mice and $-\mathcal{C}$ indicates that the infection is passed at the given rate. Note that although $\mathcal{C}$ is referred to as the "rate", its unit depends on the dimensionality of the problem.

This two-walker infection problem is equivalent to a single-walker trapping problem as follows. The method of analyzing the problem of the transmission of infection between two walkers executing an s-dimensional walk by mapping it to a $2s$-dimensional walk of a composite two-walker point is taken from the problem worked out in the 80's by Kenkre [5] concerning the annihilation of a pair of Frenkel excitons.

The annihilation problem is more complex compared to the infection problem in the sense that there, the motions of random walkers can be either quantum mechanical or classical with an arbitrary degree of coherence. On the other hand, our infection problem bears more complexity in that the motion of the walkers are *not* translationally invariant in its homogeneous problem whereas that of the annihilation problem is translationally invariant.

For the ease of description, consider a 1-dimensional infection problem, where the positions of the infected and the susceptible walkers are given by x_1 and x_2, respectively. Instead of putting them both on a 1-dimensional coordinate x, consider representing their position as a point in the position phase-space of the mice, x_1-x_2 space, where a unique positions of the mice is described as a point, (x_1, x_2). By doing this, we have described the two 1-dimensional mice as a single 2-dimensional "quasi-particle". Notice that in this space, the infection event takes place on the infinite line $x_1 = x_2$, which is stationary, and when the quasi-particle is on this line, the configuration that the infected mouse is at x_1 and the susceptible mouse is at x_2 vanishes at a rate $\mathcal{C}$, marking an infection transmission event. But this description of the infection problem is nothing but that of the trapping of the 2-dimensional quasi-particle by the infinite line-trap. In this manner, the infection model in s-dimensions is equivalent to the corresponding trapping problem in $2s$-dimensions. This equivalence between the two problems allows a straight forward solution for the infection problem just as in the Frenkel exciton annihilation problem [5].

We now focus our attention back to the study of infection transmission. In the corresponding homogeneous problem, *i.e.*, when there is no infection term in equation 4.1, the motion of the infected and the susceptible mice are independent of one another. This means that the propagator for the homogeneous problem is the

product of the homogeneous propagators of each mouse:

$$\Pi(\boldsymbol{r}_1, \boldsymbol{r}_1', \boldsymbol{r}_2, \boldsymbol{r}_2', t) = \left(\frac{1}{4\pi D\mathcal{T}(t)}\right)^s \prod_{\beta=1}^{s} e^{-\frac{\left(x_1^\beta - h_1^\beta - (x_1'^\beta - h_1^\beta)e^{-\gamma t}\right)^2 + \left(x_2^\beta - h_2^\beta - (x_2'^\beta - h_2^\beta)e^{-\gamma t}\right)^2}{4D\mathcal{T}(t)}}, \tag{4.2}$$

where the superscript $\beta = 1, 2, \ldots, s$ denotes each spatial dimension, and $\mathcal{T}(t)$ is given in equation (2.11). Then the homogeneous solution, $\eta(\boldsymbol{r}_1, \boldsymbol{r}_2, t)$, to this problem is given by

$$\eta(\boldsymbol{r}_1, \boldsymbol{r}_2, t) = \int_{-\infty}^{\infty}\int_{-\infty}^{\infty} d^s r_1' d^s r_2' \; \Pi(\boldsymbol{r}_1, \boldsymbol{r}_1', \boldsymbol{r}_2, \boldsymbol{r}_2', t) P(\boldsymbol{r}_1', \boldsymbol{r}_2', 0). \tag{4.3}$$

where $P(\boldsymbol{r}_1', \boldsymbol{r}_2', 0)$ is the initial placement of the mice. With this, when the infection term is present, the solution to equation (4.1) is found by the Green function method and is given by

$$P(\boldsymbol{r}_1, \boldsymbol{r}_2, t) = \eta(\boldsymbol{r}_1, \boldsymbol{r}_2, t) - \mathcal{C}\int_0^t dt' \int_{-\infty}^{\infty} d^s r_1' \; \Pi(\boldsymbol{r}_1, \boldsymbol{r}_1', \boldsymbol{r}_2, \boldsymbol{r}_1', t-t') P(\boldsymbol{r}_1', \boldsymbol{r}_1', t'). \tag{4.4}$$

We are interested in the infection probability, *i.e.*, the probability for the susceptible mouse to contract the disease from the infected one at a given time. We denote this quantity by $\mathcal{I}(t)$. The defect technique is again useful in obtaining the expression for $\mathcal{I}(t)$ (in the Laplace domain) for this reaction-diffusion scenario.

4.2.1 Expression for the Infection Probability in the Laplace Domain: Result From the Defect Technique

The infection probability, $\mathcal{I}(t)$ is defined in terms of $\mathcal{Q}(t)$, the 'survival probability' of the configuration that the first mouse is infected and the second is not, and is given by

$$\mathcal{I}(t) = 1 - \mathcal{Q}(t) = 1 - \int_{-\infty}^{\infty} d^s r_1 \int_{-\infty}^{\infty} d^s r_2 \, P(\boldsymbol{r}_1, \boldsymbol{r}_2, t), \tag{4.5}$$

where $\mathcal{Q}(t)$ starts at unity and decays to zero as the susceptible mouse gets infected. Therefore, $\mathcal{I}(t)$ starts out at zero initially and grows to unity in time. Substituting equation (4.4) for $P(\boldsymbol{r}_1, \boldsymbol{r}_2, t)$ in this equation yields

$$\mathcal{I}(t) = \mathcal{C} \int_0^t dt' \int_{-\infty}^{\infty} d^s r_1 \int_{-\infty}^{\infty} d^s r_2 \int_{-\infty}^{\infty} d^s r_1' \; \Pi(\boldsymbol{r}_1, \boldsymbol{r}_1', \boldsymbol{r}_2, \boldsymbol{r}_1', t-t') P(\boldsymbol{r}_1', \boldsymbol{r}_1', t'). \quad (4.6)$$

To proceed, we Laplace transform equation (4.6), which gives

$$\widetilde{\mathcal{I}}(\epsilon) = \mathcal{C} \int_{-\infty}^{\infty} d^s r_1' \, \widetilde{P}(\boldsymbol{r}_1', \boldsymbol{r}_1', \epsilon) \int_{-\infty}^{\infty} d^s r_1 \int_{-\infty}^{\infty} d^s r_2 \, \widetilde{\Pi}(\boldsymbol{r}_1, \boldsymbol{r}_1', \boldsymbol{r}_2, \boldsymbol{r}_1', \epsilon), \quad (4.7)$$

where each integral is assumed to act on all of the terms on its right. The spatial integral over $\boldsymbol{r}_1$ and $\boldsymbol{r}_2$ of the propagator becomes $1/\epsilon$, and hence, our task is to find the spatial integral over $\widetilde{P}(\boldsymbol{r}_1', \boldsymbol{r}_1', \epsilon)$. The defect technique is applied to equation (4.4) to obtain this term, $\int d^s r_1' \widetilde{P}(\boldsymbol{r}_1', \boldsymbol{r}_1', \epsilon)$, which is the probability to find the mice together at a given time in the Laplace space. The Laplace transform of equation (4.4) is

$$\widetilde{P}(\boldsymbol{r}_1, \boldsymbol{r}_2, \epsilon) = \tilde{\eta}(\boldsymbol{r}_1, \boldsymbol{r}_2, \epsilon) - \mathcal{C} \int_{-\infty}^{\infty} d^s r_1' \; \widetilde{\Pi}(\boldsymbol{r}_1, \boldsymbol{r}_1', \boldsymbol{r}_2, \boldsymbol{r}_1', \epsilon) \widetilde{P}(\boldsymbol{r}_1', \boldsymbol{r}_1', \epsilon). \quad (4.8)$$

The defect technique here specifically means to let $\boldsymbol{r}_2 = \boldsymbol{r}_1$ in this equation and integrating $\boldsymbol{r}_1$ over all space, *i.e.*,

$$\int_{-\infty}^{\infty} d^s r_1 \tilde{P}(\boldsymbol{r}_1, \boldsymbol{r}_1, \epsilon) = \int_{-\infty}^{\infty} d^s r_1 \tilde{\eta}(\boldsymbol{r}_1, \boldsymbol{r}_1, \epsilon) - \mathcal{C} \int_{-\infty}^{\infty} d^s r_1' \; \tilde{P}(\boldsymbol{r}_1', \boldsymbol{r}_1', \epsilon) \int_{-\infty}^{\infty} d^s r_1 \widetilde{\Pi}(\boldsymbol{r}_1, \boldsymbol{r}_1', \boldsymbol{r}_1, \boldsymbol{r}_1', \epsilon). \quad (4.9)$$

As was done in Chapters 2 and 3, we define the functions $\mu(t)$ and $\nu(t)$ by

$$\mu(t) = \int_{-\infty}^{\infty} d^s r_1 \eta(\boldsymbol{r}_1, \boldsymbol{r}_1, t), \quad (4.10)$$

$$\nu(t) = \int_{-\infty}^{\infty} d^s r_1 \Pi(\boldsymbol{r}_1, \boldsymbol{r}_1', \boldsymbol{r}_1, \boldsymbol{r}_1', t), \quad (4.11)$$

where for this specific problem the resulting quantity of the integral $\int_{-\infty}^{\infty} d^s r_1 \Pi(\boldsymbol{r}_1, \boldsymbol{r}_1', \boldsymbol{r}_1, \boldsymbol{r}_1', t)$ in the equation for $\nu(t)$ happens to be independent of $\boldsymbol{r}_1'$. It should be noted that the

precise physical meaning of $\mu(t)$ and $\nu(t)$ in this chapter differs from that in Chapter 3 (where the trapping problem was analyzed) but both chapters follow the same lines as set out in Chapter 2. With these definitions of $\mu(t)$ and $\nu(t)$, equation (4.9) can be solved for $\int_{-\infty}^{\infty} d^s r_1' \tilde{P}(\boldsymbol{r}_1', \boldsymbol{r}_1', \epsilon)$ and yields

$$\int_{-\infty}^{\infty} d^s r_1' \tilde{P}(\boldsymbol{r}_1', \boldsymbol{r}_1', \epsilon) = \frac{\tilde{\mu}(\epsilon)}{1 + \mathcal{C}\tilde{\nu}(\epsilon)}. \tag{4.12}$$

Applying this result in equation (4.7), the infection probability in the Laplace domain is given exactly by

$$\tilde{\mathcal{I}}(\epsilon) = \frac{1}{\epsilon}\left[\frac{\tilde{\mu}(\epsilon)}{(1/\mathcal{C}) + \tilde{\nu}(\epsilon)}\right]. \tag{4.13}$$

In our study, we consider delta-function initial conditions for the mice, $P(\boldsymbol{r}_1', \boldsymbol{r}_2' 0) = \delta^s(\boldsymbol{r}_1' - \boldsymbol{r}_1^0)\delta^s(\boldsymbol{r}_2' - \boldsymbol{r}_2^0)$, where $\boldsymbol{r}_1^0$ and $\boldsymbol{r}_2^0$ are the initial locations of the infected and susceptible mice, respectively. The specific expressions of $\mu(t)$ for this case, and $\nu(t)$ are then given by

$$\mu(t) = \left(\frac{1}{\sqrt{8\pi D\mathcal{T}(t)}}\right)^s \prod_{\beta=1}^{s} e^{-\frac{\left(h_1^\beta - h_2^\beta + \left(\left(x_1^{0\beta} - h_1^\beta\right) - \left(x_2^{0\beta} - h_2^\beta\right)\right)e^{-\gamma t}\right)^2}{8D\mathcal{T}(t)}}, \tag{4.14}$$

$$\nu(t) = \left(\frac{1}{\sqrt{8\pi D\mathcal{T}(t)}}\right)^s \prod_{\beta=1}^{s} e^{-\frac{\left(1-e^{-\gamma t}\right)^2\left(h_1^\beta - h_2^\beta\right)^2}{8D\mathcal{T}(t)}}. \tag{4.15}$$

Using these results, we investigate the effect of the confinement of the mice to their respective home ranges on the infection probability, $\mathcal{I}(t)$. As was done in Chapter 3, numerical methods are employed to evaluate $\mathcal{I}(t)$ from its Laplace transform given in equation (4.13).

4.3 Infection Probability Curve and its Non-monotonic Dependence: A Study in 1-Dimension

The functions $\mu(t)$ and $\nu(t)$ in equations (4.14) and (4.15) take the form

$$\mu(t) = \frac{1}{\sqrt{8\pi D\mathcal{T}(t)}} e^{-\frac{H^2}{8D\mathcal{T}(t)}}, \tag{4.16}$$

$$\nu(t) = \frac{1}{\sqrt{8\pi D\mathcal{T}(t)}} e^{-\frac{H^2}{8D\mathcal{T}(t)}\left(1-e^{-\gamma t}\right)^2}, \tag{4.17}$$

in 1-dimension. Here, $H \equiv h_1 - h_2$ is the inter-home distance of the mice, and the mice are initialized at their respective home-centers. We let the positions of the infected and susceptible mice be denoted by $x_1^1 \equiv x_1$ and $x_2^2 \equiv x_2$, and their home centers by $h_1^1 \equiv h_1$ and $h_2^1 \equiv h_2$, respectively. Using these $\mu(t)$ and $\nu(t)$, $\mathcal{I}(t)$ is found from two numerical procedures. First, the Laplace transform of $\mathcal{I}(t)$ is calculated via equation (4.13), using the numerically evaluated Laplace transforms of $\mu(t)$ and $\nu(t)$. Then numerical Laplace inverse is performed to obtain $\mathcal{I}(t)$.

The result is shown in figure 4.1, where $\mathcal{I}(t)$ is plotted against time. Each $\mathcal{I}(t)$ curve corresponds to a different value of the confinement strength γ whose corresponding dimensionless parameter is given by $\sqrt{\gamma\tau_H} = H/\sigma$. The 1-dimensional infection rate (which has the dimensions of velocity) is taken to be $\mathcal{C}_1 = 0.3$ in units of $2D/H$. The time is scaled to $\tau_H = H^2/2D$, the diffusive time to travel the distance between the two homes H. We follow the $\mathcal{I}(t)$-curve in the order of increasing $\sqrt{\gamma\tau_H} = H/\sigma$. The thick solid line corresponds to $\sqrt{\gamma\tau_H} = 0$, and is the infection probability in the diffusive limit, *i.e.*, when $\gamma \to 0$. As the attraction of the mice to their respective homes is introduced and made stronger gradually, the infection curve grows faster as seen in the thin-solid curve with $\sqrt{\gamma\tau_H} = 0.6$ and the dotted curve with $\sqrt{\gamma\tau_H} = 1.0$. Upward arrows are drawn to indicate the increased infection rates. However, when $\sqrt{\gamma\tau_H}$ is increased further to 1.64, the infection occurs slower,

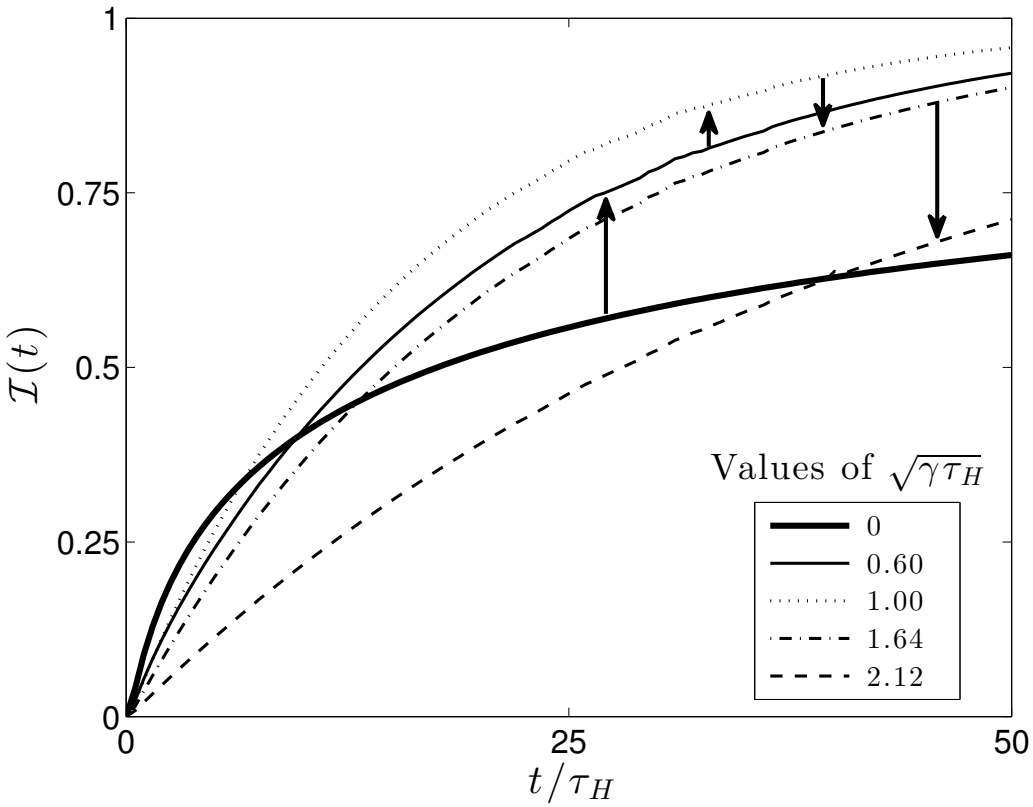

Figure 4.1: Non-monotonic variation is seen in the infection curve $\mathcal{I}(t)$ with the change in the value of γ, the strength of the confinement of the mice to their home ranges, as in Figure 1 of ref. [57]. Time is given in the units of τ_H. The infection rate $\mathcal{C}_1$ is scaled to $2D/H$ and equals 0.3. Small values of γ makes the infection-transmission to take place more efficiently. However, this trend is reversed for larger values of γ. The corresponding unit-less parameter to γ is given by H/σ, the ratio of the inter-home distance to the steady-state Smoluchowski width, and the values are shown in the legend.

as indicated by the reversal of the arrow pointing to the dash-dotted curve, and a further decline is seen for the higher value of $\sqrt{\gamma\tau_H}$ at 2.12 in the dashed curve. It is thus that we see the explicit emergence of the non-monotonic effect of confinement.

4.3.1 Analysis of the Result

In Chapter 3, the survival probability of the Smoluchowski walker to survive the trap was analyzed in the limit of small capture rate, and revealed that the observed non-monotonicity was due to the behavior of the probability density to find the walker at the trap site. Because the infection transmission problem studied here is equivalent to a trapping problem in 2-dimensions, the non-monotonic behavior of the infection probability has the same origin as the trapping problem. Without repeating the detail of the analysis, we present the essence of the non-monotonic behavior specific to this problem.

We refer to the limit of small infection rate, $\mathcal{C}_1$, such that the effect of $\mathcal{C}_1$ overwhelms that of $\tilde{\nu}(\epsilon)$ in equation (4.13), as the *contact* limit. In this limit, the time scale for an occurrence of an infection transmission event becomes much longer than that of the motion of the mice to reach its steady-state in the absence of infection. For such a case the time rate of change of the infection probability can be given approximately as the product of $\mathcal{C}_1$ and the homogeneous solution, $\mu(t)$, to find the mice together:

$$\frac{d\mathcal{I}(t)}{dt} \sim \mathcal{C}_1 \mu(t). \tag{4.18}$$

It is appropriate to replace to replace $\mu(t)$ by its steady-state form, in μ_{ss}, in this case, which is given by

$$\mu_{ss} = \frac{1}{\sqrt{2\pi}\sigma} e^{-\frac{H^2}{2\sigma^2}}. \tag{4.19}$$

Then $\mathcal{I}(t)$ in the contact limit becomes

$$\mathcal{I}(t) \sim \left(\frac{\mathcal{C}_1}{\sqrt{2\pi}\sigma} e^{-\frac{H^2}{2\sigma^2}} \right) \cdot t. \tag{4.20}$$

The non-monotonic effect in $\mathcal{I}(t)$ is now clearly found in the Gaussian function on the right hand side, *i.e.*, μ_{ss}. In Figure 4.2, we plot μ_{ss} with respect to the ratio

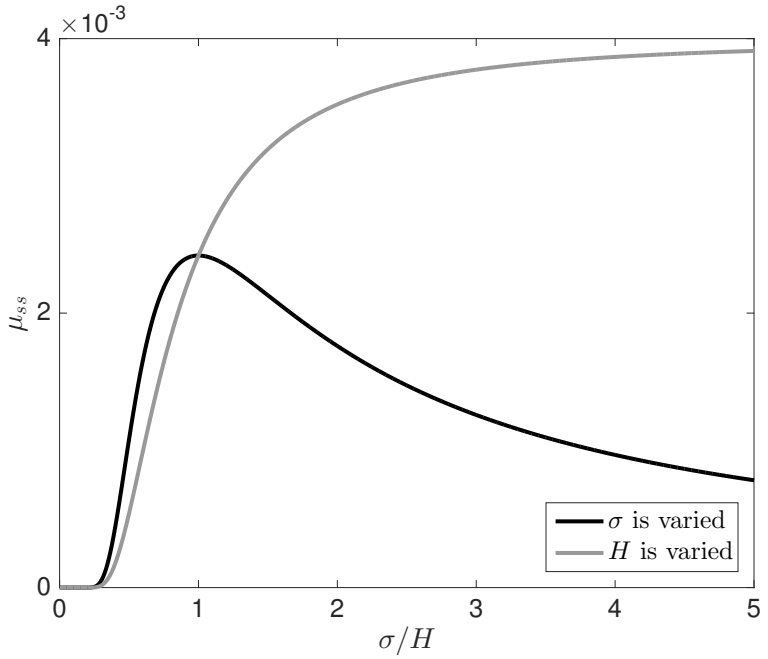

Figure 4.2: The steady-state of the probability to find the mice at a same location, μ_{ss}, as given in equation (4.19), plotted as a function of the non-dimensionalised Smoluchowski width, σ/H. The infection rate was held fixed at $\mathcal{C}_1 = 0.005$ in the units of $2D/H$. The black curve shows μ_{ss} as σ is varied whereas in the gray curve, H is varied.

of the important length scales of the system: σ/H. In producing this plot, we have re-expressed μ_{ss} as

$$\mu_{ss} = \frac{1}{H\sqrt{2\pi}z} e^{-\frac{1}{z^2}}, \tag{4.21}$$

where $z = \sigma/H$. The black curve shows μ_{ss} as σ is varied, where the non-monotonic behavior is pronounced by its peak at $\sigma/H = 1$. The gray curve on the other hand, shows μ_{ss} as H is varied, and its value only increases with increased value of σ/H, *i.e.*, decreasing value of H. This rise of the curve for smaller H indicates that infection transmission is encouraged by decreasing the inter-home distance, and there is *no* non-monotonic effect of the inter-home distance. This makes sense as bringing the mice' homes together only increases the chances of them finding each other, and

hence the chance of the transmission of infection. In addition, the analysis of the first and second derivatives of equation (4.20) confirms these results and explicitly gives $H = \sigma$ as the condition for maximal infection in this contact limit.

We close our analysis by examination of the function $\mu(t)$, whose most general definition for the infection problem is given in equation (4.10). Here, $\mu(t)$ is given by the spatial integral of the homogeneous solution, $\eta(\boldsymbol{r}_1, \boldsymbol{r}_1, t)$, to find the mice together at a given time, given the initial condition of the mice, in the *absence* of infection transmission interaction between the mice. When there is *no* occurrence of infection, $\eta(\boldsymbol{r}_1, \boldsymbol{r}_2, t)$ is given by the joint probability density of the animals, $P(\boldsymbol{r}_1, \boldsymbol{r}_2, t)$, which is the product of the homogeneous densities of each mouse: $P(\boldsymbol{r}_1, \boldsymbol{r}_2, t) = P(\boldsymbol{r}_1, t)P(\boldsymbol{r}_2, t)$. Hence, $\mu(t)$ is the amount of *overlap* between the probability densities of the mice, and this is the underlying quantity that behaves non-monotonically as a function of σ, and is manifested in μ_{ss} as shown above.

To demonstrate that the overlap of the probability density of the infected and susceptible mice shows a non-monotonic behavior we have made a plot of the steady-state joint probability density, $P_{ss}(x_1, x_2)$ along with the steady-state densities of each infected and susceptible mouse, $P_{ss}(x_1)$, $P_{ss}(x_2)$, respectively, for different value of the Smoluchowski width, σ. Figure 4.3 shows $P_{ss}(x_1)$ and $P_{ss}(x_2)$ in the left column, where the black and the gray curves respectively represent $P_{ss}(x_1)$ and $P_{ss}(x_2)$. In the right column, corresponding $P_{ss}(x_1, x_2)$ to the plot of $P_{ss}(x_1)$ and $P_{ss}(x_2)$ to its left is given in the solid curve. The dashed curves seen in the second to fourth rows are the $P_{ss}(x_1, x_2)$ curves given in the plot one above for comparison, and are drawn to scale. In both columns, h_1 and h_2 mark respective home centers. Each row in the figure corresponds to a value of H/σ that characterizes the extent of confinement of the mice to their home ranges. In the first row, $H/\sigma = 0.5$ is taken, and when

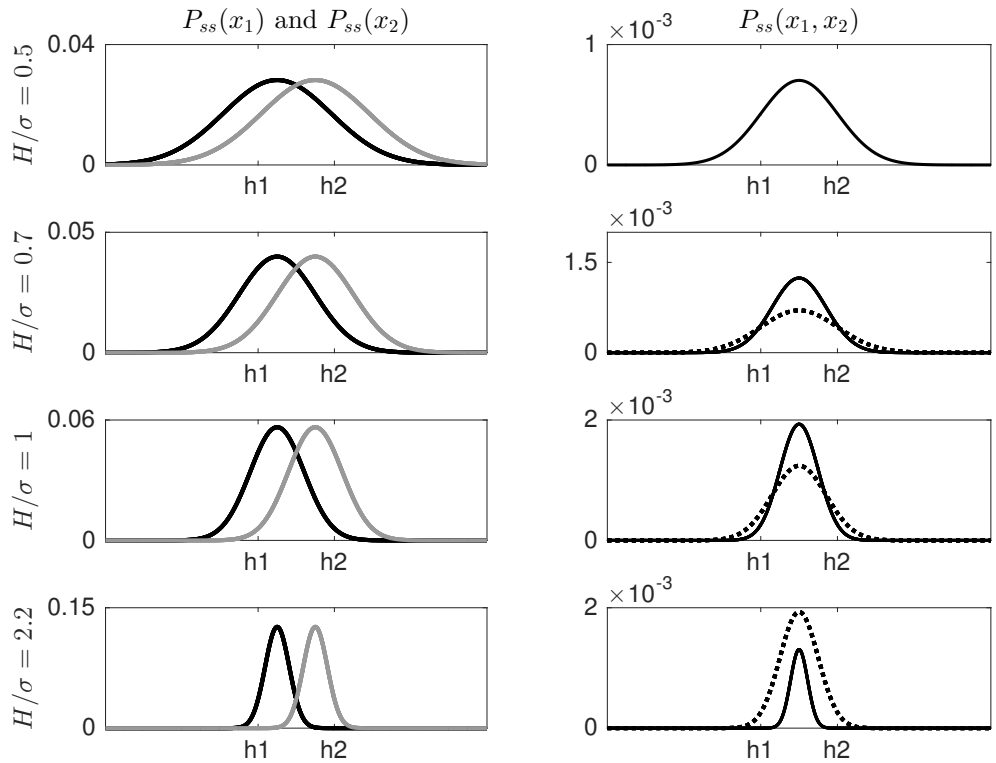

Figure 4.3: The steady-state densities of infected and susceptible mice, $P_{ss}(x_1)$ and $P_{ss}(x_2)$, respectively, and corresponding joint probability density, $P_{ss}(x_1, x_2)$ plotted for four different values of H/σ. On the left column, $P_{ss}(x_1)$ is depicted in the black curve and $P_{ss}(x_2)$ is given in the gray curve. On the right column, corresponding $P_{ss}(x_1, x_2)$ is plotted in the black curve. The dashed curve is the $P_{ss}(x_1, x_2)$ in the previous panel and is drawn to scale. In both columns, h_1 and h_2 mark respective home centers. Each row corresponds to a value of H/σ whose value is indicated on its left. The non-monotonic behavior of $P_{ss}(x_1, x_2)$ is shown as a function of increased H/σ.

the value is increased to 0.7 and to 1 as seen in the second and third rows, the joint probability density increases. However, a further increase to $H/\sigma = 2.2$, where the mice are more tightly confined to their homes, the joint density decreases, marking an instance of the non-monotonic behavior. Before we close this section, we present

an analytic expression of $\mathcal{I}(t)$ in the diffusion limit.

4.3.2 Analytic Expressions in the Diffusion Limit

We present here the infection probability in the diffusion limit, where analytic expressions are possible. In the limit $\gamma \to 0$, the expressions of $\mu(t)$ and $\nu(t)$ become simple. They are obtained from the propagator for the homogeneous diffusion equation, which can be found in a standard Statistical Mechanics textbook, ex., [58], and is given by

$$\Pi(x_1, x_1', x_2, x_2', t) = \frac{1}{\sqrt{8\pi Dt}} e^{-\frac{(x_1 - x_1')^2 + (x_2 - x_2')^2}{8Dt}}. \tag{4.22}$$

Using this propagator in equations (4.10) and (4.11), assuming that both mice start at their respective home center, $\mu(t)$ and $\nu(t)$ in the diffusion limit are

$$\nu(t) = \frac{1}{\sqrt{8\pi Dt}}, \tag{4.23}$$

$$\mu(t) = \frac{1}{\sqrt{8\pi Dt}} e^{-\frac{H^2}{8Dt}}. \tag{4.24}$$

Their Laplace transforms are known and found in a table of Laplace transforms [59]. Using such $\tilde{\mu}(\epsilon)$ and $\tilde{\nu}(\epsilon)$, the infection probability given via equation (4.13) is

$$\widetilde{I}(\epsilon) = \frac{1}{\epsilon} \left(\frac{e^{-\sqrt{\epsilon \tau_H}}}{1 + \sqrt{\epsilon \theta}} \right), \tag{4.25}$$

where $\theta = 8D/(\pi \mathcal{C}_1^2)$ is the new parameter for time, which incorporates the diffusion constant and the capture rate. The inverse transformation is also found in a table [59] and the analytic result in the time domain is

$$I(t) = \operatorname{erfc}\left(\sqrt{\frac{\tau_H}{4t}} \right) - e^{\left(\sqrt{\frac{\tau_H}{4t}} + \frac{t}{\theta} \right)} \operatorname{erfc}\left(\sqrt{\frac{\tau_H}{4t}} + \sqrt{\frac{t}{\theta}} \right), \tag{4.26}$$

where $\operatorname{erfc}(x)$ is the complementary error function. Although we have not found a previous discovery of this result in the literature pertaining to epidemics, the

expression has been reported in a wide range of reaction-diffusion contexts by several authors independently [11, 60, 60, 61]. In the case of instant infection, *i.e.*, when the infection is transmitted to the susceptible mouse one-hundred percent of the time when it meets the infected one (for such a case the value of $\mathcal{C}_1$ is infinite and $\theta \to 0$), the infection probability reduces to a complementary error function of argument $\sqrt{\tau_H/4t}$, *i.e.*,

$$\mathcal{I}(t) = \text{erfc}\left(\sqrt{\frac{\tau_H}{4t}}\right). \tag{4.27}$$

The infection curve given by equation (4.26) is plotted in the solid line ($\gamma = 0$) in figure 4.1.

4.4 Effective Rate of Infection and Extension to Dense Systems

Here we define a single parameter characterizing an infection curve that reflects the effect of important parameters in our problem: the confinement strength γ, the diffusion constant D, and the infection rate $\mathcal{C}$. We define the quantity as the effective rate of infection and denote by α.

In extracting the effective rate from our pair-mouse model, we notice that the shape of the infection curve is similar to the exponentially increasing function of the form

$$\mathcal{I}(t) \sim 1 - e^{-\alpha t}, \tag{4.28}$$

where α would be the effective infection rate. We ask the question: If $\mathcal{I}(t)$ were the exponential curve as given in this equation, what would be the decay constant α that

approximates the actual curve? We develop the following and obtain α in terms of relevant quantities of our problem: $\mu(t)$, $\nu(t)$, and $\mathcal{C}_1$. The development of such a quantity is inspired by the study of sensitized luminescence in molecular crystals as given in [62], in a quite different physical context.

If the infection probability were the suggested exponential function, then its Laplace transform is given by

$$\tilde{\mathcal{I}}(\epsilon) = \frac{\alpha}{\epsilon(\epsilon+\alpha)}. \tag{4.29}$$

We equate this equation with the definition of $\mathcal{I}(\epsilon)$ given in equation (4.13) and solve for α. Doing so gives the definition of an ϵ-dependent quantity, $\tilde{\alpha}(\epsilon)$,

$$\tilde{\alpha}(\epsilon) = \frac{\epsilon\tilde{\mu}(\epsilon)}{(1/\mathcal{C}) + \tilde{\nu}(\epsilon) - \tilde{\mu}(\epsilon)}. \tag{4.30}$$

In order to extract a *constant* effective infection rate from this $\tilde{\alpha}(\epsilon)$, we consider the Markoffian limit of this quantity, i.e., taking the limit $\epsilon \to 0$. It can be seen that taking this limit is the same as calculating the accumulative effect of $\alpha(t)$ over time:

$$\lim_{\epsilon\to 0}\tilde{\alpha}(\epsilon) = \lim_{\epsilon\to 0}\int_0^\infty dt\, e^{-\epsilon t}\alpha(t) = \int_0^\infty dt\, \alpha(t). \tag{4.31}$$

In this spirit, α is similar to the Fermi golden rule rate in describing transitions in quantum systems, although the prescription differs. The effective rate is then defined as

$$\alpha \equiv \lim_{\epsilon\to 0}\tilde{\alpha}(\epsilon) = \frac{\mu(\infty)}{(1/\mathcal{C}) + (1/\mathcal{M})}. \tag{4.32}$$

where an Abelian theorem, $\lim \epsilon \to 0\ \{\epsilon\tilde{\mu}(\epsilon)\} = \mu(t=\infty)$, has been used to obtain $\mu(\infty)$ in the numerator, and $\mathcal{M}$ is defined as

$$\frac{1}{\mathcal{M}} \equiv \int_0^\infty dt\, [\nu(t) - \mu(t)]\,. \tag{4.33}$$

4.4.1 The Contact and Motion Limits

We now discuss each quantity that constitutes α. The most straightforward one is $\mu(\infty) = \mu_{ss}$ given in equation (4.19). The unit of $\mu(\infty)$ is given by $[length]$. The length is that associated with pure random motion of the animals. The quantity we have been referring to as the infection rate, $\mathcal{C}_1$, as mentioned in passing, actually has a dimension of velocity, $[length/time]$, which can be seen by performing a dimensional analysis on the starting equation, equation (4.1). Wherever $\mathcal{C}_1$ appears in the equations, it always comes with the multiplication with the probability-density type quantity which has the unit of $[1/length]$, giving the product the unit of $[1/time]$, and in this manner, $\mathcal{C}_1$ is the rate of infection. The last quantity, $\mathcal{M}$ has the same unit as $\mathcal{C}_1$, *i.e.*, $[length/time]$. This can be seen from its definition given in equation (4.33). The integral over time gives the unit of time, and the integrand gives the reciprocal of length. Its definition also gives its physical meaning: it is the 'velocity' for the probability of the mice to meet at the same location, $P(x_1, x_1, t)$, to reach its steady-state in an absence of infection. Because the meetings of the mice are property of their motion, we call $\mathcal{M}$ the motion parameter. The product of $\mu(\infty)$ and the reciprocal of the additive sum of $1/\mathcal{C}_1$ and $1/\mathcal{M}$ gives the infection rate α, with the unit $[1/time]$.

Thus, α gives a combined effect of the two important time scales to our problem. One scale is of infection, $1/\mathcal{C}_1$, and the other of the mice' meeting probability to reach its steady-state, $1/\mathcal{M}$. The two important limits to consider are the limits $1/\mathcal{C}_1 \ll 1/\mathcal{M}$ and $1/\mathcal{C}_1 \gg 1/\mathcal{M}$. The latter is called the motion limit where the time scale for an occurrence of infection is much smaller than that associated with the meeting probability of the mice to come to a steady-state. In this case, the infection can be transmitted immediately once the mice meet, and the infection occurrence is dominated by the time scale of the *motion* of the mice. The opposite limit, the

former, is called the contact limit where the time scale for infection is much greater than that associated with reaching the steady-state. In this case, the mice spend a relatively longer time moving about and meeting one another before the infection is passed, and the infection event is dominated by the time scale of infection, $\mathcal{C}_1$. Thus, depending on the relative magnitudes of $\mathcal{C}_1$ and $\mathcal{M}$, the nature of the infection dynamics can differ widely. Such difference in the underlying dynamics is significant in understanding the physical phenomenon as shown in the pioneering work by Kenkre and his collaborators in [7, 8], in their work in the field of sensitized luminescence.

The motion and the contact limits of α are displayed in the left panel of figure 4.4 where α is plotted against the infection rate $\mathcal{C}_1$ where it is scaled to $2D/H$ and α to $1/\tau_H$, the diffusive time to travel the inter-home distance. These limits are indicated by the text with the arrows. In the contact limit, $\mathcal{C}_1 \to 0$, the effective rate approaches zero, $\alpha \to 0$, revealing that the time scale for infection becomes infinite and an infection never happens. In the motion limit where the infection takes place immediately as the two mice meet, α asymptotes the value in the limit $\mathcal{C}_1 \to \infty$, which is indicated by the dotted line. In the right panel, α is plotted against the potential strength γ, both scaled to τ_H, for the fixed value of $\mathcal{C}_1/(2D/H) = 15$. The non-monotonic effect of confinement on α is seen in the existence of the peak, and this plot also demonstrates the robustness of the effective rate α compared to the infection rate $\mathcal{I}(t)$ in understanding the dependence of an infection event on the varied parameters: γ, D, $\mathcal{C}_1$.

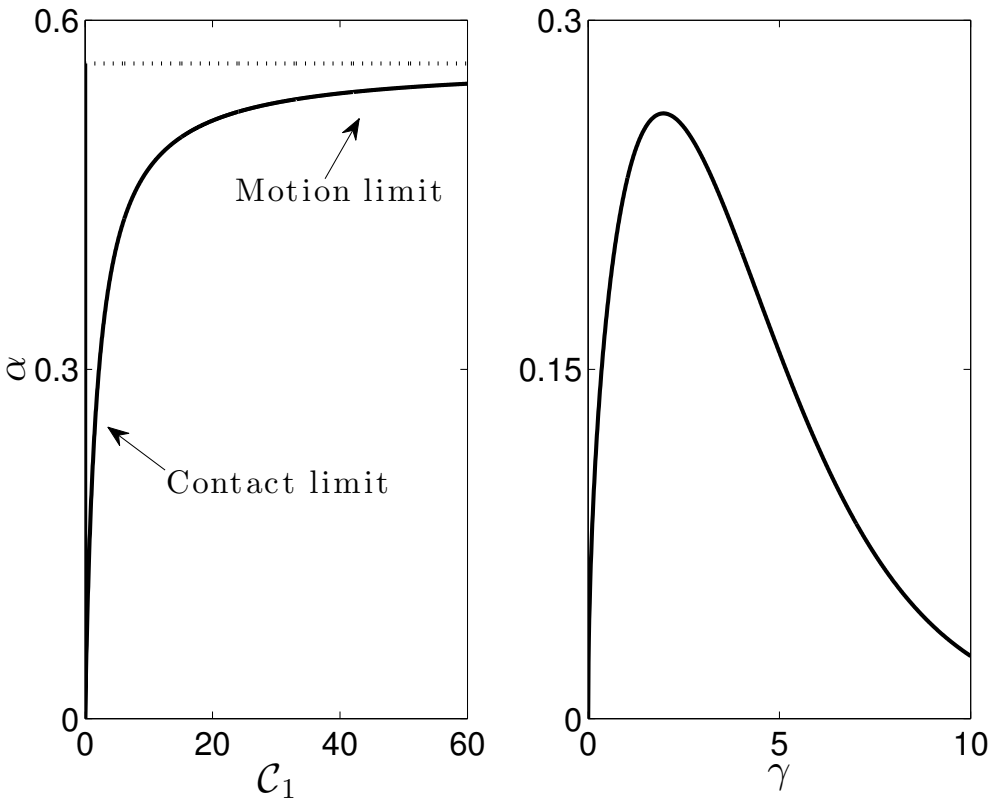

Figure 4.4: The effective infection rate, α, plotted against the infection rate, $\mathcal{C}_1$, and the confining potential strength, γ, as in Figure 2 of ref. [57]. The left panel shows α from Eq. (4.32), as a function of $\mathcal{C}_1$ (scaled to $2D/H$), where it is seen to be linear in $\mathcal{C}_1$ for small values while it saturates to a constant in the motion-limited value (0.56 here) in the other limit. The right panel shows α as a function of γ and the non-monotonic effect is seen in the peaking behavior. Here, $\mathcal{C}_1$ is in units of $2D/H$ and equals 15.

4.5 Summary

We have introduced a theory for infection transmission between two mice that is applicable in the case of a dilute population. We let the two mice, one infected with a disease and the other without but susceptible to the disease, to be Smoluchowski random walkers with distinct potential center locations, where they represent the

centers of the home ranges of the mice. We assumed that the susceptible mouse contracts the disease at a certain rate when it comes to meet the infected one. A useful intuition from the exciton annihilation problem found in [5] made us aware of an illuminating connection between the single Smoluchowski walker trapping problem studied in the previous chapter and the current problem of transmission of infection between two mice, and allowed us a straightforward solution. The connection is that a two s-dimensional-mouse infection problem is equivalent to a corresponding one $2s$-dimensional single walker trapping problem.

We studied the effect of the home ranges of the mice on the infection probability, $\mathcal{I}(t)$, and found that $\mathcal{I}(t)$ behaves non-monotonically as a function of the confinement strength. Specifically, the optimal condition for the infection transmission is found to be when the inter-home distance, H, is on the order of the characteristic size of the home range, the steady-state Smoluchowski width σ.

We borrowed an insight from the study of sensitized luminescence in molecular crystals as seen in [62], to extract a single parameter characterizing an infection curve. We sought to approximate the infection probability $\mathcal{I}(t)$ as an exponential function $\mathcal{I}(t) = 1 - e^{-\alpha t}$, where α is the parameter of interest, the effective infection rate. Resulting α shows the non-monotonic behavior as well as the contact and motion limits of the infection dynamics. Application of this theory to higher dimensions is studied in the next Chapter.

Chapter 5

Explicit Extension of the Theory in Arbitrary Dimensions

5.1 A Technical Problem in Higher Dimensions and Its Solution

The two-mouse model of infection transmission presented in the previous chapter is formulated in this chapter to arbitrary number of dimensions. The most relevant application of the theory would be in 2-dimensions as the Hantavirus-carrying population of mice (specifically the Sin Nombre strain) is found in New Mexico, moving about in a 2-dimensional space, on the desert terrain. There is, apparently, a well-known difficulty in the reaction-diffusion problem that we encounter and solve in this chapter. We thereby demonstrate a practical extension of our theory to higher dimensions.

The specific problem we encounter in our calculation is that the Laplace trans-

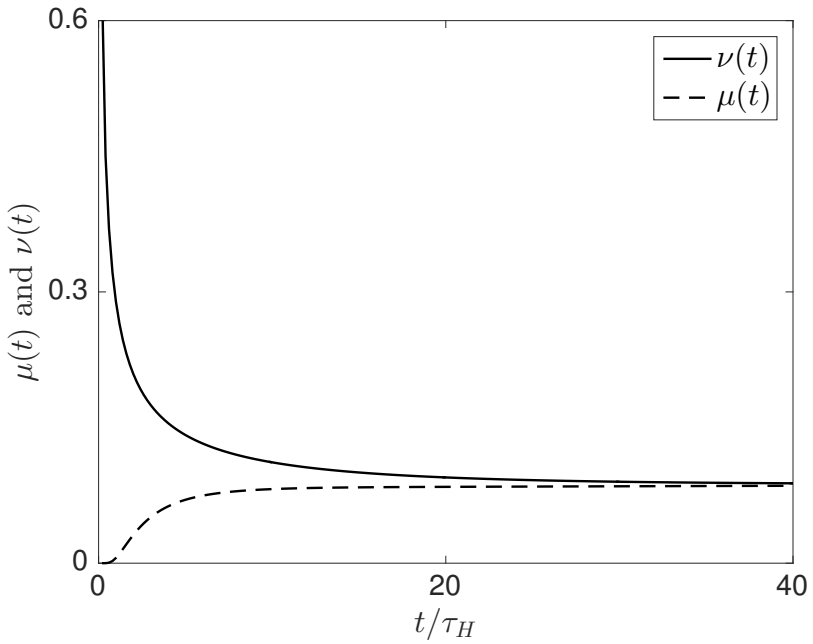

Figure 5.1: $\mu(t)$ and $\nu(t)$ in 1-dimension plotted against time. The functions are scaled to the inter-home distance H and the time to τ_H. The initial conditions of the mice are chosen arbitrarily away from each other.

form of the self-propagator, $\widetilde{\nu}(\epsilon)$, becomes non-existent in higher dimensions as demonstrated below. In the Laplace space, $\tilde{\mathcal{I}}(\epsilon)$ is given as a product of $\tilde{\mu}(\epsilon)$ and $1/(1/\mathcal{C} + \tilde{\nu}(\epsilon))$. While there is no problem in finding $\tilde{\mu}(\epsilon)$ in higher dimensions, $\tilde{\nu}(\epsilon)$ cannot be evaluated because of its short-time behavior. Figure 5.1 shows $\nu(t)$ and $\mu(t)$ plotted against time, which is scaled to τ_H in 1-dimensions. The initial conditions of the mice are arbitrarily chosen so that they are located away from each other. Shown in the solid curve is $\nu(t)$, which is divergent at $t = 0$ while $\mu(t)$ starts at 0 indicated by the dashed curve, and they converge in time. The two functions behave in a similar manner in higher dimensions with $\nu(t)$ showing stronger divergence at $t = 0$. We show the manner of this divergence below.

In the limit of $t \to 0$, $\mathcal{T}(t)$ and $e^{-\gamma t}$ in the expressions of $\nu(t)$ given in equation (4.15) become

$$\mathcal{T}(t) \to t \tag{5.1}$$

$$e^{-\gamma t} \to 1 - \gamma t, \tag{5.2}$$

and $\nu(t)$ at a small time becomes

$$\begin{aligned} \nu(t \to 0) \quad &\to \quad \left(\frac{1}{\sqrt{8\pi D t}}\right)^s \prod_{\beta=1}^{s} e^{-\frac{\gamma^2 t \left(h_1^\beta - h_2^\beta\right)^2}{8D}} \\ &\to \quad \left(\frac{1}{\sqrt{8\pi D t}}\right)^s \prod_{\beta=1}^{s} \left(1 - \frac{(\gamma H^\beta)^2}{8D} t + \cdots\right) \\ &\to \quad \left(\frac{1}{8\pi D}\right)^{\frac{s}{2}} \prod_{\beta=1}^{s} \left(t^{-\frac{s}{2}} - \frac{(\gamma H^\beta)^2}{8D} t^{-\frac{s}{2}+1} + \cdots\right), \end{aligned} \tag{5.3}$$

where in obtaining the second line, the exponential was expanded for a small argument. To the leading order, $\nu(t)$ diverges as $t^{-s/2}$ as $t \to 0$. Consequently, when its Laplace transform is considered, *i.e.*,

$$\tilde{\nu}(\epsilon) = \int_0^\infty dt\, \nu(t) e^{-\epsilon t}, \tag{5.4}$$

its divergent behavior at short-time limit leads to the divergence of the integral at $t = 0$, *except* in 1-dimension. This is the precise reason why $\tilde{\nu}(\epsilon)$ cannot be calculated for higher dimensions when the mice *meet at a point*. In order to verify the short time approximation of $\nu(t)$, equation (5.3) is plotted along with the exact expression given in equation (4.15) in 1-dimension in Figure 5.2, where $\nu(t)$ is plotted against time that is scaled to τ_H. The exact expression is shown in the solid curve and the approximation is shown by the circles. The approximation deviates from the exact $\nu(t)$ for a larger time, however, correctly converges to the latter for short times.

The problem of the divergence of $\tilde{\nu}(\epsilon)$ at $t = 0$ can be resolved simply by taking the infection region to have a finite extent of at least $(s-1)$-dimensions when

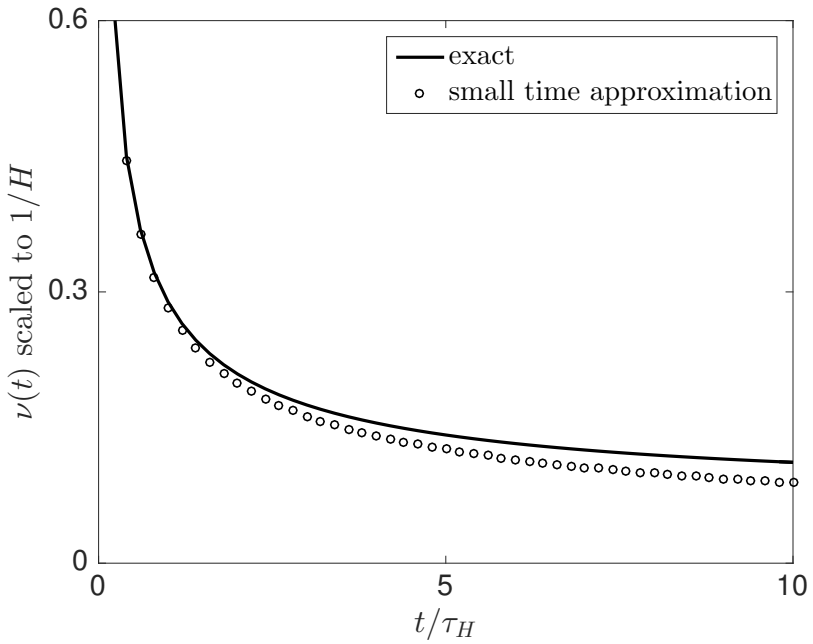

Figure 5.2: An exact and approximate $\nu(t)$, given in equations (4.15) and (5.3), respectively, plotted against t/τ_H. The approximation, depicted by circles, gives a correct behavior for short times as it converges to the exact $\nu(t)$, given by the solid curve, towards $t \to 0$.

applying our theory in s-dimensions ("regularization of the delta-function"). A systematic study, conducted in a collaboration with Chase and Kenkre, is presented in Appendix B. We make an appropriate modification to our theory in this chapter and present an explicit example in 2-dimensions and show how the non-monotonic effect of the confinement is generalized to higher dimensions.

5.1.1 Practical Extension of the Formalism to Higher Dimensions

We start by writing down a generalization of equation (4.1), the equation of motion for the configuration of the mice, $P(\boldsymbol{r}_1, \boldsymbol{r}_2, t)$, to find the infected and susceptible mice at their respective positions, $\boldsymbol{r}_1$, $\boldsymbol{r}_2$, at time t. This generalization extends the possibility of an occurrence of infection transmission to take place on a *finite region* rather than at a point:

$$\begin{aligned}\frac{\partial P(\boldsymbol{r}_1, \boldsymbol{r}_2, t)}{\partial t} &= \nabla_1 \cdot \left[\gamma \left(\boldsymbol{r}_1 - \boldsymbol{R}_1\right) P(\boldsymbol{r}_1, \boldsymbol{r}_2, t)\right] + \nabla_2 \cdot \left[\gamma \left(\boldsymbol{r}_2 - \boldsymbol{R}_2\right) P(\boldsymbol{r}_1, \boldsymbol{r}_2, t)\right] \\ &\quad + D \left(\nabla_1^2 + \nabla_2^2\right) P(\boldsymbol{r}_1, \boldsymbol{r}_2, t) \\ &\quad - \mathcal{C} \int^{'} \delta(\boldsymbol{r}_1 - \boldsymbol{r}_1')\delta(\boldsymbol{r}_2 - \boldsymbol{r}_2') P(\boldsymbol{r}_1, \boldsymbol{r}_2, t) d^s\boldsymbol{r}_1' d^s\boldsymbol{r}_2'. \end{aligned} \tag{5.5}$$

Here the first three terms are exactly the same as given in equation (4.1) and they describe the Smoluchowski motion of the mice: the attraction of the mice to their respective home centers, which in turn confine the mice to their home ranges, is given in the first two terms, where $\boldsymbol{R}_1$ and $\boldsymbol{R}_2$ denote the s-dimensional coordinates of the home centers of the infected and the susceptible mice, respectively; the third term represents the pure random motions of the mice. The last term, $-\mathcal{C} \int^{'} \delta(\boldsymbol{r}_1 - \boldsymbol{r}_1')\delta(\boldsymbol{r}_2 - \boldsymbol{r}_2') P(\boldsymbol{r}_1, \boldsymbol{r}_2, t) d^s r_1' d^s r_2'$, represents the infection-transmission event taking place in a finite region of arbitrary dimensions. The delta-functions and their arguments indicate that the transmission of infection takes place when the infected mouse is at $\boldsymbol{r}_1 = \boldsymbol{r}_1'$ and the susceptible mouse is at $\boldsymbol{r}_2 = \boldsymbol{r}_2'$. The primed integral integrates such locations over an arbitrary infection region. The infection is assumed to occur at a rate $\mathcal{C}$, which we have taken to be constant for simplicity. The unit of $\mathcal{C}$ depends on the dimension of the infection region.

We now show that the calculations, to arrive at the infection probability in the

Laplace space, are found to become easier when our problem is transformed to the center of mass (CM) and relative coordinates.

Transformation to Center of Mass and Relative Coordinates

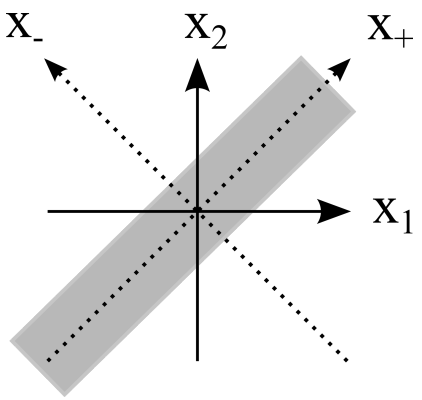

Figure 5.3: The original coordinate, x_1-x_2, is shown in the solid coordinate axes, where x_1 and x_2 denote the coordinates of the infected and susceptible mice, respectively. The center of mass (CM) and the relative coordinates are superimposed on the original axes in the dotted, x_+-x_- axes. The gray region shows the infection region, which lies along the CM (x_+) coordinate and is perpendicular to the relative (x_-) coordinate. This diagram depicts the case for 1-dimension.

We first show visually, the reduction that occurs in the spatial degrees of freedom in Figure 5.3, where the effect of the transformation is shown in the first dimension. Denoting the first coordinates of the infected and susceptible mice by x_1 and x_2, respectively, consider the 2-dimensional x_1-x_2 space as we would consider the corresponding trapping problem. In this case, the locations of the two mice are represented as a point, (x_1, x_2), and the infection region becomes stationary. We let the corresponding CM and relative coordinates to be denoted respectively by + and $-$: the coordinates of the first dimension are given by x_+ and x_-. In the figure, the original and the CM and relative coordinates are superimposed on each other.

The latter is depicted by dotted lines and the solid lines give the former. Supposing that the infection can be transmitted when the mice are within a certain distance from each other, the gray region shows the infection region, which lies diagonally to the original, and along the CM coordinate and perpendicularly to the relative coordinate. This figure reveals that an infection event takes place everywhere in the CM coordinate, leaving the position dependence only in the relative coordinate. The same happens for higher dimensions.

The transformation we use is given by

$$\boldsymbol{r}_{\pm} = \frac{1}{\sqrt{2}} \left(\boldsymbol{r}_1 \pm \boldsymbol{r}_2 \right) \quad \Longleftrightarrow \quad \boldsymbol{r}_{1,2} = \frac{1}{\sqrt{2}} \left(\boldsymbol{r}_+ \pm \boldsymbol{r}_- \right). \tag{5.6}$$

The specific choice of the constant coefficient, $1/\sqrt{2}$, is made to preserve the form of the homogeneous part of equation (5.5), *i.e.*, the the transformed equation becomes

$$\begin{aligned} \frac{\partial P(\boldsymbol{r}_+, \boldsymbol{r}_-, t)}{\partial t} &= \nabla_+ \cdot \left[\gamma \left(\boldsymbol{r}_+ - \boldsymbol{R}_+ \right) P(\boldsymbol{r}_+, \boldsymbol{r}_-, t) \right] + \nabla_- \cdot \left[\gamma \left(\boldsymbol{r}_- - \boldsymbol{R}_- \right) P(\boldsymbol{r}_+, \boldsymbol{r}_-, t) \right] \\ &\quad + D \left(\nabla_+^2 + \nabla_-^2 \right) P(\boldsymbol{r}_+, \boldsymbol{r}_-, t) \\ &\quad - \mathcal{C} \int' d^s r'_+ d^s r'_- \, \delta(\boldsymbol{r}_+ - \boldsymbol{r}'_+) \delta(\boldsymbol{r}_- - \boldsymbol{r}'_-) P(\boldsymbol{r}_1, \boldsymbol{r}_2, t), \end{aligned} \tag{5.7}$$

where $\boldsymbol{R}_{\pm}$ are given by

$$\boldsymbol{R}_{\pm} = \frac{1}{\sqrt{2}} \left(\boldsymbol{R}_1 \pm \boldsymbol{R}_2 \right). \tag{5.8}$$

The details of the preservation of the homogeneous part of the equation is given in Appendix C. We note that the coordinate transformation rule for a delta-function is given by

$$\delta(\boldsymbol{a}) = \frac{1}{|J|} \delta(\boldsymbol{b}), \tag{5.9}$$

where the transformation between an arbitrary coordinate vectors $\boldsymbol{a}$ and $\boldsymbol{b}$ is assumed not singular, and J is the Jacobian of the transformation, which turns out to

be -1 between each element of $\boldsymbol{r}_1$ and $\boldsymbol{r}_2$ here.

Because the homogeneous part of equations (5.5) and (5.7) have the same form, so do the functional forms of the propagators. Therefore, the homogeneous propagator, $\Pi(\boldsymbol{r}_+, \boldsymbol{r}'_+, \boldsymbol{r}_-, \boldsymbol{r}'_-, t)$, in the transformed coordinate is

$$\Pi(\boldsymbol{r}_+, \boldsymbol{r}'_+, \boldsymbol{r}_-, \boldsymbol{r}'_-, t) = \left(\frac{1}{4\pi D\mathcal{T}(t)}\right)^s \prod_{\beta=1}^{s} e^{-\frac{\left(x_+^\beta - h_+^\beta - (x_+'^\beta - h_+^\beta)e^{-\gamma t}\right)^2 + \left(x_-^\beta - h_-^\beta - (x_-'^\beta - h_-^\beta)e^{-\gamma t}\right)^2}{4D\mathcal{T}(t)}}, \tag{5.10}$$

where β denotes each dimension. Using the Green function method, the solution to equation (5.7) is

$$P(\boldsymbol{r}_+, \boldsymbol{r}_-, t) = \eta(\boldsymbol{r}_+, \boldsymbol{r}_-, t) - \mathcal{C}\int_0^t dt' \int^{'} d^s r'_+ d^s r'_- \, \Pi(\boldsymbol{r}_+, \boldsymbol{r}'_+, \boldsymbol{r}_-, \boldsymbol{r}'_-, t-t') P(\boldsymbol{r}'_+, \boldsymbol{r}'_-, t), \tag{5.11}$$

where $\eta(\boldsymbol{r}_+, \boldsymbol{r}_-, t)$ is the homogeneous solution. With an arbitrary initial condition $P(\boldsymbol{r}_+^0, \boldsymbol{r}_-^0, 0)$, where $\boldsymbol{r}_+^0$ and $\boldsymbol{r}_-^0$ are the initial locations, the homogeneous solution $\eta(\boldsymbol{r}_+, \boldsymbol{r}_-, t)$ is given by

$$\eta(\boldsymbol{r}_+, \boldsymbol{r}_-, t) = \int_{-\infty}^{\infty}\int_{-\infty}^{\infty} d^s r_+^0 d^s r_-^0 \, \Pi(\boldsymbol{r}_+, \boldsymbol{r}_+^0, \boldsymbol{r}_-, \boldsymbol{r}_-^0, t) P(\boldsymbol{r}_+^0, \boldsymbol{r}_-^0, 0). \tag{5.12}$$

From this point, the steps taken to arrive at the infection probability, $\mathcal{I}(t)$, in the Laplace domain, $\tilde{\mathcal{I}}(\epsilon)$, are very similar to that presented in the previous chapter, with one crucial difference which comes about in the calculation of the function $\nu(t)$. In order to calculate this quantity with the extended region of infection, the ν-function method [6, 7] is employed as presented below.

The Infection Probability and $\mu(t)$ and $\nu(t)$ Functions: the ν-function Method

The definition of the infection probability, $\mathcal{I}(t)$, is given in euqation (4.5). For this specific case, in the CM and relative coordinates, it becomes

$$\mathcal{I}(t) = 1 - \int_{-\infty}^{\infty} d^s r_+ d^s r_- \; P(\boldsymbol{r}_+, \boldsymbol{r}_-, t). \tag{5.13}$$

As was done in the previous chapter, we Laplace transform this equation and obtain

$$\begin{aligned}\widetilde{\mathcal{I}}(\epsilon) = \frac{1}{\epsilon} &- \int_{-\infty}^{\infty}\int_{-\infty}^{\infty} d^s r_+ d^s r_- \tilde{\eta}(\boldsymbol{r}_+, \boldsymbol{r}_-, \epsilon) \\ &+ \mathcal{C}\int' d^s r'_+, d^s r'_- \widetilde{P}(\boldsymbol{r}'_+, \boldsymbol{r}'_-, \epsilon)\int_{-\infty}^{\infty}\int_{-\infty}^{\infty} d^s r_+ d^s r_- \widetilde{\Pi}(\boldsymbol{r}_+, \boldsymbol{r}^0_+, \boldsymbol{r}_-, \boldsymbol{r}^0_-, \epsilon),\end{aligned} \tag{5.14}$$

where $P(\boldsymbol{r}_+, \boldsymbol{r}_-, t)$ given in equation (5.11) was explicitly written. On the right hand side, the spatial integrals of $\tilde{\eta}(\boldsymbol{r}_+, \boldsymbol{r}_-, \epsilon)$ of the second term and that of $\widetilde{\Pi}(\boldsymbol{r}_+, \boldsymbol{r}^0_+, \boldsymbol{r}_-, \boldsymbol{r}^0_-, \epsilon)$ in the third term both yield $1/\epsilon$. With this, the infection probability in the Laplace space becomes

$$\widetilde{\mathcal{I}}(\epsilon) = \frac{\mathcal{C}}{\epsilon}\int' d^s r'_+, d^s r'_- \widetilde{P}(\boldsymbol{r}'_+, \boldsymbol{r}'_-, \epsilon). \tag{5.15}$$

The integrated quantity on the right hand side yields the probability to find the infected and susceptible mice within the region of infection at a given time in the Laplace domain. As mentioned above, in the current problem with a finite infection region, the defect technique must be extended via the ν-function method [6, 7]. The use of the defect technique here means integrating equation (5.11) over the infection region in the coordinate variables $\boldsymbol{r}_+$ and $\boldsymbol{r}_-$ in the Laplace domain, which yields

$$\begin{aligned}\int' d^s r_+ d^s r_- \widetilde{P}(\boldsymbol{r}_+, \boldsymbol{r}_-, \epsilon) = &\int' d^s r_+ d^s r_- \tilde{\eta}(\boldsymbol{r}_+, \boldsymbol{r}_-, \epsilon) \\ &- \mathcal{C}\int' d^s r'_+ d^s r'_- \; \widetilde{P}(\boldsymbol{r}'_+, \boldsymbol{r}'_-, \epsilon)\int' d^s r_+ d^s r_- \widetilde{\Pi}(\boldsymbol{r}_+, \boldsymbol{r}'_+, \boldsymbol{r}_-, \boldsymbol{r}'_-, \epsilon),\end{aligned} \tag{5.16}$$

Now, we define the functions $\mu(t)$ and $\nu(t)$ specifically for the problem at hand. The former is defined by

$$\mu(t) = \int' d^s r_+ d^s r_- \; \eta(\boldsymbol{r}_+, \boldsymbol{r}_-, t). \tag{5.17}$$

Defining $\nu(t)$ is not as straightforward. The integral over the infection region of the propagator in the second term of the right hand side of equation (5.16), viz.,

$$\int' d^s r_+ d^s r_- \widetilde{\Pi}(\boldsymbol{r}_+, \boldsymbol{r}'_+, \boldsymbol{r}_-, \boldsymbol{r}'_-, \epsilon), \tag{5.18}$$

leaves $\boldsymbol{r}'_+$ and $\boldsymbol{r}'_-$-dependence in the integrated quantity, and describes the probability density to find the mice within the infection region given that they were at ($\boldsymbol{r}'_+$,$\boldsymbol{r}'_-$) some time earlier, *i.e.*, within the region of infection. The ν-function method [6, 7] ensemble-averages such ($\boldsymbol{r}'_+$,$\boldsymbol{r}'_-$) and yields $\nu(t)$ that only depends on time. Hence, as was done in Chapter 2, we define $\nu(t)$ by

$$\nu(t) = \frac{\int' d^s r'_+ d^s r'_- \int' d^s r_+ d^s r_- \Pi(\boldsymbol{r}_+, \boldsymbol{r}'_+, \boldsymbol{r}_-, \boldsymbol{r}'_-, t)}{\int' d^s r'_+ d^s r'_-}. \tag{5.19}$$

With this approximation, equation (5.16) yields

$$\int' d^s r'_+ d^s r'_- \; \widetilde{P}(\boldsymbol{r}'_+, \boldsymbol{r}'_-, \epsilon) = \frac{\tilde{\mu}(t)}{1 + \mathcal{C}\tilde{\nu}(t)}, \tag{5.20}$$

where we note that the from on the right hand side is identical to that given in equation (4.12). Substituting this equation into the expression of $\widetilde{\mathcal{I}}(\epsilon)$ given in equation (5.15) yields the same expression of $\widetilde{\mathcal{I}}(\epsilon)$ found for a point infection region in the last chapter, and is given by equation (4.13). Thus, the use of the defect technique and the ν-function method allowed for the solution of $\widetilde{\mathcal{I}}(\epsilon)$ solely in terms of the knowledge of the homogeneous propagator, $\Pi(\boldsymbol{r}_+, \boldsymbol{r}'_+, \boldsymbol{r}_-, \boldsymbol{r}'_-, t)$ via equations (5.17) and (5.19).

Reduction of the Spatial Degrees of Freedom

We calculate $\mu(t)$ and $\nu(t)$ explicitly for a delta-function initial condition of the mice: $P(\boldsymbol{r}'_+, \boldsymbol{r}'_-, 0) = \delta^s\left(\boldsymbol{r}'_+ - \boldsymbol{r}^0_+\right)\delta^s\left(\boldsymbol{r}'_- - \boldsymbol{r}^0_-\right)$. We bring our attention to Figure 5.3, and emphasize that the infection region indicated by the gray region lies along the CM coordinate. This means that the integrals in equations (5.17) and (5.19) can be written in a more explicit form as

$$\int' d^s r'_+ d^s r'_- \quad \rightarrow \quad \int_{-\infty}^{\infty} d^s r'_+ \int' d^s r'_-, \tag{5.21}$$

where the prime for the relative coordinate integral is to be specified later. Together with the form of propagator given in equation (5.10), $\mu(t)$ and $\nu(t)$ of equations (5.17) and (5.19) are then written as

$$\mu(t) = \int_{-\infty}^{\infty} d^s r_+ \int' d^s r_- \left(\frac{1}{4\pi D\mathcal{T}(t)}\right)^s \prod_{\beta=1}^{s} e^{-\frac{\left(x_+^\beta - h_+^\beta - (x_+^{0\beta} - h_+^\beta)e^{-\gamma t}\right)^2 + \left(x_-^\beta - h_-^\beta - (x_-^{0\beta} - h_-^\beta)e^{-\gamma t}\right)^2}{4D\mathcal{T}(t)}}, \tag{5.22}$$

$$\nu(t) = \frac{\int' d^s r'_- \int_{-\infty}^{\infty} d^s r_+ \int' d^s r_- \left(\frac{1}{4\pi D\mathcal{T}(t)}\right)^s \prod_{\beta=1}^{s} e^{-\frac{\left(x_+^\beta - h_+^\beta - (x_+'^\beta - h_+^\beta)e^{-\gamma t}\right)^2 + \left(x_-^\beta - h_-^\beta - (x_-'^\beta - h_-^\beta)e^{-\gamma t}\right)^2}{4D\mathcal{T}(t)}}}{\int' d^s r'_-}. \tag{5.23}$$

The Gaussian integral over the CM coordinate is trivial, and we yield simpler forms of $\mu(t)$ and $\nu(t)$ as

$$\mu(t) = \int' d^s r_- \left(\frac{1}{4\pi D\mathcal{T}(t)}\right)^{\frac{s}{2}} \prod_{\beta=1}^{s} e^{-\frac{\left(x_-^\beta - h_-^\beta - (x_-^{0\beta} - h_-^\beta)e^{-\gamma t}\right)^2}{4D\mathcal{T}(t)}}, \tag{5.24}$$

$$\nu(t) = \frac{\int' d^s r'_- \int' d^s r_- \left(\frac{1}{4\pi D\mathcal{T}(t)}\right)^{\frac{s}{2}} \prod_{\beta=1}^{s} e^{-\frac{\left(x_-^\beta - h_-^\beta - (x_-'^\beta - h_-^\beta)e^{-\gamma t}\right)^2}{4D\mathcal{T}(t)}}}{\int' d^s r'_-}. \tag{5.25}$$

Thus, the CM coordinate dependence of the problem is integrated out to a constant in each dimension and the spatial degrees of freedom is reduced to half. We present

the use of this theory explicitly in 2-dimensions next.

5.2 Explicit Calculations in 2-dimensions

Two dimensional calculations of our model not only provide the simplest example of the extended theory, but also, and more importantly, possess practical applications to an infection spread among mice moving on a terrain. Surely, it is more appropriate to choose infection as occurring as an arbitrary function of the relative distance of the mice. However in this chapter, we present the simplest case where the transmission of infection is assumed to occur when the mice are *at* a certain distance A, the infection range, from each other in 2-dimensions, in other words, anywhere on the circumference of a given radius surrounding the other mouse.

We proceed with the calculation of $\mu(t)$ and $\nu(t)$ specific to a finite-range infection in 2-dimensions. With the definitions of $\mu(t)$ and $\nu(t)$ derived in the last section, in equations (5.24) and (5.25), in 2-dimensions they becomes

$$\mu(t) = \int' dxdy \left(\frac{1}{4\pi D\mathcal{T}(t)}\right) e^{-\frac{\left(x-h-(x^0-h)e^{-\gamma t}\right)^2+\left(y-f-(y^0-f)e^{-\gamma t}\right)^2}{4D\mathcal{T}(t)}}, \tag{5.26}$$

$$\nu(t) = \frac{\int' dx'dy' \int' dxdy \left(\frac{1}{4\pi D\mathcal{T}(t)}\right) e^{-\frac{\left(x-h-(x'-h)e^{-\gamma t}\right)^2+\left(y-f-(y'-f)e^{-\gamma t}\right)^2}{4D\mathcal{T}(t)}}}{\int' dx'dy'}, \tag{5.27}$$

where the relative coordinate in the first dimension is denoted by $x^1_- \equiv x$, that of the second dimension by $x^2_- \equiv y$, the relative home-center coordinate in the first dimension by $h^1_- \equiv h$, and that of the second dimension by $h^2_- \equiv f$. The integrals above become easier in the corresponding polar coordinate, where the infection region is given by a circle of radius A: $x^2 + y^2 = A^2$. Thus we make another coordinate

transformation according to

$$\begin{cases} \rho^2 = x^2 + y^2 \\ \tan\theta = y/x \end{cases} \Rightarrow \begin{cases} x = \rho\cos\theta \\ y = \rho\sin\theta \end{cases} . \tag{5.28}$$

We first transform the integrand of $\mu(t)$ and $\nu(t)$. The numerator of the exponent of the Gaussian in equations (5.26) and (5.27) transforms to

$$\begin{aligned} &\left(x - h - (x' - h)e^{-\gamma t}\right)^2 + \left(y - f - (y' - f)e^{-\gamma t}\right)^2 \\ &= B(\rho, \rho', \theta) - 2\rho\left[E(\rho', \theta')\cos\theta + F(\rho', \theta')\sin\theta\right], \end{aligned} \tag{5.29}$$

where

$$B(\rho, \rho', \theta') = \rho^2 + \rho'^2 e^{-2\gamma t} + H^2\left(1 - e^{-\gamma t}\right)^2 + 2H\rho'^2 e^{-\gamma t}\left(1 - e^{-\gamma t}\right)\cos(\theta' - \phi), \tag{5.29a}$$

$$E(\rho', \theta') = \rho' e^{-\gamma t}\cos\theta' + H\cos\phi\left(1 - e^{-\gamma t}\right), \tag{5.29b}$$

$$F(\rho', \theta') = \rho' e^{-\gamma t}\sin\theta' + H\sin\phi\left(1 - e^{-\gamma t}\right), \tag{5.29c}$$

$$H^2 = h^2 + f^2, \tag{5.29d}$$

$$\tan\phi = f/h. \tag{5.29e}$$

We define three additional quantities to simplify equation (5.29) so that the resulting expression becomes a known integral. First we define

$$\cos\Omega = \frac{F(\rho', \theta')}{\sqrt{E^2(\rho', \theta') + F^2(\rho', \theta')}}, \qquad \sin\Omega = \frac{E(\rho', \theta')}{\sqrt{E^2(\rho', \theta') + F^2(\rho', \theta')}}, \tag{5.30}$$

and additionally define the function $\mathcal{F}(\rho', \theta')$ as

$$\mathcal{F}(\rho', \theta') = E^2(\rho', \theta') + F^2(\rho', \theta'). \tag{5.31}$$

We recognize that

$$B(\rho, \rho', \theta') = \rho^2 + E^2(\rho', \theta') + F^2(\rho', \theta') = \rho^2 + \mathcal{F}(\rho', \theta'). \tag{5.32}$$

With these, equation (5.29) becomes

$$\begin{aligned}&\left(x-h-(x'-h)e^{-\gamma t}\right)^2+\left(y-f-(y'-f)e^{-\gamma t}\right)^2\\&=\rho^2+\mathcal{F}(\rho',\theta')-2\rho\sqrt{\mathcal{F}(\rho',\theta')}\cos\left(\theta-\Omega\right).\end{aligned}\tag{5.33}$$

The integral over the infection region in the polar coordinate becomes

$$\int' dxdy\to\int_0^\infty d\rho\int_0^{2\pi}\rho d\theta\,\frac{1}{\rho 2\pi}\delta\left(\rho-A\right)=\int_0^\infty d\rho\int_0^{2\pi}d\theta\,\frac{1}{2\pi}\delta\left(\rho-A\right).\tag{5.34}$$

Then the integrals of $\mu(t)$ and $\nu(t)$ can be recognized as the 0-th order modified Bessel function of the first kind [50], $\mathrm{I}_0(z)$, and $\mu(t)$ and $\nu(t)$ become

$$\mu(t)=\left(\frac{1}{4\pi D\mathcal{T}(t)}\right)e^{-\frac{A^2+\mathcal{F}(\rho_0,\theta_0)}{4D\mathcal{T}(t)}}\mathrm{I}_0\left(\frac{A\sqrt{\mathcal{F}(\rho_0,\theta_0)}}{2D\mathcal{T}(t)}\right),\tag{5.35}$$

and

$$\nu(t)=\frac{1}{2\pi}\int_0^{2\pi}d\theta'\left(\frac{1}{4\pi D\mathcal{T}(t)}\right)e^{-\frac{A^2+\mathcal{F}(A,\theta')}{4D\mathcal{T}(t)}}\mathrm{I}_0\left(\frac{A\sqrt{\mathcal{F}(A,\theta')}}{2D\mathcal{T}(t)}\right),\tag{5.36}$$

where the integral over θ' needs to be evaluated numerically.

5.2.1 Result for 2-dimensional Finite-Range Infection: Recovery of $\nu(t)$ and the non-monotonic effect

We now show that the $\nu(t)$ obtained above behaves as $t^{-1/2}$ as $t\to 0$ and therefore the Laplace transformable behavior is recovered. As $t\to 0$, the argument of the Bessel function becomes large where its asymptotic form is appropriate. For a large argument, $z\to\infty$, the asymptotic behavior of $\mathrm{I}_0(z)$ is given by [50]

$$\mathrm{I}_0(z)\to\frac{e^z}{\sqrt{z}},\quad z\to\infty,\tag{5.37}$$

and $\nu(t)$ behaves, at short times, as

$$\nu(t\to 0)\to\frac{1}{2\pi}\int_0^{2\pi}d\theta'\left(\frac{1}{4\pi Dt}\right)e^{-\frac{A^2+A^2}{4Dt}}\sqrt{\frac{2Dt}{A^2}}e^{\frac{A^2}{2Dt}}\sim\frac{1}{\sqrt{t}}.\tag{5.38}$$

Hence, $\nu(t)$ at short times behaves as was seen in the case of a point infection region in one dimension, and its Laplace transform, $\widetilde{\nu}(t)$ can be calculated.

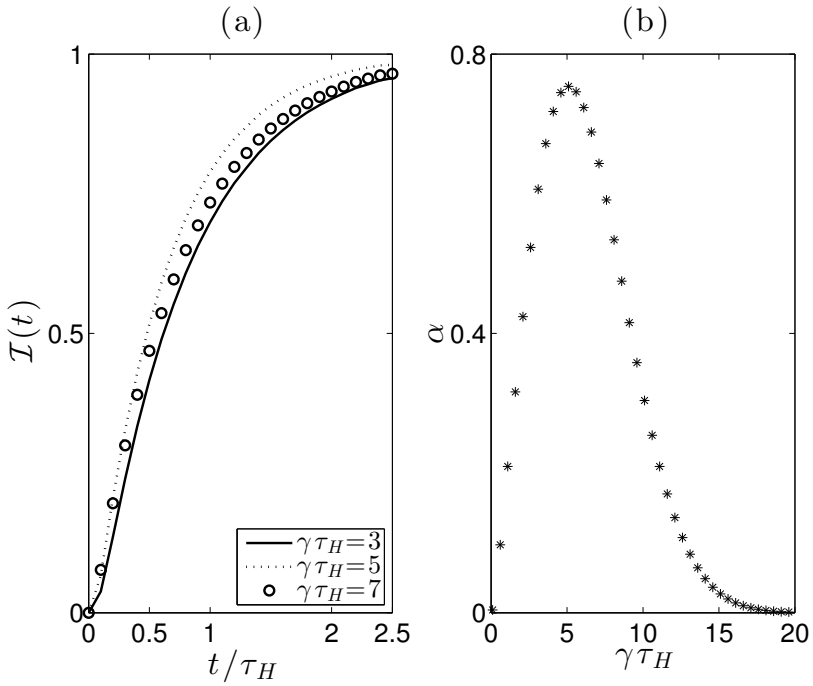

Figure 5.4: (a)The non-monotonic effect of infection probability as a function of monotomically increasing $\gamma\tau_H$, the strength of cofinement. The numerically calculated infection probability $\mathcal{I}(t)$ is plotted against time in units of the diffusive time to for the walker to traverse the inter-home distance H. Each infection curve corresponds to a different value of $\gamma\tau_H$, the strength of confinement to homes. The behavior of the $\mathcal{I}(t)$ is identical to that as seen in figure 4.1 of the previous chapter. (b) The effective rate α scaled to τ_h plotted against $\gamma\tau_H$, whose peak indicates the optimal value of $\gamma\tau_H$ for infection.

The Laplace transforms of $\mu(t)$ and $\nu(t)$ were found numerically in order to calculate $\tilde{\mathcal{I}}(\epsilon)$ via equation (4.13), which was numerically inverted to obtain $\mathcal{I}(t)$. The effective rate α was calculated via equation (4.32). The resulting infection curve and the effective rate showing the non-monotonic behavior due to the effect of confinement are shown in figure 5.4. In panel (a), the infection curve is plotted against

time scaled to τ_H. Each curve corresponds to a value of $\gamma\tau_H$, effectively to a given potential strength γ. Panel (b) of Figure 5.4 shows the effective rate α scaled to $1/\tau_H$, plotted against $\gamma\tau_H$ again showing the non-monotonic effect. Thus, we show how explicitly the result in 1-dimension is generalized to 2-dimensions.

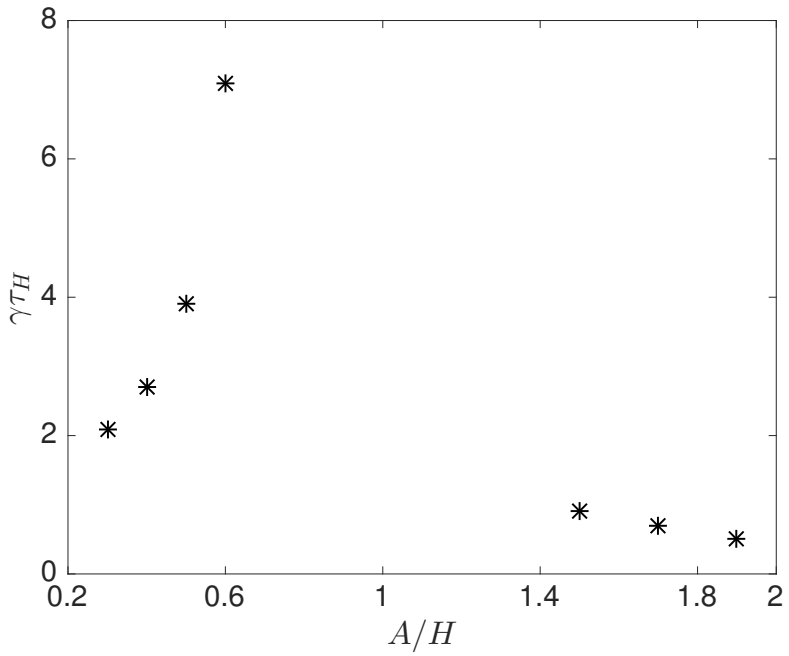

Figure 5.5: The optimal value of $\gamma\tau_H$ is plotted for a given ratio of the infection range to the inter-home distance A/H. The optimal values are found numerically through α-curve as shown in panel b) of Figure 5.4 for each value of A while the diffusion constant D, the inter-home distance H, and the infection rate $\mathcal{C}$ were held fixed.

The infection range, A, provides a new length scale in our problem and, therefore, we investigate its effect on the transmission of infection, specifically on the optimal value of $\gamma\tau_H$. To do this, an optimal value of $\gamma\tau_H$ was numerically found from the α-curve as shown in panel (b) of Figure 5.4 for a value of A. The resulting A-dependency of the optimal $\gamma\tau_H$ values are plotted in Figure 5.5, where A is scaled

to H. One striking feature is the seemingly diverging value of $\gamma\tau_H$ at $A/H = 1$, however such behavior of $\gamma\tau_H$ is not surprising as $A = H$ means that the infection occurs as if though the two mice share their home center. When the mice live at the same home, a stronger confinement only encourages infection transmission by the increased chance of their encounter. In order to elucidate the effect of A on the behavior of the optimal $\gamma\tau_H$ values in a simplest manner, we analyze the finite-range infection in 1-dimension below.

5.3 Effect of Varying the Infection Range: Analysis in 1-dimension

The finite-range infection is not specific to 2-dimensions, and the essence of its effect on infection transmission is captured already in 1-dimension. We show the 1-dimensional analysis here because it leads to a more tractable expressions that embodies the effect of the infection range. As was done in Chapters 3 and 4, we perform our analysis in the contact limit where it is appropriate to express the infection probability as a product of the infection rate and the steady-state homogeneous probability to find the animals at the infection site. The steady-state probability to find the mice at the infection site is obtained through the joint probability density, $P_{ss}(x_1, x_2)$, to find the infected mouse at x_1 and the susceptible one at x_2. In the absence of infection, the joint distribution is the product of individual densities of the mice, where we denote that of the infected and susceptible by $P_1(x)$ and $P_2(x)$, respectively, where

$$P_i(x) = \frac{1}{\sqrt{\pi}\sigma} e^{-\frac{(x-A-h_i)^2}{\sigma^2}}, \quad i = 1, 2. \tag{5.39}$$

The joint density to find the mice at an infection range A apart is

$$P_1(x)P_2(x-A)+P_1(x)P_2(x+A) = \frac{1}{\pi\sigma^2}\left(e^{-\frac{2(x-(h_1+h_2+A)/2)^2}{\sigma^2}}e^{-\frac{(H-A)^2}{2\sigma^2}} + e^{-\frac{2(x-(h_1+h_2-A)/2)^2}{\sigma^2}}e^{-\frac{(H+A)^2}{2\sigma^2}}\right), \tag{5.40}$$

where $H = h_1 - h_2$. Integrating x over all space yields the probability, which in turn gives $\mathcal{I}(t)$ in the contact limit as

$$\mathcal{I}(t) \sim \mathcal{C}_1\frac{1}{\sqrt{2\pi}\sigma}\left(e^{-\frac{(H-A)^2}{\sigma^2}} + e^{-\frac{(H+A)^2}{\sigma^2}}\right)\ t. \tag{5.41}$$

Finding the condition for maximum value of $\mathcal{I}(t)$ as a function of σ yields the transcendental relation

$$\frac{1-2\gamma\tau_H(1-A/H)^2}{1-2\gamma\tau_H(1+A/H)^2} = -e^{-4\gamma\tau_H(A/H)}. \tag{5.42}$$

Figure 5.6 shows the optimal value of $\gamma\tau_H$, found by numerically solving equation (5.42), plotted against A/H. We find that $\gamma\tau_H$ behaves similarly to that found for 2-dimensional boxer infection as a function of A/H, with diverging behavior at $A/H = 1$. The inset of the figure shows $\gamma\tau_H$ plotted against the normalized difference between A and H, $|A-H|/H$ to show the expected asymmetry, although such feature is less pronounced here in 1-dimension than that seen in 2-dimensions (see figure 5.5).

We note that it is possible, however much more cumbersome, to calculate the *exact* infection probability in the Laplace domain, and arrive at equation (5.42). The interested reader is referred to Appendix D for the detail.

5.4 Summary

In this chapter, we gave a practical extension of the reaction-diffusion theory for infection-transmission given in Chapter 4 to higher dimensions. It is well known that

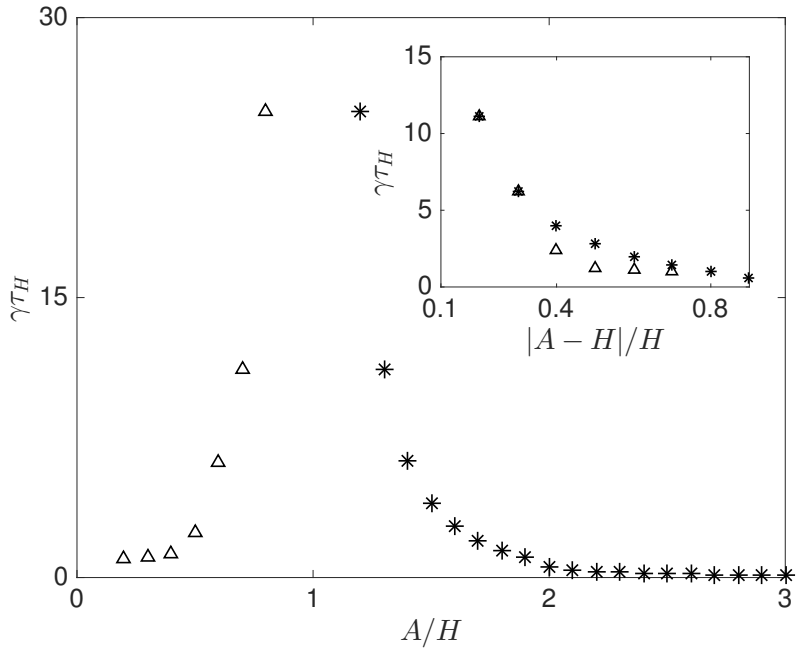

Figure 5.6: Optimal value of the confining potential steepness γ (scaled to $1/\tau_H$) for maximum infection rate as a function of (A/H). In the inset, the optimal $\gamma\tau_H$ is plotted against the normalized difference between A and H to show the asymmetry in the behavior of $\gamma\tau_H$ as a function of $|A-H|/H$.

the Laplace transform of the self-propagator is not defined in such cases. The "self"-propagator refers to a point (zero-dimensional region) and leads to a mathematical problem. The general resolution lies in enlarging the spatial extent of the meeting region of the mice to a finite region as explicitly pointed out in ref [57]. Our study of reaction-diffusion theory in higher dimensions, conducted in collaboration with Chase and Kenkre and given in this thesis as Appendix B, clarifies that point [57], *i.e.*, how such a problem can be resolved by extending the infection-occurring region to a finite region of at least $(s-1)$-dimensions when an s-dimensional problem is considered.

We also studied the effect of the variation of the range of infection A on the

optimal confinement strength in detail in 1-dimension. Essentially, A modulates the role of the inter-home distance, H, in the problem of point infection region. We found that the relationship among A, H, and γ that yields an optimal confinement strength for infection transmission becomes much more complex compared to that found in the trapping and infection problems considered in Chapters 3 and 4.

Chapter 6

Concluding Remarks

6.1 Summary

We conclude with a summary of the work presented in this thesis and mention briefly some related projects. In this thesis, we applied reaction-diffusion theory to model infectious disease transmission between a mouse that carries a disease to another mouse that is without infection but susceptible to it. In our simple model, applicable directly to the Hantavirus epidemic as seen in refs. [25–32], we described an underlying process of an epidemic spread in a dilute population, with the assumption that the mice move as tethered random walkers and that the disease is transmitted at a certain rate upon their encounter.

In Chapter 2, we introduced the tools of our investigation, viz., the Smoluchowski equation and the defect technique. The method of solution was summarized in Appendix A and the characteristics of the probability density is discussed at length. The "defect technique" explained there is an important method to solve the reaction-diffusion equations considered in this thesis, and its basic procedure was presented

in a context of a trapping problem of a random walker.

The simplest reaction-diffusion scenario was studied in Chapter 3, viz., trapping of a Smoluchowski random walker by a single stationary trap, in order to investigate the effect of the attractive potential on the survival probability of the walker. We found that the survival probability behaves non-monotonically as a function of the potential strength unless the trap is located precisely at the center of the potential, a configuration that generally would seldom occur. Such an effect arises due to the property of a Smoluchowski walker that its steady-state density is a Gaussian centered at the potential center with the width $\sigma = \sqrt{2D/\gamma}$. As the width of the Gaussian varies with the potential strength γ, so does the probability density to find the walker at the trap site. This change in the density occurs non-monotonically, causing such effect in the survival probability.

The above result and the tools were used in Chapter 4 to address the central problem of this thesis, the transmission of infection. The procedure was to convert the two-walker infection problem to a trapping problem in twice the number of dimensions by following the methodology used by Kenkre [5] many years ago for treating exciton annihilation in molecular crystals. The non-monotonic effect of the confining potential found was shown to extend to this infection problem also. Here, the effect is observed as one varies the the ratio of the inter-home distance to the steady-state Smoluchowski width. We also defined the effective infection rate that characterizes the infection probability (that depends on time) as a single quantity which reflects the effects of the important parameters: the diffusion constant, the confining potential strength, and the infection rate. The non-monotonic effect was also manifested in the effective rate; the two limits in the dynamics of infection transmission, viz., the motion and contact limits were discussed.

Although the two-mouse model is formulated in any number of dimensions, such that the infection is transmitted when they co-locate at a point, this condition of 'co-location at a point' causes the Laplace transform of the quantity $\nu(t)$, the probability to find the mice together given that they were together before, to cease to exist in higher dimensions. This appears to be a well-known problem in reaction-diffusion theory. In chapter 5, we presented some analysis in this context by extending the region where the infection takes place, from a point to a finite region. Appendix B was given for a detailed discussion on this matter. Using that work, an extension of the 1-dimensional theory [57] to a realistic n-dimensional situation was done next in Chapter 5 and the non-monotonic effect of the confinement was confirmed in 2-dimensions. Appendix D is provided for further elucidation. This extension to higher dimensions is a primary constitution of this thesis.

6.2 Comments Regarding Possible Future Work

The ultimate goal of the research initiated in this thesis is to construct a kinetic equation for epidemic spread incorporating the consideration of the home ranges of the mice. Such a kinetic equation would take the equation proposed by Abramson and Kenkre [18] as a springboard. It would thus be an equation for the macroscopic variable, the population densities of the mice, susceptible and infected. It would incorporate the effect of the tethered nature of the random walks. The problem of obtaining infection rates in a *dilute* system has been solved in this thesis. The general problem presented by a system of arbitrary density requires the completion of several difficult tasks which are beyond the scope of this thesis. One of these tasks is to obtain a macroscopic equation for the mouse density given the microscopic equa-

tions for the probability density of mice in a dilute system. This is a very difficult undertaking. The number as well as the identity of interacting infected-susceptible mouse pairs varies dynamically. Even the passage to a macroscopic equation for the total mouse density from individual probability densities is a very hard task. Work on the latter issue was carried out a number of years ago by MacInnis and Kenkre [44] who proposed a macroscopic equation that included the effect of home ranges. We made a number of attempts during the course of this thesis to investigate the validity of that equation and to complete the other aspects of the construction of the kinetic framework discussed above. We have only met with partial success and have not included a report of those activities in the present thesis. It is hoped that the dilute system calculations presented in this thesis will play an essential role in a theory that addresses dense systems as appropriately .

Appendices

Appendix A

Solving the Smoluchowski Equation

One standard way to solve the Smoluchowski equation given in equation (2.8), is by the method of characteristics performed in the Fourier domain. Thus, we begin by Fourier transforming the equation. Defining

$$\hat{P}(\boldsymbol{k},t) = \int_{-\infty}^{\infty} \cdots \int_{-\infty}^{\infty} d^n \boldsymbol{r} e^{-i\boldsymbol{k}\cdot\boldsymbol{r}} P(\boldsymbol{r},t), \tag{A.1}$$

where $\boldsymbol{k} = (k_1, k_2, \ldots, k_n)$ is the vector of Fourier variables, equation (2.8) in the Fourier domain is given by

$$\frac{\partial \hat{P}(\boldsymbol{k},t)}{\partial t} = -\gamma \boldsymbol{k} \cdot \nabla_{\boldsymbol{k}} \hat{P} - i\gamma \boldsymbol{k} \cdot \boldsymbol{r}_h \hat{P} - D\boldsymbol{k} \cdot \boldsymbol{k} \hat{P}, \tag{A.2}$$

This first-order partial differential equation is solved by transforming to an ordinary differential equation (the method of characteristic) by introducing another variable, say s, such that $s = s(k_1, k_2, \ldots, k_n, t)$, whose specific functional form is determined by

$$1 = \frac{dt}{ds}, \tag{A.3}$$

and

$$\gamma k_1 = \frac{dk_1}{ds}, \quad \gamma k_2 = \frac{dk_2}{ds}, \ldots, \quad \gamma k_n = \frac{dk_n}{ds}. \tag{A.4}$$

Such prescription allows us to write equation (A.2) as

$$\frac{d\hat{P}(s)}{ds} = -\left(i\gamma \boldsymbol{k}(s)\cdot \boldsymbol{r}_h + D\boldsymbol{k}^2(s)\right)\hat{P}(s). \tag{A.5}$$

To proceed, first solve for the functional relations between s, t, and each of the k's, by choosing the initial condition $s = 0$ when $t = 0$, and $k_\beta(s=0) \equiv k_\beta^0$, which gives

$$t(s) = s \tag{A.6}$$

$$k_\beta(s) = k_\beta^0 e^{\gamma s}. \tag{A.7}$$

Substituting these into eq. (A.5) and solving the equation gives

$$\hat{P}(s) = \hat{P}(s=0)\prod_{\beta=1}^{n} e^{-ik_\beta^0 h_\beta (e^{\gamma s}-1) - \frac{D(k_\beta^0)^2}{2\gamma}\left(e^{2\gamma s}-1\right)}. \tag{A.8}$$

Transforming the variable back from s to k's and t, and assuming a delta-function initial condition, $P(\boldsymbol{r},0) = \delta^n(\boldsymbol{r}-\boldsymbol{r}')$, the solution in the Fourier domain is given by

$$\hat{P}(\boldsymbol{k},\boldsymbol{r}',t) = e^{-i\boldsymbol{k}\cdot\boldsymbol{r}'e^{-\gamma t}} e^{-i\boldsymbol{r}_h\cdot\boldsymbol{k}(1-e^{-\gamma t}) - \frac{D\boldsymbol{k}^2}{2\gamma}(1-e^{-2\gamma t})}. \tag{A.9}$$

Inverse Fourier transforming this equation according to

$$\Pi(\boldsymbol{r},\boldsymbol{r}',t) \equiv \left(\frac{1}{2\pi}\right)^n \int_{-\infty}^{\infty}\cdots\int_{-\infty}^{\infty} d^n\boldsymbol{k} e^{i\boldsymbol{k}\cdot\boldsymbol{r}}\hat{P}(\boldsymbol{k},\boldsymbol{r}',t) \tag{A.10}$$

gives the propagator shown in equation (2.10) of the main text.

Appendix B

Reaction-Diffusion Theory in Arbitrary Number of Dimensions

In this Appendix we show explicitly how one may resolve the technical problem that arises for reaction-diffusion calculations involving encounters at a single point in 2-dimensions. The problem has been mentioned in our earlier work [57] where it has been pointed out that the solution lies simply in extending the reaction region from a point to a region of higher dimensions. We give supporting and explicit calculations below (this work, done in collaboration with Chase as well as my thesis advisor, is part of a preprint "S. Sugaya, M. Chase, and V. M. Kenkre, Comments on Reaction-Diffusion Theory in Dimensions Higher Than One"). Given that an infection problem involving two walkers meeting is equivalent to a trapping problem of a single representative walker in twice the number of dimensions [5], we work here only with a trapping problem.

Given that the point problem arises in the case also of a pure random walker (rather than a Smoluchowski random walker) we give our study in this Appendix

with a free (unconfined) walker that interacts with a stationary trap that captures the walker at a constant rate $\mathcal{C}$. The formalism to obtain the walker's survival probability, $\mathcal{Q}(t)$, is presented in Chapter 2. The expression of $\mathcal{Q}(t)$ in the Laplace domain, $\widetilde{\mathcal{Q}}(\epsilon)$, is found in equation (2.31), where it is given by the product of $\tilde{\mu}(\epsilon)$ and $1/(1/\mathcal{C} + \tilde{\nu}(\epsilon))$. In Chapter 5, it is shown that $\nu(t)$ yielded for the point trap in s-dimensions cannot be Laplace transformed because of its strongly divergent behavior at short times. Here, we assess, in 1 and 2-dimensions, how the short time behavior of $\nu(t)$ depends on the respective trap dimension to the dimension of the walker, and in turn affects the existence of $\tilde{\nu}(\epsilon)$. We do this by considering trap with various trap-dimensions and finding $\nu(t)$ for each type of trap considered. The long time behavior of such $\nu(t)$ is also analyzed to assure that its behavior toward $t \to \infty$ is appropriate for the existence of $\tilde{\nu}(t)$.

B.1 Calculation in 1-dimension

We consider three different traps for a 1-dimensional walker. The first of which is a single point, another one consists of two separated points, and the last one is a finite line segment. The point traps have one less dimension whereas the line-segment trap has the same dimension compared to that in which the motion of the walker occurs. The definition of $\nu(t)$ in s-dimensions is given in equation (5.20). For 1-dimension, $\nu(t)$ becomes

$$\nu(t) = \frac{\int dx_1 \int dx\, \Pi(x, x_1, t)}{\int dx_1}, \tag{B.1}$$

where the integrals of x and x_1 are over the trapping region. The propagator $\Pi(x, x', t)$ is given by

$$\Pi(x, x_1, t) = \frac{1}{\sqrt{4\pi D t}} e^{-\frac{(x-x_1)^2}{4Dt}}, \tag{B.2}$$

with D being the diffusion constant. We provide the description of each trap and present the corresponding $\nu(t)$ and analyze its short and long time behaviors below.

Single-Point Trap:

Without loss of generality, we place the trap at the origin. Then $\nu(t)$ is given exactly by

$$\begin{aligned}\nu(t) &= \frac{\int_{-\infty}^{\infty} dx_1 \delta(x_1) \int_{-\infty}^{\infty} dx \delta(x) \Pi(x, x_1, t)}{\int_{-\infty}^{\infty} dx_1 \delta(x_1)} \\ &= \Pi(0, 0, t) \\ &= \frac{1}{\sqrt{4\pi D t}}. \end{aligned} \tag{B.3}$$

Needless to say, the short and long time behaviors go as $\sim 1/\sqrt{t}$.

Two-Point Trap:

Let the two traps be separated by an arbitrary distance $2a$, and the origin be placed at the midpoint without loss of generality. Then $\nu(t)$ is given exactly by

$$\begin{aligned}\nu(t) &= \frac{\int_{-\infty}^{\infty} dx_1 \left[\delta(x_1 + a) + \delta(x_1 - a)\right] \int_{-\infty}^{\infty} dx \left[\delta(x + a) + \delta(x - a)\right] \Pi(x, x_1, t)}{\int_{-\infty}^{\infty} dx_1 \left[\delta(x_1 + a) + \delta(x_1 - a)\right]} \\ &= \frac{1}{2} \left[\Pi(-a, -a, t) + \Pi(a, -a, t) + \Pi(-a, a, t) + \Pi(a, a, t)\right] \\ &= \frac{1}{\sqrt{4\pi D t}} \left(1 + e^{-\frac{a^2}{Dt}}\right). \end{aligned} \tag{B.4}$$

We see that merely having two-point trap does not change the short and long time behaviors of $\nu(t)$, *i.e.*, it goes as $\sim 1/\sqrt{t}$. We note that $1/\sqrt{t}$ is the leading term in the case of $t \to \infty$.

A Finite-Segment Trap:

Let the length of the segment be $2a$ with the origin placed at the midpoint. Here,

$\nu(t)$ becomes an averaged quantity and is given by

$$\begin{aligned}\nu(t) &= \frac{\int_{-a}^{a} dx' \int_{-a}^{a} dx\, \Pi(x, x', t)}{\int_{-a}^{a} dx'} \\ &= \mathrm{erf}\left(\frac{a}{\sqrt{Dt}}\right) - \frac{\sqrt{4\pi Dt}}{\pi a} e^{-\frac{a^2}{2Dt}} \sinh\left(\frac{a^2}{2Dt}\right). \end{aligned} \tag{B.5}$$

When $t \to 0$, the argument of the error function becomes infinite and the first term becomes unity while the second term vanishes, resulting in $\nu(t \to 0) \to 1$. On the other hand the error function vanishes as $t \to \infty$, and the second term with the hyperbolic sine becomes $1/\sqrt{t}$, to the leading order. Hence, keeping to the leading order, $\nu(t \to \infty) \to a/\sqrt{\pi Dt}$.

The results of our calculation are summarized in Table B.1, and each $\nu(t)$ is plotted against time (scaled to $\tau_a = a^2/2D$, the diffusive time to ravel the distance a) in Figure B.1. The divergent behaviors for the point traps (dashed line for the single-point and dotted line for the two-point) and the convergent behavior for the line trap (solid line) is seen. Although $\nu(t)$ is divergent at $t = 0$ for the point traps, there is no problem in Laplace-transforming all the $\nu(t)$ presented above as we know that the integral of $1/\sqrt{t}$ evaluated at $t = 0$ is convergent. We point out that, for the trap of 1 dimension less than that of the walker, $\nu(t)$ diverges as $1/\sqrt{t}$ as $t \to 0$, whereas when the dimensions of the trapping region and of the walker's motion are the same, as in the finite-segment trap, $\nu(t)$ is convergent. We find a similar result in 2-dimensions.

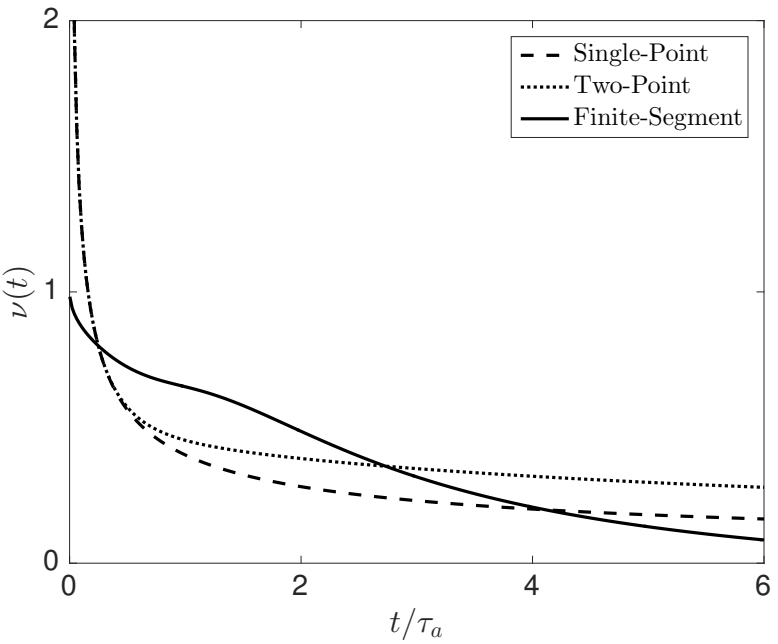

Figure B.1: The function $\nu(t)$ plotted against $t/\tau_a = a^2/2D$ where τ_a is the diffusive time to travel the distance a. The dashed, dotted, and solid curves correspond, respectively, to trap made up of a single point, two separate points, and of a finite segment. For point traps, $\nu(t)$ diverge as $t \to 0$, whereas it is convergent (to unity) for the line-segment.

B.2 Calculation in 2-dimensions

We repeat our calculations above in 2-dimensions, *i.e.*, we consider 0, 1, and 2-dimensional traps in 2-dimensions. Here, $\nu(t)$ is calculated by

$$\nu(t) = \frac{\int dx_1 dy_1 \int dx dy \Pi(x, x_1, y, y_1, t)}{\int dx_1 dy_1}, \tag{B.6}$$

where the propagator $\Pi(x, x_1, y, y_1, t)$ is

$$\Pi(x, x_1, y, y_1, t) = \frac{1}{4\pi D t} e^{-\frac{(x-x_1)^2+(y-y_1)^2}{4Dt}}. \tag{B.7}$$

We consider a point trap, an infinite-line trap, a ring trap, and a disk trap. A point trap has 2 dimensions less, an infinite-line and ring traps have 1 dimension less, and

Trap Type	$\nu(t)$	Short time	Long time
	$\frac{1}{\sqrt{4\pi Dt}}$	$\frac{1}{\sqrt{t}}$	$\frac{1}{\sqrt{t}}$
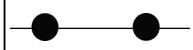	$\frac{1}{\sqrt{4\pi Dt}}\left(1+e^{-\frac{a^2}{Dt}}\right)$	$\frac{1}{\sqrt{t}}$	$\frac{1}{\sqrt{t}}$
	$\mathrm{erf}\left(\frac{a}{\sqrt{Dt}}\right)-\frac{\sqrt{4\pi Dt}}{\pi a}e^{-\frac{a^2}{2Dt}}\sinh\left(\frac{a^2}{2Dt}\right)$	1	$\frac{1}{\sqrt{t}}$

Table B.1: Summary of the analysis in 1-dimension. For each trap shape indicated by the picture on the left most column, the corresponding $\nu(t)$ and the short and long time behaviors are given.

a disk trap has the same dimension as that of the motion of the walker.

Point Trap:

We chose to place the trap at origin without loss of generality. $\nu(t)$ is given exactly by

$$\begin{aligned}\nu(t) &= \frac{\int_{-\infty}^{\infty}\int_{-\infty}^{\infty} dx_1 dy_1 \delta(x_1)\delta(y_1) \int_{-\infty}^{\infty}\int_{-\infty}^{\infty} dx dy \delta(x)\delta(y)\Pi(x,x_1,y,y_1,t)}{\int_{-\infty}^{\infty}\int_{-\infty}^{\infty} dx_1 dy_1 \delta(x_1)\delta(y_1)} \\ &= \Pi(0,0,0,0,t) \\ &= \frac{1}{4\pi Dt}. \end{aligned} \tag{B.8}$$

The short and long time behaviors are apparent from this expression and they both take the form of $1/t$.

Infinite-Line Trap:

Without loss of generality, we choose the infinite line to lie on the diagonal, $y = x$. For this case, $\nu(t)$ is exactly given by

$$\begin{aligned}\nu(t) &= \frac{\int_{-\infty}^{\infty}\int_{-\infty}^{\infty} dx_1 dy_1 \int_{-\infty}^{\infty}\int_{-\infty}^{\infty} dx dy \delta(y_1 - x_1)\delta(y - x)\Pi(x, x_1, y, y_1, t)}{\int_{-\infty}^{\infty}\int_{-\infty}^{\infty} dx_1 dy_1 \delta(y_1 - x_1)} \\ &= \frac{1}{\sqrt{8\pi D t}}. \end{aligned} \tag{B.9}$$

The short and long time behaviors are the same as that found for the point traps in 1-dimension and they go as $1/\sqrt{t}$.

Ring Trap:

We choose the center of the ring to be the origin without loss of generality, and let the radius of the ring be a. The calculation is easier performed in the polar coordinate where the coordinate transformation, $x, r \to \rho, \theta$, is made according to $\rho^2 = x^2 + y^2$, $\theta = \tan^{-1}(y/x)$. We obtain $\nu(t)$ in two steps; we calculate $\nu(\rho_1, \theta_1, t)$ first, and then find its average over the ring trap. The form of the transformed propagator is given by

$$\Pi(\rho, \rho_1, \theta, \theta_1, t) = \frac{1}{4\pi D t} e^{-\frac{\rho^2 + \rho_1^2 - 2\rho\rho_1\cos(\theta - \theta_1)}{4Dt}}. \tag{B.10}$$

With this, calculation of $\nu(\rho_1, \theta_1, t)$ yields

$$\begin{aligned}\nu(\rho_1, \theta_1, t) &= \int_0^{\infty} d\rho \int_0^{2\pi} \rho d\theta \, \frac{1}{2\pi\rho}\delta(\rho - a)\Pi(\rho, \rho_1, \theta, \theta_1, t) \\ &= \frac{1}{2\pi}\frac{1}{4\pi D t} e^{-\frac{\rho^2 + \rho_1^2}{4Dt}} \int_0^{2\pi} d\theta \, e^{\frac{2\rho\rho_1\cos(\theta - \theta_1)}{4Dt}} \Big|_{\rho = a}. \end{aligned} \tag{B.11}$$

The integral becomes a modified Bessel function of zero-th order [12], and due to the azimuthal symmetry of the trap, the resulting quantity becomes independent of θ_1. We here define $\nu_{\text{ring}}(\rho, \rho_1, t)$ as

$$\nu_{\text{ring}}(\rho, \rho_1, t) = \frac{1}{4\pi D t} e^{-\frac{\rho^2 + \rho_1^2}{4Dt}} \mathrm{I}_0\left(\frac{\rho\rho_1}{2Dt}\right), \tag{B.12}$$

where we have left the ρ a variable, as this function becomes useful in the calculation for a disk trap. Using the ν-function method, $\nu(t)$ for the ring trap is obtained by taking the average over the ring:

$$\begin{aligned}\nu(t) &= \frac{\int_0^\infty d\rho_1 \int_0^{2\pi} \rho_1 d\theta_1 \frac{1}{2\pi\rho_1}\delta(\rho_1 - a)\nu_{\text{ring}}(a, \rho_1, t)}{\int_0^\infty d\rho_1 \int_0^{2\pi} \rho_1 d\theta_1 \frac{1}{2\pi\rho_1}\delta(\rho_1 - a)} \\ &= \frac{1}{4\pi Dt} e^{-\frac{a^2}{2Dt}} \mathrm{I}_0\left(\frac{a^2}{2Dt}\right). \end{aligned} \tag{B.13}$$

When $t \to 0$, the argument of the Bessel function becomes large, hence the asymptotic form of the function is appropriate, where $\mathrm{I}_0(z) \sim e^z/\sqrt{z}$ for large z [50]. This approximation gives the short time behavior as $\nu(t \to 0) \to 1/\sqrt{4\pi Dt}$. For $t \to \infty$, the argument of the Bessel function becomes small and the Bessel function approaches unity so does the exponential function, yielding $\nu(t) \sim 1/4\pi Dt$ to the leading order.

Disk Trap:

Let the radius of the disk be a. We can obtain $\nu(t)$ for a disk trap from $\nu_{\text{ring}}(\rho, \rho_1, t)$ given in equation (B.12) by integrating the radius from 0 to a, *i.e.*,

$$\nu(t) = \frac{\int_0^a d\rho_1\, 2\pi\rho_1 \int_0^a d\rho\, 2\pi\rho\, \nu_{\text{ring}}(\rho, \rho_1, t)}{\int_0^a d\rho_1\, 2\pi\rho_1} \tag{B.14}$$

$$= \frac{2}{a^2}\int_0^a d\rho_1 \int_0^a d\rho\, \frac{\rho\rho_1}{2Dt} e^{-\frac{\rho^2+\rho'^2}{4Dt}} \mathrm{I}_0\left(\frac{\rho\rho_1}{2Dt}\right), \tag{B.15}$$

where a is the radius of the disk, and the quadrature requires a numerical evaluation. Because the integrals are over the spatial variable, we can perform the analysis to find the short and long time behaviors nonetheless. For $t \to 0$, we express the Bessel function in its asymptotic form as was done for the ring trap case, and yield the integrand to become $\sqrt{\rho\rho_1}\delta(\rho - \rho_1)$. Note that we have used the definition of delta-function given by

$$\delta(\rho - \rho_1) = \lim_{t\to 0^+} \frac{1}{\sqrt{4\pi Dt}} e^{-\frac{(\rho-\rho_1)^2}{4Dt}}. \tag{B.16}$$

We see now that the short-time behavior is given by $\nu(t \to 0) \sim 1$. In the other limit, $t \to \infty$, the Bessel and exponential functions become unity and $\nu(t \to \infty) \sim 1/4\pi Dt$.

Disk Trap with Radius-dependent Capture Rate $\mathcal{C}(\rho)$:

We conclude this series of calculations by considering a case that includes radius-dependent capture rate, $\mathcal{C}(\rho)$, for a future application. For this case, the definition of $\nu(t)$ needs modification to accommodate the effect due to $\mathcal{C}(\rho)$. Following the formalism found in Chapter 2, but employing an averaging approximation, the survival probability appropriate for this case is found to be, in the Laplace domain,

$$\widetilde{\mathcal{Q}}(\epsilon) = \frac{1}{\epsilon}\left[1 - \frac{\tilde{\mu}(\epsilon)/\mathcal{C}}{1/\mathcal{C} + \tilde{\nu}(\epsilon)/\mathcal{C}}\right], \tag{B.17}$$

where $\mathcal{C}$, and corresponding $\mu(t)$, and $\nu(t)$ are given by

$$\mathcal{C} = \int d^s r\, \mathcal{C}(\boldsymbol{r}), \tag{B.18}$$

$$\mu(t) = \int d^s r\, \mathcal{C}(\boldsymbol{r})\eta(\boldsymbol{r}, t), \tag{B.19}$$

$$\nu(t) = \frac{\int d^s r_1 \int d^s r\, \mathcal{C}(\boldsymbol{r})\Pi(\boldsymbol{r}, \boldsymbol{r}_1, t)}{\int d^s r_1}, \tag{B.20}$$

where $\eta(\boldsymbol{r}, t)$ is the homogeneous solution, and the integrals over r and r_1 are to be performed over the trap region. Under the averaging approximation, in 2-dimensions, $\nu(t)$ becomes

$$\nu(t) = \frac{\int_0^a d\rho_1\, 2\pi\rho_1 \int_0^a d\rho\, 2\pi\rho\, \mathcal{C}(\rho)\nu_{\text{ring}}(\rho, \rho_1, t)}{\int_0^a d\rho_1\, 2\pi\rho_1}, \tag{B.21}$$

and specifically for the disk trap,

$$\nu(t) = \frac{2}{a^2}\int_0^a d\rho_1 \int_0^a d\rho\, \mathcal{C}(\rho)\frac{\rho\rho_1}{2Dt} e^{-\frac{\rho^2+\rho_1^2}{4Dt}} \mathrm{I}_0\left(\frac{\rho\rho_1}{2Dt}\right). \tag{B.22}$$

The short- and long-time behaviors are as seen for the disk trap with a constant capture rate, and therefore,

$\nu(t \to 0) \to \int_0^a d\rho\, \rho\, \mathcal{C}(\rho)$ and $\nu(t \to \infty) \to (1/a^2 Dt) \int_0^a d\rho \int_0^a d\rho'\, \rho\rho'\, \mathcal{C}(\rho)$.

The result of the calculations is summarized in Table B.2 where we plot in Figure B.2 $\nu(t)$ for a point, an infinite-segment, a ring, and a disk traps (only for a constant $\mathcal{C}$). In the figure, $\nu(t)$ is shown against time scaled to $\tau_a = a^2/2D$, and dashed, dotted, dash-dotted, and solid lines correspond to a point, an infinite line, a ring, and a disk traps, respectively. The short-time behaviors of the first three are divergent, and that of the disk is convergent. As seen from Table B.2, the divergence of $\nu(t)$ for the infinite line and the ring traps occurs as $1/\sqrt{t}$, which allows for the existence of the corresponding Laplace transforms. In contrast, in the case of a point trap, the divergence of $1/t$ is too strong for the $\tilde{\nu}(\epsilon)$ to exist.

The calculations in 1 and 2-dimensions that we have displayed suggest that the Laplace transform of $\nu(t)$ cannot be found when the dimensionality of the trap is more than 1-dimension smaller than that of the walker, due to the strongly divergent behavior of such $\nu(t)$ at $t = 0$. Moreover, our calculations indicate that when the trap-dimension is the same as the walker-dimension, $\nu(t)$ is convergent at $t = 0$. When the former is 1-dimension less than the latter, then $\nu(t)$ is divergent as $\nu(t) \sim t^{-1/2}$, and for any smaller trap-dimensions, the $\nu(t)$ diverges stronger. We thus suggest that the trapping in $(s-1)$-dimensions or higher where the walker moves in s-dimensions presents no divergence problems of the kind we have discussed.

Trap Type	$\nu(t)$	Short time	Long time
	$\frac{1}{4\pi Dt}$	$\frac{1}{t}$	$\frac{1}{t}$
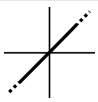	$\frac{1}{\sqrt{8\pi Dt}}$	$\frac{1}{\sqrt{t}}$	$\frac{1}{\sqrt{t}}$
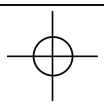	$\frac{1}{4\pi Dt} e^{-\frac{a^2}{2Dt}} \mathrm{I}_0\left(\frac{a^2}{2Dt}\right)$	$\frac{1}{\sqrt{t}}$	$\frac{1}{t}$
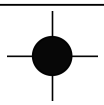	$\frac{2}{a^2}\int_0^a d\rho' \int_0^a d\rho\, \frac{\rho\rho'}{2Dt} e^{-\frac{\rho^2+\rho'^2}{4Dt}} \mathrm{I}_0\left(\frac{\rho\rho'}{2Dt}\right)$	1	$\frac{1}{t}$
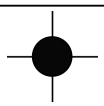	$\frac{2}{a^2}\int_0^a d\rho' \int_0^a d\rho\, \mathcal{C}(\rho) \frac{\rho\rho'}{2Dt} e^{-\frac{\rho^2+\rho'^2}{4Dt}} \mathrm{I}_0\left(\frac{\rho\rho'}{2Dt}\right)$	$\int_0^a d\rho\ \rho\mathcal{C}(\rho)$	$\frac{1}{t}$

Table B.2: A summary of 2-dimensional calculation. Each trap type is depicted in the left-most column, and corresponding $\nu(t)$ and its short and long time behaviors are given. The last row is the result for the disk trap with radius-dependent capture rate while the second row gives that for a constant rate.

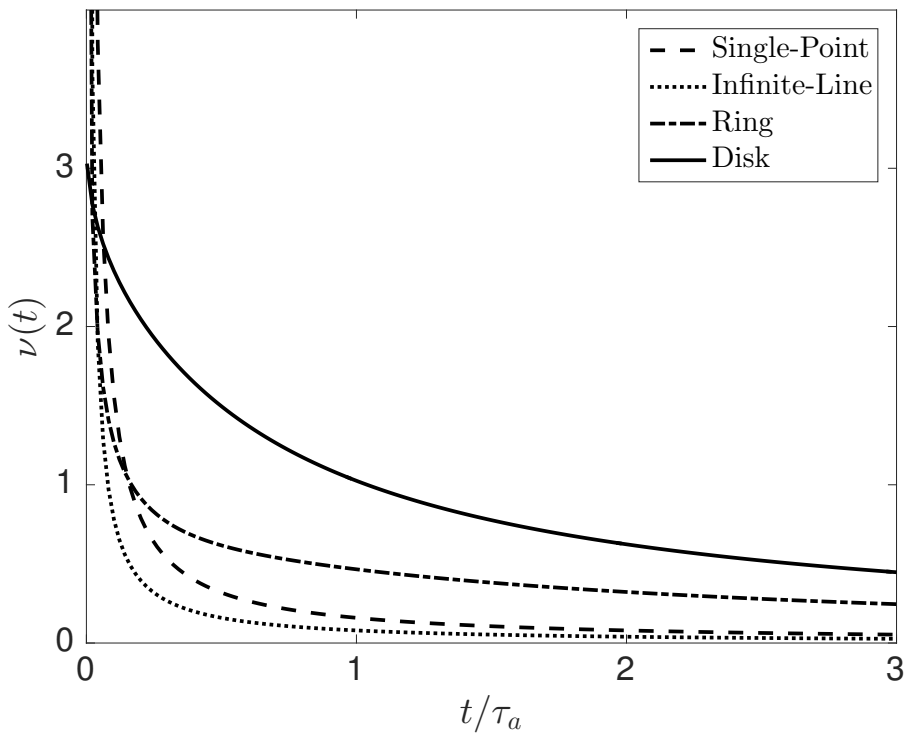

Figure B.2: $\nu(t)$ plotted against $t/\tau_a = a^2/2D$. The dashed, dotted, dash-dotted, and solid curves corresponds to $\nu(t)$ for a point, an infinite line, a ring, and a disk traps.

Appendix C

Transformation of the Homogeneous Smoluchowski Equation to Center of Mass and Relative Coordinates

In this Appendix, we show that the form of the homogeneous Smoluchowski equation describing the probability density, $P(\boldsymbol{r}_1, \boldsymbol{r}_2, t)$, to find the first walker at $\boldsymbol{r}_1$ and the second at $\boldsymbol{r}_2$ at time t, in an arbitrary number of dimensions in the Cartesian coordinate, is preserved when it is transformed to the center of mass (CM) and relative coordinates, via the transformation given equation (5.6) of Chapter 5. The Smoluchowski equation in the Cartesian coordinate is

$$\frac{\partial P(\boldsymbol{r}_1, \boldsymbol{r}_2, t)}{\partial t} = \nabla_1 \cdot \left[\gamma \left(\boldsymbol{r}_1 - \boldsymbol{R}_1\right) P(\boldsymbol{r}_1, \boldsymbol{r}_2, t)\right] + \nabla_2 \cdot \left[\gamma \left(\boldsymbol{r}_2 - \boldsymbol{R}_2\right) P(\boldsymbol{r}_1, \boldsymbol{r}_2, t)\right] + D\left(\nabla_1^2 + \nabla_2^2\right) P(\boldsymbol{r}_1, \boldsymbol{r}_2, t), \tag{C.1}$$

where $\boldsymbol{R}_1$ and $\boldsymbol{R}_2$ are the positions of the home-center of the first and second walker, respectively. According to the specific form of the transformation given, the differ-

ential operators in the Cartesian coordinate and CM and relative coordinates are related by

$$\nabla_{\pm} = \frac{1}{\sqrt{2}} \left(\nabla_1 \pm \nabla_2 \right) \quad \Rightarrow \quad \nabla_{1,2} = \frac{1}{\sqrt{2}} \left(\nabla_+ \pm \nabla_- \right). \tag{C.2}$$

First, we apply this transformation to the terms presenting the attraction of the walkers to the respective potential centers. The first two terms of equation (C.1) transforms as

$$\begin{aligned}
&\nabla_1 \cdot \left[\gamma \left(\boldsymbol{r}_1 - \boldsymbol{R}_1 \right) P(\boldsymbol{r}_1, \boldsymbol{r}_2, t) \right] + \nabla_2 \cdot \left[\gamma \left(\boldsymbol{r}_2 - \boldsymbol{R}_2 \right) P(\boldsymbol{r}_1, \boldsymbol{r}_2, t) \right] \\
&= \gamma \left[\frac{1}{\sqrt{2}} \left(\nabla_+ + \nabla_- \right) \cdot \left(\boldsymbol{r}_1 - \boldsymbol{R}_1 \right) + \frac{1}{\sqrt{2}} \left(\nabla_+ - \nabla_- \right) \cdot \left(\boldsymbol{r}_1 - \boldsymbol{R}_1 \right) \right] P(\boldsymbol{r}_1, \boldsymbol{r}_2, t) \\
&= \gamma \left[\nabla_+ \cdot \left\{ \frac{1}{\sqrt{2}} \left(\boldsymbol{r}_1 + \boldsymbol{r}_2 \right) - \frac{1}{\sqrt{2}} \left(\boldsymbol{R}_1 + \boldsymbol{R}_2 \right) \right\} \right. \\
&\qquad \left. + \nabla_- \cdot \left\{ \frac{1}{\sqrt{2}} \left(\boldsymbol{r}_1 - \boldsymbol{r}_2 \right) - \frac{1}{\sqrt{2}} \left(\boldsymbol{R}_1 - \boldsymbol{R}_2 \right) \right\} \right] P(\boldsymbol{r}_1, \boldsymbol{r}_2, t) \\
&= \nabla_+ \cdot \left[\gamma \left(\boldsymbol{r}_+ - \boldsymbol{R}_+ \right) P(\boldsymbol{r}_+, \boldsymbol{r}_-, t) \right] + \nabla_- \cdot \left[\gamma \left(\boldsymbol{r}_- - \boldsymbol{R}_- \right) P(\boldsymbol{r}_+, \boldsymbol{r}_-, t) \right],
\end{aligned} \tag{C.3}$$

where in arriving at the last line from the third one, we have used the definitions of $\boldsymbol{r}_{\pm}$ and $\boldsymbol{R}_{\pm}$ given in equations (5.6) and (5.8), respectively. Next, we focus on the pure diffusion term, the third term of equation (C.1). The Laplacians, ∇_1^2 and ∇_2^2, in terms of ∇_+ and ∇_- via equation C.2) become

$$\nabla_1^2 = \frac{1}{2} \left(\nabla_+ + \nabla_- \right) \cdot \left(\nabla_+ + \nabla_- \right) = \frac{1}{2} \left(\nabla_+^2 + \nabla_+ \nabla_- + \nabla_- \nabla_+ + \nabla_-^2 \right), \tag{C.4}$$

$$\nabla_2^2 = \frac{1}{2} \left(\nabla_+ - \nabla_- \right) \cdot \left(\nabla_+ - \nabla_- \right) = \frac{1}{2} \left(\nabla_+^2 - \nabla_+ \nabla_- - \nabla_- \nabla_+ + \nabla_-^2 \right). \tag{C.5}$$

The addition of these quantities yields

$$\nabla_1^2 + \nabla_2^2 = \nabla_+^2 + \nabla_-^2, \tag{C.6}$$

and hence the pure diffusion term transforms to

$$D \left(\nabla_1^2 + \nabla_2^2 \right) P(\boldsymbol{r}_1, \boldsymbol{r}_2, t) = D \left(\nabla_+^2 + \nabla_-^2 \right) P(\boldsymbol{r}_+, \boldsymbol{r}_-, t). \tag{C.7}$$

Putting these results together the homogeneous Smoluchowski equation in the CM and relative coordinate is given by

$$\frac{\partial P(\boldsymbol{r}_+, \boldsymbol{r}_-, t)}{\partial t} = \nabla_+ \cdot \left[\gamma \left(\boldsymbol{r}_+ - \boldsymbol{R}_+\right) P(\boldsymbol{r}_+, \boldsymbol{r}_-, t)\right] + \nabla_- \cdot \left[\gamma \left(\boldsymbol{r}_- - \boldsymbol{R}_-\right) P(\boldsymbol{r}_+, \boldsymbol{r}_-, t)\right] + D\left(\nabla_+^2 + \nabla_-^2\right) P(\boldsymbol{r}_+, \boldsymbol{r}_-, t), \tag{C.8}$$

and we show that form of equation (C.1) is preserved under the transformation given in equation (5.6).

Appendix D

Finite-range Infection in $1D$

The equation of motion for the configuration $P(x_+, x_-, t)$, to find the CM location of the mice at x_+ and relative location at x_- at time t, for a 1-dimensional finite-range infection is

$$\begin{aligned}\frac{\partial P(x_+,x_-,t)}{\partial t} = &\frac{\partial}{\partial x_+}\gamma\left(x_+ - h_+\right)P(x_+,x_-,t) + \frac{\partial}{\partial x_-}\gamma\left(x_- - h_-\right)P(x_+,x_-,t)\\ &+ D\left(\frac{\partial^2}{\partial x_+^2} + \frac{\partial^2}{\partial x_-^2}\right)P(x_+,x_-,t)\\ &- \mathcal{C}_1\delta\left(x_- - A\right)P(x_+,x_-,t) - \mathcal{C}_1\delta\left(x_- + A\right)P(x_+,x_-,t),\end{aligned} \tag{D.1}$$

where A is the infection range in this coordinate, the first three terms represent the Smoluchowski motion, and the infection transmission is described in the last two terms. The infection is transmitted to the susceptible mouse from the infected one when they are a distance A apart, *i.e.*, when $x_- = \pm A$, as indicated by the arguments of the delta functions, and at a 1-dimensional infection rate $\mathcal{C}_1$. Because there are only two locations at which a transmission of infection occur, $\tilde{\nu}(\epsilon)$ can be calculated exactly without the use of the ν-function method. The propagator for this problem

is given by

$$\Pi(x_+, x'_+, x_-, x'_-, t) = \frac{1}{4\pi D\mathcal{T}(t)} e^{-\frac{\left(x_+ - h_+ - (x'_+ - h_+)e^{-\gamma t}\right)^2 + \left(x_- - h_- - (x'_- - h_-)e^{-\gamma t}\right)^2}{4D\mathcal{T}(t)}}. \quad \text{(D.2)}$$

The procedure to arrive at $\widetilde{\mathcal{I}}(\epsilon)$ for this specific case starts to deviate from the general method presented earlier in section 5.1.1 at equation (5.16), which for this case becomes

$$\widetilde{\mathcal{I}}(\epsilon) = \frac{\mathcal{C}_1}{\epsilon}\left[\int_{-\infty}^{\infty} dx_+ \widetilde{P}(x_+, A, \epsilon) + \int_{-\infty}^{\infty} dx_+ \widetilde{P}(x_+, -A, \epsilon)\right]. \quad \text{(D.3)}$$

To calculate the quantity in the square parenthesis, we start with the counter part of equation (5.11) specific for 1-dimensional finite-range infection, which is

$$\begin{aligned}\tilde{P}(x_+, x_-, \epsilon) = \tilde{\eta}(x_+, x_-, \epsilon) \\ - \mathcal{C}_1 \int_{-\infty}^{\infty} dx'_+ \tilde{\Pi}(x_+, x'_+, x_-, -A, \epsilon)\tilde{P}(x'_+, -A, \epsilon) \\ - \mathcal{C}_1 \int_{-\infty}^{\infty} dx'_+ \tilde{\Pi}(x_+, x'_+, x_-, A, \epsilon)\tilde{P}(x'_+, A, \epsilon). \end{aligned} \quad \text{(D.4)}$$

Use of the defect technique, *i.e.*, setting $x_- = \pm A$ and integrating x_+ over all space, after some algebra, yields

$$\begin{aligned}&\int_{-\infty}^{\infty} dx_+ \widetilde{P}(x_+, A, \epsilon) + \int_{-\infty}^{\infty} dx_+ \widetilde{P}(x_+, -A, \epsilon) \\ &= \frac{1}{\mathcal{C}_1} \frac{\left[1/\mathcal{C}_1 + \tilde{\nu}^{++}(\epsilon) - \tilde{\nu}^{+-}(\epsilon)\right]\tilde{\mu}^-(\epsilon) + \left[1/\mathcal{C}_1 + \tilde{\nu}^{--}(\epsilon) - \tilde{\nu}^{-+}(\epsilon)\right]\tilde{\mu}^+(\epsilon)}{\left[1/\mathcal{C}_1 + \tilde{\nu}^{--}(\epsilon)\right]\left[1/\mathcal{C}_1 + \tilde{\nu}^{++}(\epsilon)\right] - \tilde{\nu}^{-+}(\epsilon)\tilde{\nu}^{+-}(\epsilon)}, \end{aligned} \quad \text{(D.5)}$$

where

$$\mu^{+}(t) = \int_{-\infty}^{\infty} dx_{+}\eta(x_{+}, A, t) = \frac{1}{\sqrt{4\pi D\mathcal{T}(t)}}\, e^{-\frac{\left(A-H-(x_{-}^{0}-H)e^{-\gamma t}\right)^{2}}{4D\mathcal{T}(t)}} \tag{D.6}$$

$$\mu^{-}(t) = \int_{-\infty}^{\infty} dx_{+}\eta(x_{+}, -A, t) = \frac{1}{\sqrt{4\pi D\mathcal{T}(t)}}\, e^{-\frac{\left(A+H+(x_{-}^{0}-H)e^{-\gamma t}\right)^{2}}{4D\mathcal{T}(t)}} \tag{D.7}$$

$$\nu^{++}(t) = \int_{-\infty}^{\infty} dx_{+}\Pi(x_{+}, A, x'_{+}, A) = \frac{1}{\sqrt{4\pi D\mathcal{T}(t)}}\, e^{-\frac{\left[(A-H)(1-e^{-\gamma t})\right]^{2}}{4D\mathcal{T}(t)}} \tag{D.8}$$

$$\nu^{+-}(t) = \int_{-\infty}^{\infty} dx_{+}\Pi(x_{+}, A, x'_{+}, -A) = \frac{1}{\sqrt{4\pi D\mathcal{T}(t)}}\, e^{-\frac{\left[A-H+(A+H)e^{-\gamma t}\right]^{2}}{4D\mathcal{T}(t)}} \tag{D.9}$$

$$\nu^{-+}(t) = \int_{-\infty}^{\infty} dx_{+}\Pi(x_{+}, -A, x'_{+}, A) = \frac{1}{\sqrt{4\pi D\mathcal{T}(t)}}\, e^{-\frac{\left[A+H+(A-H)e^{-\gamma t}\right]^{2}}{4D\mathcal{T}(t)}} \tag{D.10}$$

$$\nu^{--}(t) = \int_{-\infty}^{\infty} dx_{+}\Pi(x_{+}, -A, x'_{+}, -A) = \frac{1}{\sqrt{4\pi D\mathcal{T}(t)}}\, e^{-\frac{\left[(A+H)(1-e^{-\gamma t})\right]^{2}}{4D\mathcal{T}(t)}}. \tag{D.11}$$

Note that in the calculation of the $\mu(t)$'s, the delta-function initial condition was assumed. With this, the infection rate in the Laplace domain is given exactly by

$$\widetilde{\mathcal{I}}(\epsilon) = \frac{1}{\epsilon}\frac{\left[1/\mathcal{C}_1 + \tilde{\nu}^{++}(\epsilon) - \tilde{\nu}^{+-}(\epsilon)\right]\tilde{\mu}^{-}(\epsilon) + \left[1/\mathcal{C}_1 + \tilde{\nu}^{--}(\epsilon) - \tilde{\nu}^{-+}(\epsilon)\right]\tilde{\mu}^{+}(\epsilon)}{\left[1/\mathcal{C}_1 + \tilde{\nu}^{--}(\epsilon)\right]\left[1/\mathcal{C}_1 + \tilde{\nu}^{++}(\epsilon)\right] - \tilde{\nu}^{-+}(\epsilon)\tilde{\nu}^{+-}(\epsilon)}. \tag{D.12}$$

Now, considering the contact limit where $1/\mathcal{C}_1$ is much greater than any of the $\nu(t)$'s and $\mu(t)$'s in its effect, and where it is appropriate to replace all the $\mu(t)$'s and $\nu(t)$'s by their steady state counter parts, the infection probability is given approximately by

$$\mathcal{I}(t) \sim \mathcal{C}_1\left(\mu^{+}(\infty) + \mu^{-}(\infty)\right)\cdot t, \tag{D.13}$$

where we note that $\nu^{++}(\infty) = \nu^{+-}(\infty) = \mu^{+}(\infty)$ and $\nu^{--}(\infty) = \nu^{-+}(\infty) = \mu^{-}(\infty)$. The condition for the optimal value of $\gamma\tau_H$ value found from this result yields the transcendental relation given in equation (5.42).

References

[1] M. V. Smoluchowski. Drei Vortrage uber Diffusion, Brownsche Bewegung und Koagulation von Kolloidteilchen. *Zeitschrift fur Physik*, 17:557–585, 1916.

[2] E. W. Montroll and B. West. Scattering of waves by irregularities in periodic discrete lattice spaces. i. reduction of problem to quadratures on a discrete model of the schrdinger equation. *Journal of Statistical Physics*, 13(1):17–42, feb 1975.

[3] V. M. Kenkre and Y. M. Wong. Theory of migration experiments with imperfectly absorbing end detectors. *Physical Review B*, 22(12):5716–5722, dec 1980.

[4] V. M. Kenkre and Y. M. Wong. Effect of transport coherence on trapping: Quantum-yield calculations for excitons in molecular crystals. *Physical Review B*, 23(8):3748–3755, apr 1980.

[5] V. M. Kenkre. Theory of exciton annihilation in molecular crystals. *Physical Review B*, 22(4):2089–2098, aug 1980.

[6] V. M. Kenkre. A theoretical approach to exciton trapping in systems with arbitrary trap concentration. *Chemical Physics Letters*, 93(3):260–263, dec 1982.

[7] V. M. Kenkre and P. E. Parris. Exicton trapping and sensitized luminescence: A generalized theory for all trap concentrations. *Physical Review B*, 27(6):3221–3234, mar 1983.

[8] V. M. Kenkre, P. E. Parris, and D. Schmid. Investigation of the appropriateness of sensitized luminescence to determine exciton motion parameters in pure molecular crystals. *Physical Review B*, 32(8):4946, oct 1985.

[9] A. Szabo, G. Lamm, and G. H. Weiss. Localized partial traps in diffusion processes and random walks. *Journal of Statistical Physics*, 34(1):225–238, jan 1984.

[10] S. Redner and D. ben Avraham. Nearest-neighbor distances of diffusing particles from a single trap. *Journal of Physics A: Math. Gen.*, 23:L1169, sep 1990.

[11] G. Abramson and H. S. Wio. Time behaviour for diffusion in the presence of static imperfect traps. *Chaos, Solitons & Fractals*, 6(1):1–5, 1995.

[12] K. Spendier and V. M. Kenkre. Analytic solution for some reaction-diffusion scenarios. *The Journal of Theoretical Chemistry B*, 117:15639–15650, jul 2013.

[13] R. M. Anderson and R. M. May. *Infectious Disease of Humans*. Oxford University Press Inc., New York, 1995.

[14] H. W. Hethcote. The mathematics of infectious diseases. *SIAM Review*, 42(4):599–653, 2000.

[15] A. Okubo and S. A. Levin. *Diffusion and Ecological Problems*. Springer, New York, second edition, 2001.

[16] R. S. Cantrell and C. Cosner. *Spatial Ecology Via Reaction-diffusion Equations*. Wiley, Chichester, England, 2003. In Wiley Series in Mathematical and Computational Biology.

[17] E. E. Holmes, M. A. Lewis, J. E. Banks, and R. R. Veit. Partial differential equations in ecology: Spatial interactions and population dynamics. *Ecology*, 75(1):17–29, jan 1994.

[18] G. Abramson and V. M. Kenkre. Spatiotemporal patters in the hantavirus infection. *Physical Review E*, 66(1):011912, jul 2002.

[19] G. Abramson, V. M. Kenkre, T. L. Yates, and R. R. Parmenter. Traveling waves of infection in the hantavirus epidemics. *Bulletin of Mathematical Biology*, 65:519–534, 2003.

[20] T. C. Reluga, J. Medlock, and A. P. Galavani. A model of spatial epidemic spread when individuals move within overlapping home ranges. *Bulletin of Mathematical Biology*, 68:401–416, apr 2006.

[21] V. M. Kenkre, L. Giuggioli, G. Abramson, and G. Camelo-Neto. Theory of hantavirus infection spread incororating localized adult and itinerant juvenile mice. *European Physical Journal B*, 55:461–470, mar 2007.

[22] N. Kumar, R. R. Parmenter, and V. M. Kenkre. Extinction of refugia of hantavirus infection in a spatially heterogeneous environment. *Physical Review E*, 82(1):011920, jul 2010.

[23] G. Abramson, L. Giuggioli, R. R. Parmenter, and V. M. Kenkre. Quasi-one-dimensional waves in rodent populations in heterogeneous habitats: A consequence of elevational gradients on spatio-temporal dynamics. *Journal of Theoretical Biology*, 319:96–101, dec 2013.

[24] L. Giuggioli and V. M. Kenkre. Consequences of animal interactions on their dynamics: Emergence of home ranges and territoriality. *Movement Ecology*, 2:20–41, 2014.

[25] C. Schmaljohn and B. Hjelle. Hantavirus: A global disease problem. *Emerging Infectious Diseases*, 3(2):95–104, apr 1997.

[26] J. N. Mills, T. L. Yates, T. G. Ksiazek, G. J. Peters, and J. E. Childs. Long-term studies of hantavirus reservoir populations in the southwestern united states: Rationale, potential, and methods. *Emerging Infectious Diseases*, 5(1):95–101, jan 1999.

[27] K. D. Abbott, T. G. Ksiazek, and J. N. Mills. Long-term hantavirus persistence in rodent populations in central arizona. *Emerging Infectious Diseases*, 5(1):102–112, jan 1999.

[28] A. J. Kuenzi, M. L. Morrison, D. E. Swann, P. C. Hardy, and G. T. Downard. A longitudinal study of sin nombre virus prevalence in rodents, southeastern arizona. *Emerging Infectious Diseases*, 5(1):113–117, jan 1999.

[29] C. A. Parmenter, T. L. Yates, R. R. Parmenter, and J. L. Dunnum. Statistical sensitivity for detection of spatial and temporal patterns in rodent population densities. *Emerging Infectious Diseases*, 5(1):118–125, jan 1999.

[30] C. H. Calisher, W. Sweeney, J. N. Mills, and B. J. Beaty. Natural history of sin nombre virus in western colorado. *Emerging Infectious Diseases*, 5(1):126–134, jan 1999.

[31] J. N. Mills, T. G. Ksiazek, G. J. Peters, and J. E. Childs. Long-term studies of hantavirus reservoir populations in the southwestern united states: A synthesis. *Emerging Infectious Diseases*, 5(1):135–142, jan 1999.

[32] G. E. Glass, J. E. Cheek, J. A. Patz, T. M. Shields, T. J. Doyle, D. A. Thoroughman, D. K. Hunt, R. E. Enscore, K. L. Gage, C. Irland, C. J. Peters, and R. Bryan. Using remotely sensed data to identify areas at risk for hantavirus pulmonary syndrome. *Emerging Infectious Disease*, 6(3):238–247, may 2000.

[33] T. L. Yates, J. N. Mills, C. A. Parmenter, T. G. Ksiazek, R. R. Parmenter, J. R. vande Castle, C. H. Calisher, S. T. Nichol, K. D. Abbott, J. C. Young, M. L.

Morrison, B. J. Beaty, J. L. Dunnum, R. J. Baker, J. Salazar-Bravo, and C. J. Peters. The ecology and evolutionary history of an emergent disease: Hantavirus pulmonary syndrome. *Bio Science*, 52(11):989, nov 2002.

[34] J. D. Murray. *Mathematical Biology I: An Introduction*, volume I. Springer, New York, third edition, 2004.

[35] G. Abramson, V. M. Kenkre, and A. R. Bishop. Analytic solutions for nonlinear waves in coupled reacting systems. *Physica A*, 305:427–436, 2002.

[36] M. A. Aguirre, G. Abramson, A. R. Bishop, and V. M. Kenkre. Simulations in the mathematical modeling of the spread of the hantavirus. *Physical Review E*, 66(4):041908, oct 2002.

[37] 242-248 (2004). V. M. Kenkre Physica A 342. Results from variants of the fisher equation in the study of epidemics and bacteria. *Physica A*, 342:242–248, may 2004.

[38] L. Giuggioli, G. Abramson, V. M. Kenkre, G. Suzán, and E. Marcé T. L. Yates. Diffusion and home range parameters from rodent population measurements in panama. *Bulletin of Mathematical Biology*, 67:1135–1149, 2005.

[39] V. M. Kenkre. Statistical mechanical considerations in the theory of the spread of the hantavirus. *Physica A*, 356:121–126, jun 2005.

[40] G. Abramson, L. Giuggioli, V. M. Kenkre, J. D. Dragoo, R. R. Parmenter, C. A. Parmenter, and T. L. Yates. Diffusion and home range parameters for rodents: Peromyscus maniculatus in new mexico. *Ecological Complexity*, 3:64–67, 2006.

[41] L. Giuggioli, G. Abramson, V. M. Kenkre, R. P. Parmenter, and T. L. Yates. Theory of home range estimation from displacement measurements of animal populations. *Journal of Theoretical Biology*, 240:126–135, oct 2006.

[42] G. Camelo-Neto, A. T. C. Silva, L. Giuggioli, and V. M. Kenkre. Effect of predators of juvenile rodents on the spread of the hantavirus epidemic. *Bulletin of Mathematical Biology*, 70:179–188, aug 2008.

[43] V. M. Kenrke and N. Kumar. Nonlinearity in bacterial population dynamics: Proposal for experiments for the observation of abrupt transitioins in patches. *PNAS*, 105(48):18752–18757, dec 2008.

[44] D. R. MacInnis. *Applicatios of Nonlinear Science and Kinetic Equations to the Spread of Epidemics*. Ph.D., The University of New Mexico, Albuquerque, NM, May 2007.

[45] Hannes Risken. *The Fokker-Plank Equation: Methods of Solution and Applications, Second Ed.* Springer-Verlag, Germany, 1989.

[46] D. P. Gaver Jr. Observing stochastic processes, and approximate transform inversion. *Operations Research*, 14(3):444–459, jun 1966.

[47] Josheph Abate and Ward Whitt. Aunified framework for numerically inverting laplace transforms. *INFORMS Journal on Computing*, 18(4):408?421, 2006.

[48] K. Spendier, S. Sugaya, and V. M. Kenkre. Reaction-diffusion theory in the presence of an attractive harmonic potential. *Physical Review E*, 88(6):062142, dec 2013.

[49] K. Spendier. *Dynamics and distribution of immunoglobolin E receptors : a dialog between experiment and theory.* Ph.D., The University of New Mexico, Albuquerque, NM, May 2012.

[50] M. Abramowitz and I. A. Stegun. *Handbook of Mathematical Functions.* Dover Publications, Toronto, 1970.

[51] German Drazer, Horacio S. Wio, and Constantino Tsallis. Anomalous diffusion with absorption: Exact time-dependent solutions. *Physical Review E*, 61(2):1417–1422, feb 2000.

[52] Biman Bagchi, Graham R. Fleming, and David W. Oxtoby. Theory of electronic relaxation in solution in the absence of an activation barrier. *Journal of Chemical Physics*, 78(12):7375, jun 1983.

[53] Michelle D. Wang, Hong Tin, Robert Landick, Jeff Gelles, and Steven M. Block. Stretching dna with optical tweezers. *Biophysical Journal*, 72:1335–1346, mar 1997.

[54] Moshe Lindner, Guy Nir, Anat Vivante, Ian T. Young, and Yuval Garini. Dynamic analysis of a diffusing particle in a trapping potential. *Physical Review E*, 87(2):022716, feb 2013.

[55] Rebecca C. Wade, Razif R. Gaboulline, Susanna K. Lu´udemann, and Valére Lounas. Electrostatic steering and ionic tethering in enzyme-ligand binding: Insights from simulations. *Proceedings of National Academy of Science*, 95:5942–5949, may 1998.

[56] Dennis R. Livesay, Per Jambeck, Atipat Rojnuckarin, and Shankar Subramaniam. Conservation of electrostatic properties within enzyme families and superfamilies. *Biochemistry*, 42:3464–3473, mar 2003.

[57] V. M. Kenkre and S. Sugaya. Theory of the transmission of infection in the spread of epidemics: Interacting random walkers with and without confinement. *Bulletin of Mathematical Biology*, 76:3016–3027, nov 2014.

[58] L. E. Reichl. *A Modern Course in Statistical Physics*. Wiley-VCH Verlag, Weinheim, 2009.

[59] G. E. Roberts and H. Kaufman. *Table of Laplace Transforms*. W. B. Saunders Company, Philadelphia/London, 1966.

[60] H. S. Carslaw and J. C. Jaeger. *Conduction of Heats in Solids*. Oxford University Press, London, UK, 1959.

[61] S. Redner. *A Guide to First-Passage Process*. Cambridge University Press, Cambridge, UK, 2001.

[62] V. M. Kenkre. *Exciton Dynamics in Molecular Crystals and Aggregates*, volume 94. Springer, Berlin, 1982. Springer Tracts in Modern Physics.